UC Berkeley
UC Berkeley Electronic Theses and Dissertations

Title
Cortical Microstimulation for Neural Prostheses

Permalink
https://escholarship.org/uc/item/1j47p7g4

Author
Venkatraman, Subramaniam

Publication Date
2010

Peer reviewed|Thesis/dissertation

eScholarship.org Powered by the California Digital Library
University of California

Cortical Microstimulation for Neural Prostheses

by

Subramaniam Venkatraman

A dissertation submitted in partial satisfaction of the

requirements for the degree of

Doctor of Philosophy

in

Engineering - Electrical Engineering and Computer Sciences

in the

Graduate Division

of the

University of California, Berkeley

Committee in charge:

Professor Jose M. Carmena, Co-chair
Professor Kristofer S. J. Pister, Co-chair
Professor Yang Dan

Spring 2010

The dissertation of Subramaniam Venkatraman, titled Cortical Microstimulation for Neural Prostheses, is approved:

Co-chair Date

Co-chair Date

Date

University of California, Berkeley

Cortical Microstimulation for Neural Prostheses

Copyright 2010

by

Subramaniam Venkatraman

Abstract

Cortical Microstimulation for Neural Prostheses

by

Subramaniam Venkatraman

Doctor of Philosophy in Electrical Engineering and Computer Sciences

University of California, Berkeley

Professor Jose M. Carmena, Co-chair

Professor Kristofer S. J. Pister, Co-chair

Brain-controlled prostheses have the potential to improve the quality of life of a large number of paralyzed persons by allowing them to control prosthetic limbs simply by thought. An essential requirement for natural use of such neural prostheses is that the user should be provided with somatosensory feedback from the artificial limb. This can be achieved by electrically stimulating small populations of neurons in the cortex; a process known as cortical microstimulation. This dissertation describes the development of novel technologies for experimental neuroscience and their use to explore the neural and perceptual effects of cortical microstimulation in rodents.

The first part of this dissertation describes the various tools built to study cortical microstimulation in awake, behaving rodents. Circuits were developed to simultaneously record and stimulate neurons in the cortex; thus paving the way for future research into neural responses to stimulation. Further, electrode coatings based on conductive polymers were explored to allow chronic neural stimulation without causing long term damage to the implanted electrodes or neural tissue.

Two technologies were then developed to monitor different aspects of rodent behavior. Wireless accelerometers were built to monitor gross behavior and neural network based algorithms were developed to extract behavioral states from such acceleration data. Rats have poor visual acuity and actively scan their facial vibrissae or whiskers to feel the world around them. To study this whisking behavior, a video based whisker tracking system was developed which tracks the movement of a single whisker in real-time.

The second part of this dissertation describes advances in neuroscience enabled by these tools. The neural response to microstimulation was explored in awake, behaving rats and

it was found that microstimulation in barrel cortex evokes 15-18 Hz oscillations that are strongly modulated by motor behavior. In freely whisking rats, the power of the microstimulation evoked oscillation in the local field potential was inversely correlated to the strength of whisking. This relationship was also present in rats performing a stimulus detection task suggesting that the effect was not due to sleep or drowsiness. Further, a computational model of the thalamocortical loop is presented which recreates the observed phenomenon and predicts some of its underlying causes. These findings demonstrate that stimulus-evoked oscillations are strongly influenced by motor modulation of afferent somatosensory circuits.

The perceptual effects of cortical microstimulation were then explored using behavioral studies. Tactile exploration of the environment involves the active movement of external mechanoreceptors and the integration of information across sensory and motor modalities. To explore the encoding of somatosensory feedback in such an active sensing system, a novel behavioral paradigm was introduced which precisely controls cortical microstimulation in real-time based on the movements of the animal. Using a real-time whisker tracking system, microstimulation was delivered in barrel cortex of actively whisking rats when their whisker crossed a software-defined target. Rats learned to rapidly integrate microstimulation cues with their knowledge of whisker position to compute target location along the rostro-caudal axis. This showed that rats can perform sensorimotor integration using electrically delivered stimuli. Moreover, it was discovered that rats trained to respond to cortical microstimulation responded similarly to physical whisker deflection suggesting that microstimulation in barrel cortex induces tactile percepts. This ability to encode tactile percepts in active sensing systems may be critical for providing the sense of touch to future users of motor neuroprostheses.

Contents

List of Figures

Acknowledgments

First and foremost, I would like to thank my co-advisors Professor Jose Carmena and Professor Kris Pister. Both gave me complete freedom to explore research topics of my interest while providing support and advice at key points along the way. I owe a great deal of thanks to Jose, who provided the direction for much of the work in this dissertation. His enthusiasm and vision have helped push my research and knowledge far beyond what I would have imagined. Kris has a knack of getting to the core of any research problem and asking the right questions; he has been a fantastic role model as a researcher. I am also thankful to Professor Yang Dan for her valuable feedback on many research projects and papers.

I would like to thank all the residents of 471 Cory. Matt Last, Sarah Bergbreiter, Al Molnar, Steven Lanzisera and Chinwuba Ezekwe introduced me to the ways of grad school. A big thanks to Matt for allowing me to tag along on the microassembly project and teaching me everything I know about MEMS. Sarah, Steve and Chinwuba were the ideal 'senior grad students' you want to have around when you are new to grad school. They have provided valuable advice on many an occasion and have become great friends. A big thanks to Al for convincing me that I could be both an electrical engineer and a neuroscientist. Ankur Mehta, Erika Parra, Travis Massey, Thomas Watteyne and Anita Flynn have always been around to brainstorm crazy ideas, as well as shine lasers at campus buildings and fly model helicopters.

I would like to thank all the members of the BMI systems lab. John Long, Amy Orsborn, Karunesh Ganguly, Ryan Canolty, Rodolphe Heliot, Gireeja Ranade, Aaron Koralek and Jessica Jimenez have provided both valuable insights and a patient ear to the triumphs and defeats of grad school. Rodolphe and Amy made group meetings a pleasure with their mouth watering cakes and brownies, and have set a high bar for future postdocs and grad students. A big thanks to John Long and Natalia Caporale who helped me setup the rodent electrophysiology lab and taught me brain surgery! I would also like to thank all the other neuroscience grad students who have helped me over the years and been great friends outside of the NAF. I mentored a number of undergraduate students over the years and they have been more helpful than they might imagine. Ken Elkabany and Maria Bustamante helped me build the whisker tracking system while Sandra Truong, Pattana Lee and Darin Hoyer helped figure out the nitty gritty details of experimental neuroscience that are the key to success. A special mention to R36, my favorite and most brilliant rat, who perfected the art of escaping from locked cages.

A big thanks to all my friends at Berkeley who have been there for numerous coffee breaks, dinners and road trips. You made the journey through grad school a whole lot more fun. Finally, I would like to thank my family. Living on opposite corners of the world has certainly been difficult but my parents Dr. S. Venkatraman and Pushpa Venkatraman and sister Shweta have provided me with undying love and encouragement. Most of all, a heartfelt thanks to my wife Praveena. Over the past few years, she has experienced the numerous ups and downs of not one but two Phds and I certainly couldn't have done it without her.

Chapter 1

Introduction

During the 1780s [1], Luigi Galvani was performing experiments at the University of Bologna involving frogs. While cutting a frog's leg, Galvani's assistant touched an exposed nerve of the frog with a metal scalpel which had picked up a charge. At that moment, they saw sparks and the leg twitched! This observation made Galvani the first investigator to appreciate the relationship between electricity and life, a phenomenon he called 'animal electricity'. Later studies revealed that the electric current delivered by a Leyden jar or a rotating static electricity generator could also cause the contraction of the muscles in a frog leg. These findings provided the basis for our current understanding that neurons transmit information using electrical pulses.

Two centuries later, electrical recording and stimulation of neurons remain the predominant techniques used to study neural circuitry and function [2], map the connectivity between brain regions [3] and alleviate severe neurological disorders like epilepsy and Parkinson's disease [4]. This dissertation explores another application of neural recording and stimulation; namely, how do we provide tactile feedback to users of prosthetic limbs using electrode arrays implanted in the cortex?

The most successful neural prostheses today are cochlear implants (Figure 1.1A) which restore audition in the hearing impaired by stimulating nerve cells in the cochlea with an implanted electrode array [5]. These devices have been implanted in over 100,000 persons worldwide. Another sensory neuroprosthesis being actively researched is the retinal prosthesis (Figure 1.1B) [6], which restores some vision by stimulating the retina based on real-time video recordings. A common feature of both devices is that they use electrical stimulation of neurons to restore lost senses.

Another class of neural prostheses aims to provide users with the ability to control prosthetic limbs or computer cursors using signals recorded from the brain (Figure 1.1C). Likely beneficiaries of this technology include people paralyzed by brain or spinal-cord trauma or those with deficits caused by stroke, amyotrophic lateral sclerosis (ALS), cerebral palsy, and multiple sclerosis. Neurally controlled devices based on recordings from the surface of the

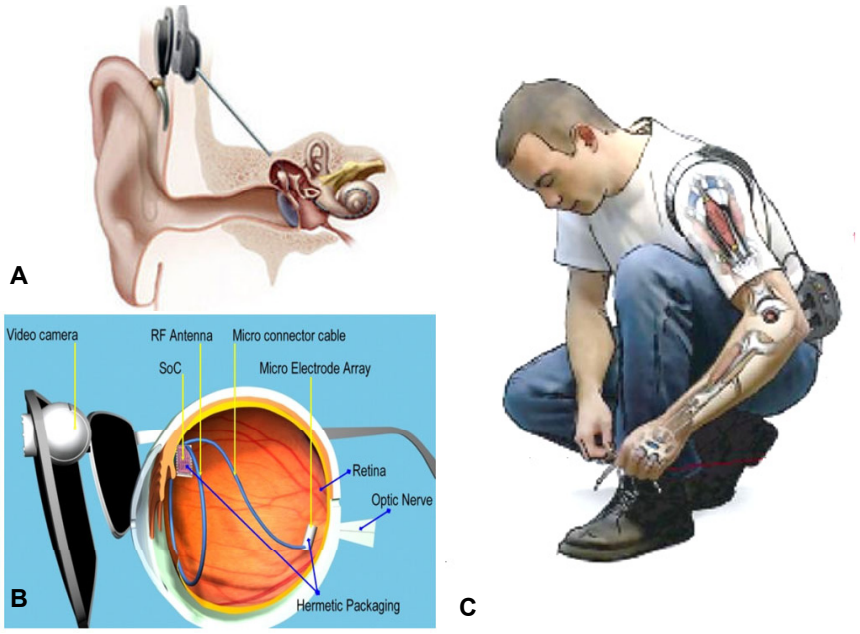

Figure 1.1: Neuroprostheses. (A) Cochlear implants which restore audition (Image courtesy NIH Medical Arts) (B) Retinal prosthesis which restore vision (Image courtesy USC). (C) Artist's conception of a future motor prosthesis [7]

scalp (Electroencephalogram - EEG) have been researched for many decades but suffer from poor spatial and temporal resolution of the recorded signals. This field has seen remarkable progress in the last decade due to advances in invasive multielectrode array neural recording technologies [8, 9]. Chapin et al. [10] first demonstrated that a rat could control a lever to feed itself using signals extracted from motor cortex in 1999 (Figure 1.2A). Since then, we have seen demonstrations of real-time control of computer cursors [11, 12, 13] and robotic arms [13, 14] by non-human primates (2002 onward) (Figure 1.2B) and the implantation of electrode arrays into the brain of a paralyzed man in 2006 [15] allowing him to control devices using his 'thoughts' (Figure 1.2C). Excellent reviews on brain-machine interfaces have been published in recent years and interested readers should peruse [7, 16, 17].

While much work needs to be done before we can achieve accurate, multi-degree of freedom control of artificial limbs using neural signals, an equally important requirement for users of such prostheses would be the ability to experience somatosensory feedback from the limb [18]. Somatosensory inputs comprise the sensory modalities of touch, temperature, proprioception and nociception (pain). Proprioception is the sense that tells us where our limbs are in space, and is essential for us to perform most day-to-day tasks like walking. Our acute dependence on proprioception in daily life only becomes apparent in the few cases where patients lose this sense. For example, patients suffering from acute sensory neuropathy can only walk by staring at their feet to know leg position since they lack proprioceptive signals which encode limb position. Other somatosensory inputs like touch and force feedback are also essential for daily activities like handling tools and delicate objects. For example,

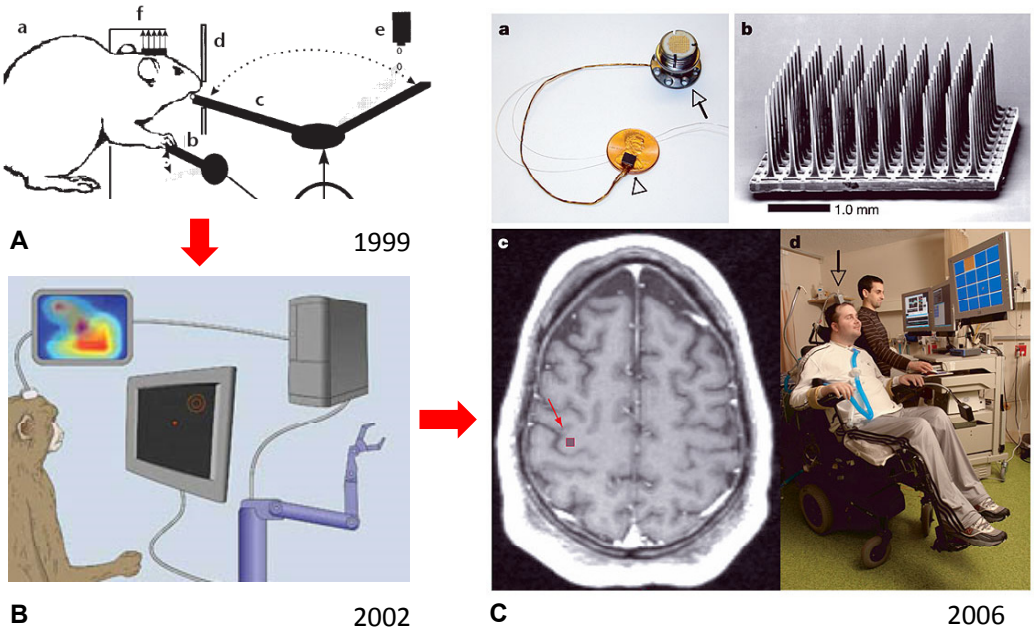

Figure 1.2: Brief history of motor prostheses. (A) Rats control a lever using signals from motor cortex [10] (B) Monkeys control computer cursors and robotic arms using neural signals and (C) First demonstration of neural control of external actuators using implanted electrode arrays in humans [15]

it would be difficult to unscrew a light bulb with a robotic hand without either crushing or dropping it (Figure 1.3) unless we provide somatosensory feedback to the user of such a hand. The work presented in this dissertation focuses on the technological and neuroscience challenges that need to be overcome to provide such somatosensory feedback to future users of prosthetic limbs.

This dissertation begins with a brief introduction to neural interfaces. This is followed by a review of recent research on encoding somatosensory feedback using cortical microstimulation. Chapter 2 describes circuits and electrodes required to record and stimulate neurons in the cortex and some technological advances in that direction. Chapter 3 describes devices which we developed to track rodent behavior, which is crucial for research on awake behaving rodents. Chapter 4 and 5 discuss two neuroscience problems which we addressed using technologies developed in previous chapters. Chapter 4 describes the modulation of the rat somatosensory system with behavior as explored using cortical microstimulation. Chapter 5 demonstrates the encoding of target location in an active sensing system using cortical microstimulation. Finally, conclusions and future directions suggested by this research are detailed in Chapter 6.

Figure 1.3: How do you unscrew a light bulb with a prosthetic hand? To do so, it is essential that sensory feedback from the robotic hand be provided to the user (Image courtesy Shadow Robot Company).

1.1 Neural Interfaces

This section presents some of the basics of neuroscience and neural interfaces which forms the foundation of the work presented in this dissertation. Interested readers are referred to the extensive body of literature on neuroscience and in particular "Principles of Neural Science" [19] which provides an excellent and comprehensive introduction to the field and "Brain Facts" published by the Society for Neuroscience [20] which provides a shorter 'lay-person' introduction.

Neurons are specialized cells which form the functional units of the brain and consist of a cell body, dendrites and an axon (Figure 1.4A). Neurons communicate by transmitting electrical impulses, called action potentials, along their axons which synapse onto the dendrites of other neurons. Action potentials form a digital code with which neurons communicate with each other, with information encoded in their timing and rate. Thus we can decode the communication between neurons by recording the precise timing of action potentials. Moreover, we can encode information by eliciting action potentials in neurons. We record and stimulate neurons in the cortex (the outermost layer of the brain) using arrays of chronically implanted extracellular microelectrodes (Figure 1.4B).

These arrays can be fabricated using microfabrication techniques (Figure 1.5A,C) [21, 9] or can be assembled using metal microwires (Figure 1.5D) [8]. More recent designs have an open architecture (Figure 1.5B) [22], flexible electrodes (Figure 1.5E,F) [23] or channels for drug delivery (Figure 1.5G,H) [24]. All the experiments presented in this work were

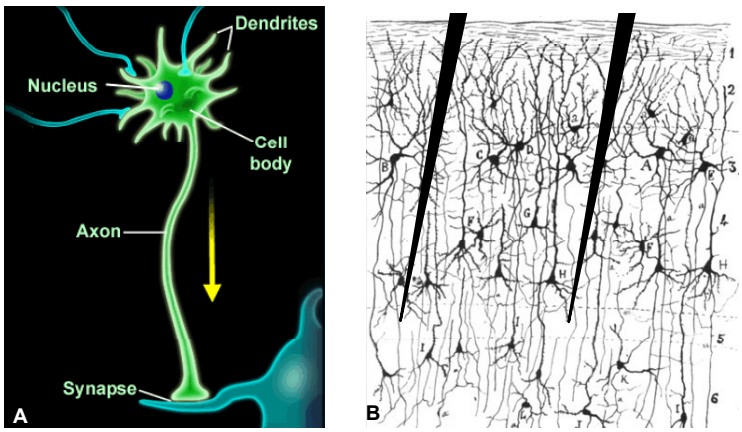

Figure 1.4: Neurons (A) Neurons consist of a cell body, dendrites and an axon. (B) Golgi stain of a slice of cortex showing different cell types and illustration of implanted extracellular microelectrodes.

performed using metal microwire arrays similar to (Figure 1.5D). The surgical procedure used for array implantation are described in Chapter 3.

An action potential results in a tens to hundreds of μV change in the extracellular voltage at points within 100μm of the neuron. This voltage change can be recorded by extracellular electrodes placed within that region and provides a signature of the firing of the neuron. Microelectrode arrays are implanted into the appropriate region of cortex (primary somatosensory cortex in this work) but do not specifically target individual neurons. They simply record spikes from a random subset of the millions of neurons which are present in the vicinity. Each electrode records action potentials from 1-4 nearby neurons and the spikes from each neuron typically have different waveform shapes and amplitudes allowing us to discriminate between them.

Injecting a small current pulse through implanted microelectrodes leads to depolarization of the cell membrane of neurons near the cathode and initiates an action potential. This process, namely electrical stimulation of small populations of neurons in the cortex, is known as intracortical microstimulation (ICMS). Reference [25] provides a good review of extracellular stimulating and recording using microelectrodes.

The animal experiments presented in this work were performed on adult rats therefore it is instructive to study the rat somatosensory system. Rats have poor visual acuity and have therefore developed a very sensitive whisker system which they use to sense the world around them (Figure 1.6). By using their whiskers, rodents can build spatial representations of their environment, locate objects, and perform fine-grain texture discrimination. Deflection of a whisker evokes action potentials in sensory neurons of the trigeminal nerve, which transmits this information to the brain stem, thalamus, and then the primary somatosensory barrel cortex. The barrel cortex has an exquisite somatotopic map where each whisker is

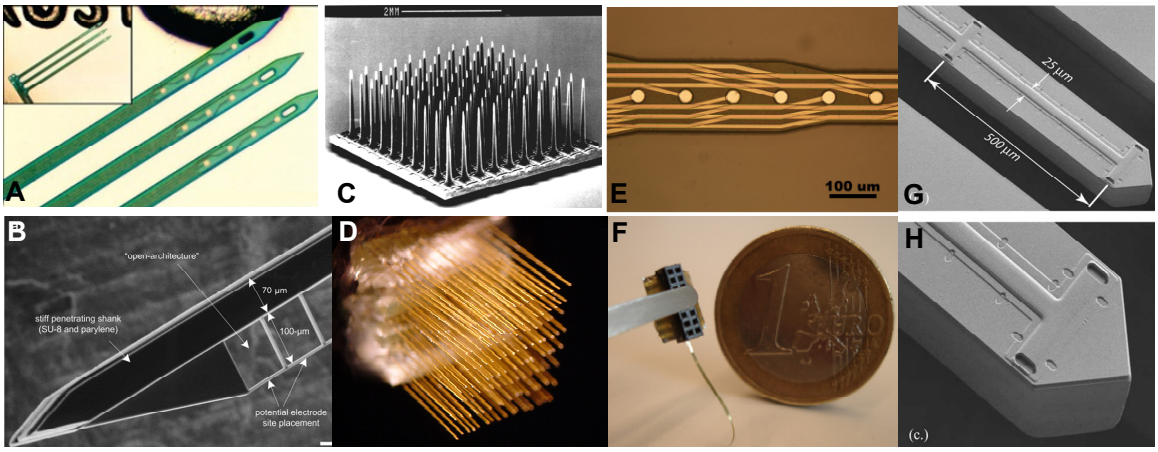

Figure 1.5: Neural Interfaces. (A,B) Michigan Probes [22] (C) The Utah array [9] (D) Microwire arrays [8] (E,F) Flexible electrode arrays [23] (G, H) Electrode arrays with microfluidics [24]

represented in a discrete anatomical unit called a barrel (Figure 1.6). Reference [26] provides an excellent review of the functional and anatomical organization of the barrel cortex.

Much of the previous research on microstimulation in the rat somatosensory system [27, 28] ignored the peculiarities of the rat vibrissa system and considered it as a simple model of somatosensory processing. Instead, in this work, we pay attention to the vast literature on the rat vibrissa system and study thalamocortical processing and active sensing in the rat whisker system using cortical microstimulation. All animal procedures conformed to the NIH and USDA regulations and were approved by the UC Berkeley Animal Care and Use Committee.

1.2 Somatosensory Feedback

Cortical microstimulation is known to evoke motor and sensory effects which mimic the contribution of the stimulated areas [29, 30, 31]. Since we know the location in cortex of regions that encode a particular sense, we can then bypass lost or damaged external sensors and recreate that sense by stimulating neurons in precise cortical locations. Excellent work in humans by Wilder Penfield and others in the 1950s [32] laid the basis for much of this work by showing that electrical stimulation of sensory cortical areas could result in sensory percepts. Later studies showed that microstimulation in visual cortex can produce the perceptual effect of visual sensation [33], and this research has led to attempts to create cortical visual prostheses. These prostheses would work by capturing video of the outside world, performing appropriate compression and stimulating the visual cortex using an array

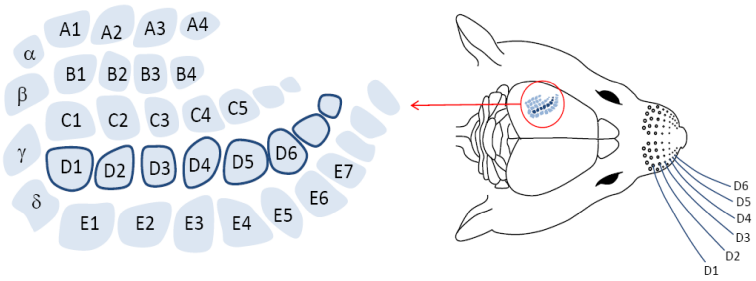

Figure 1.6: Rats have a well developed whisker system. The somatotopic arrangement of barrel cortex shows that each barrel corresponds to one whisker. (Image courtesy Neural Coding Lab, Univ. of New South Wales)

of implanted electrodes to recreate a simplified representation of the outside world.

Similarly, microstimulation in somatosensory cortex has been shown to mimic the perception of flutter vibrations on the fingers (Figure 1.7A) [34]. This study was particularly fascinating because it demonstrated that microstimulation can be used to elicit a memorizable and discriminable analog range of percepts. Moreover the fact that the percept was similar to that caused by touching the fingers agrees with other studies in humans [35, 36, 37] which have reported that microstimulation of somatosensory regions evokes tactile percepts. Therefore we can conceive of somatosensory prostheses which encode touch by stimulating neurons in the primary somatosensory cortex.

Preliminary work in this direction has shown that microstimulation of the two hemispheres of rat somatosensory cortex (Figure 1.7B) can be used to provide rats with binary information and guide them through a complex terrain [27]. While not entirely surprising from a scientific point of view, this research sparked wide public interest as a remote controlled 'roborat'. Following this line of research, it was shown that different spatiotemporal sequences of stimulation (Figure 1.7C) can be used to encode different reach directions in primates [38]. These results aim to encode information in the somatosensory cortex using microstimulation without exploring the actual sensory percept caused by this stimulation. While it is possible that this approach can have clinical applications, it is likely that mimicking natural sensory percepts (to whatever extent possible) will lead to more natural and useful somatosensory feedback for prosthetic users.

More general work on cortical microstimulation has shown that the perceived intensity of cortical microstimulation in rats is similar to the response of a leaky integrator [28]. Moreover, studies in rat auditory cortex have suggested that microstimulation results in sensory percepts similar to that encoded by the stimulated region [39]. Further, the neural response to stimulation was shown to consist of a spatiotemporal blur of activation around the stimulating electrode [40]. These studies provide some direction regarding the stimulation protocol required and the optimal site of stimulation to encode sensory percepts using cortical microstimulation. While instructive, these results represent just the tip of the iceberg and many

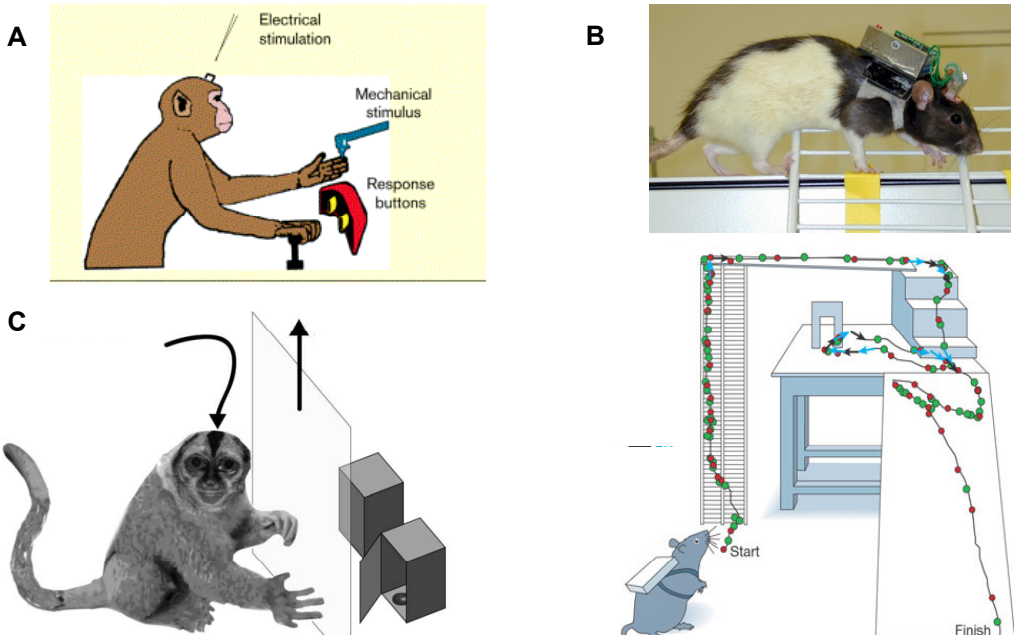

Figure 1.7: Previous experiments in microstimulation to provide somatosensory feedback. (A) Flutter stimulation in monkeys [34] (B) Remote control of a rat [27] (C) Spatiotemporal stimulation sequences in monkeys [38]

technological and neuroscience issues need to be addressed before we can use cortical microstimulation on patient populations.

Providing somatosensory feedback requires that we device ways to record and stimulate neural activity at will and that we understand the neural and perceptual effects of such stimulation. The research presented in this dissertation explores these issues and paves the way to providing the feeling of touch to future users of motor neuroprostheses.

Chapter 2

Electronic Neural Interfaces

Understanding the neural and behavioral response to cortical microstimulation is essential in order to design stimulation protocols for sensory neuroprostheses. A major technical impediment in this endeavor is the lack of commercial technologies to simultaneously stimulate and record neurons in awake, behaving animals. In this chapter we discuss the design of such a platform using off-the-shelf components, custom software, and custom printed circuits boards (PCBs). We then discuss the electrode materials which need to be developed to allow safe chronic stimulation with such a system; a necessary requirement before such technology can transition to human use.

2.1 Stimulation and Recording System

2.1.1 System Architecture

Current commercial systems allow parallel neural recordings from arrays of implanted electrodes in awake, behaving animals but do not allow simultaneous stimulation. Other commercial systems exist which perform stimulation so the first technical challenge was to integrate these systems. The overall system architecture is shown in Figure 2.1A. Neural signals are recorded from 35μm diameter microwire arrays implanted in rat somatosensory cortex using a multi-channel neural recording system (Plexon Inc., Dallas, TX). Signals are filtered into two frequency bands of interest: 3-200Hz for LFP and 0.5-9kHz for spikes. Biphasic current stimuli are delivered using a multichannel stimulation system (Triangle Biosystems, Durham, NC) and custom software. Both these systems have a frontend which consists of a light headstage with electronics connected directly to the electrode array and connected by flexible cables to further electronics. An important constraint with microstimulation and recording in awake, behaving rodents is to ensure that minimal electronics are placed next to the implanted electrodes to ensure that rats do not have to move around carrying large and heavy electronics.

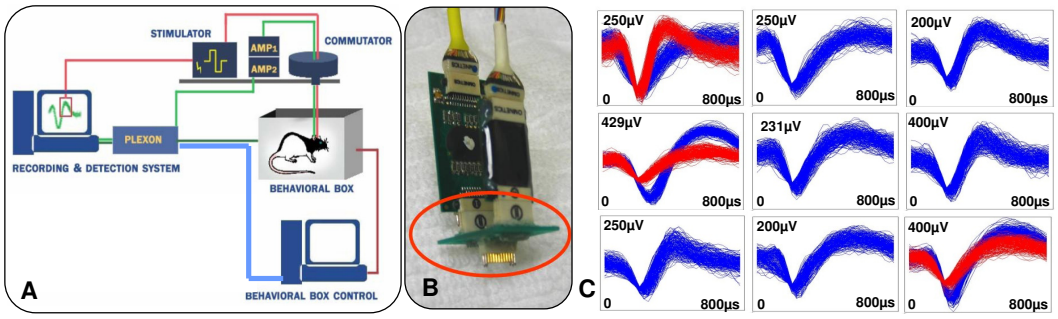

Figure 2.1: Closed-loop stimulation system. (A) System architecture showing the animal in a behavioral box, recording and stimulation systems and behavioral control PC connected to form a closed loop system (B) Stimulation and recording headstages connected with a custom connector on a small PC board (C) Waveforms recorded from a 16 channel microwire array implanted in barrel cortex of awake behaving rat.

We interfaced these two headstages by developing a simple connector, called a 'Y connector' on a printed circuit board that attaches these two headstages in parallel across the electrode array as shown in Figure 2.1B. An important constraint while doing so is to ensure that the stimulator output impedance is significantly greater than the impedance of the electrodes, which was achieved by modifying the output impedance of the stimulator to 10MΩ while not actively delivering current. The other constraint in such a system is that the stimulation voltage should not exceed the voltage compliance of the recording headstage and this was achieved by limiting the voltage excursions of the stimulation system to 5V.

Alternately a single channel stimulator from AM systems was used along with specially designed electrode arrays with dedicated stimulating channels. The advantage of this approach is that it does away with the Y connector and associated noise sources. However it does not allow simultaneous stimulation and recording from the same electrode.

2.1.2 Artifact Reduction System

The long duration of the artifact produced by microstimulation on nearby recording channels is a well known problem and has been encountered by researchers for decades [41, 42]. In the case of arrays of chronically implanted microelectrodes, this problem is further exacerbated by the close spacing of the electrodes and the mutual coupling between them. Software reduction of the artifact is possible to some extent [43] but software techniques can never recover the period during which the amplifiers are saturated and this period is often longer than 5ms. Hardware based techniques previously reported include using a low slew rate initial amplifier [44] or actively discharging the electrodes soon after stimulation [45]. These solutions require electronics to be placed on the animal next to the electrodes. This places very stringent size and weight constrains on the circuit and requires the design of a custom

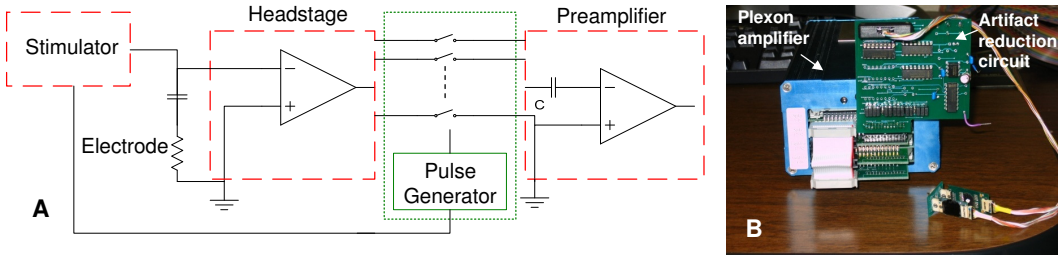

Figure 2.2: Artifact reduction circuit (A) Circuit used to reduce the length of the stimulation artifact (B) Artifact reduction circuit as fabricated is the green board shown attached to the further amplification stages.

integrated circuit. While such devices are being developed, our design provides a simple and cheap solution.

To minimize the artifact, we placed an array of switches between the first and second amplifier stages to disconnect the second stage from the first for a short period (1ms) after the stimulation (Figure 2.2A). The implemented circuit board is shown in Figure 2.2B. A variable pulse length is generated from the stimulation trigger using a monostable multivibrator. This pulse is used to turn off fault-protected analog switches MAX 4712 (Maxim Semiconductors, Sunnyvale, CA) which connect the input amplifiers to the rest of the amplifier chain. One limitation of our approach is that it cannot remove the artifact on the stimulating channel. This is due to residual polarization of the electrode itself which can only be decreased by directly discharging the electrode as in [45].

An example of the performance of the circuit is shown in Figure 2.3A. The initial artifact was 5.2ms long when the amplifiers were operated at their maximum gain of 32,000. By employing the switching circuit, this artifact was reduced to 2.0ms in length. Figure 2.3C shows the artifact length recorded from a number of channels on the same array with the circuit operational and not. The artifact length here is defined as the time for which the amplifiers are completely saturated. This figure provides a quantitative estimate of the factors which affect the artifact length. The length of the stimulation artifact strongly depends upon stimulation amplitude but this factor is not shown here since stimulation amplitude was kept constant at 30μA, 200μs biphasic pulses during these experiments. The artifact increases with increasing gain on the recording channel and decreases with increasing distance from the stimulating electrode as expected. More importantly, it also shows that using the artifact reduction circuit causes a factor of (mean $\pm$ SD) 0.28 $\pm$ 0.23 reduction in artifact length.

The voltage transient caused due to switching our circuit without actually triggering stimulation is $<20\%$ in amplitude of that caused with stimulation (Figure 2.3D(ii)). Hence we believe that the residual artifact seen is not due to the presence of DC offset on the input channels or due to switch induced charge injection. In agreement with this, we found that providing a sample and hold circuit to store the DC bias on the amplifier outputs (Figure 2.3D(iii)) or providing an impedance matched switch to balance charge injection (Figure 2.3D(iv)) did

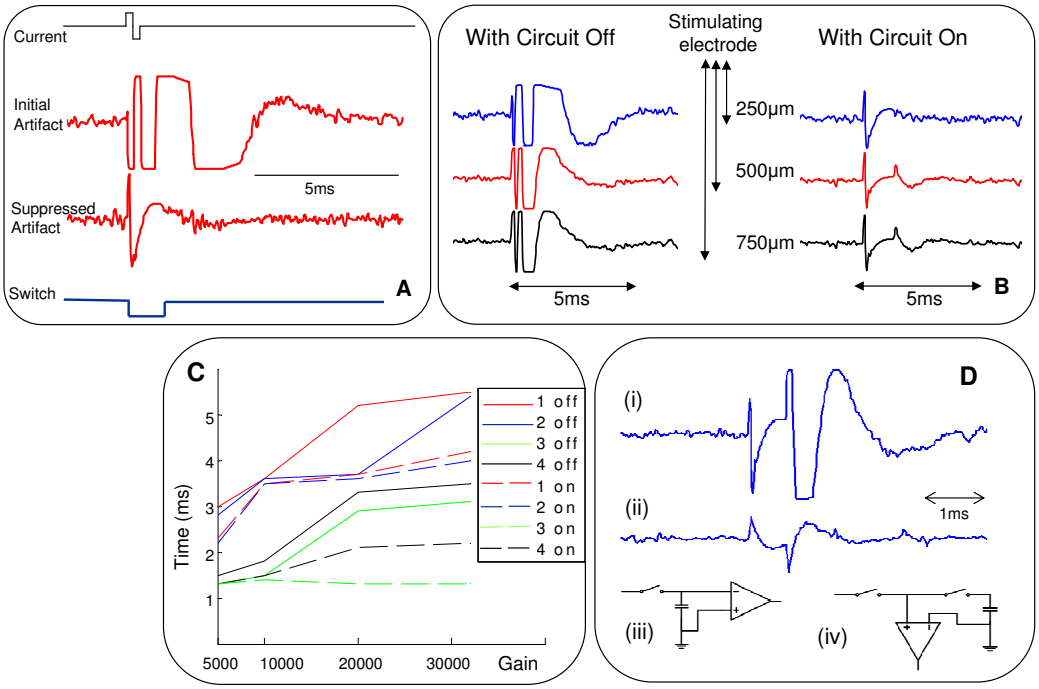

Figure 2.3: Performance of artifact reduction circuit. (A) The initial artifact caused due to stimulation and the suppressed artifact after turning on the circuit (B) The reduction of stimulation artifact across multiple recording channels at different distances from the stimulating electrode. (C) Electrodes 1,2,3 are at increasing distances from the stimulating electrode. (D) Figure (i) shows the residual artifact with the circuit on and figure (ii) shows the artifact with no stimulation. Figure (iii, iv) are two topologies commonly used to reduce artifacts which do not help in our case due to the negligible influence of DC offsets and switch induced charge injection.

not improve the artifact (data not shown). All recordings in Figure 2.3 were performed on chronically implanted electrodes in a rat anaesthetized using isofluorine to minimize neural responses to ICMS.

An artifact of less than 2ms allows us to view the initial neural response to microstimulation that typically occurs between 2-5ms after stimulation. Figure 2.4 shows the neural response to microstimulation observed in a chronically implanted electrode in the rat primary somatosensory cortex (S1). The neuron shows an initial excitation followed by a prolonged period of decreased firing rate before returning to its baseline firing rate as is evident from Figure 2.4C. This response is very similar to that observed by other groups in anesthetized animals [40].

Thus we show that a simple design, based on well known circuit techniques, can significantly improve the capability to record neural responses to ICMS in awake behaving animals, thus enabling a more thorough understanding of ICMS. Future designs will probably involve fully integrated artifact reduction systems [45] as well as multi-channel integrated neural

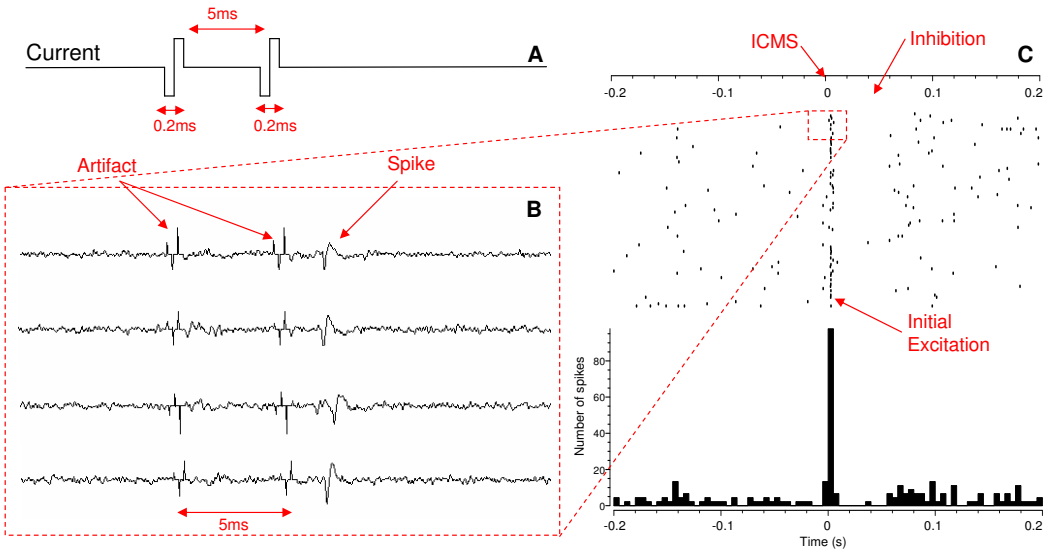

Figure 2.4: Neural Response to ICMS (A) Stimulation sequence consisting of two biphasic current pulses of amplitude 10μA. Two pulses separated by 5ms were used since this sequence reliably elicited a response from this particular neuron. (B) Traces showing a particular neuron's response to stimulation. The circuit helps to significantly reduce the period during which the amplifiers are saturated and the residual artifact is further cleaned using software. (C) Raster plot and peri-stimulus histogram showing the response of the same neuron to ICMS with initial excitation, inhibition and return to baseline firing rate.

amplifiers [46, 47, 48]. A novel topology for such amplifiers which exploits the power spectrum of recorded neural signals is presented in [49].

2.2 PEDOT coated Microelectrodes

Since sensory prostheses are expected to function for a number of years, it is essential that the electrode materials and stimulation waveforms be chosen to ensure that microstimulation does not cause any deleterious effects on either the surrounding nervous tissue or the electrodes. The amount of charge required to stimulate neurons using extracellular microelectrodes often exceeds the quantity needed to initiate irreversible faradaic reactions at the electrode interface; which in the extreme case can lead to electrolysis of water as shown in Figure 2.5.

Electrodes for neural stimulation are typically characterized by their charge-injection limit that represents the maximum charge that can be injected into tissue without initiating irreversible faradaic reactions [50]. The charge needed to stimulate neurons in the central nervous system using microelectrodes typically exceeds the established limits of noble metal

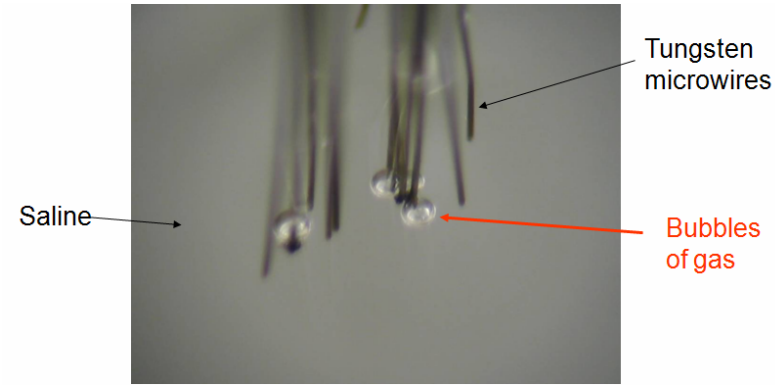

Figure 2.5: Electrolysis of water using microelectrode arrays. Applying a 5V, 1kHz square wave to the electrodes of a microelectrode array for a few seconds results in the formation of bubbles of gas due to electrolysis.

electrodes [25]. Moreover, many applications require that the same electrodes also be used for single unit neural recording and this places stringent constraints on the maximum area of electrodes ($<1250\mu m^2$). Hence, a number of electrode coatings are being explored which increase the surface area and/or charge capacity of the interface; notable among them being iridium oxide (IrOx), titanium nitride (TiN) and poly(3,4-ethylenedioxythiophene) (PEDOT).

PEDOT is an electrically conducting polymer which has been investigated for improving the long-term performance of microfabricated neural prosthetic devices. PEDOT coatings on electrodes lead to significant reduction in electrical impedance and increase in charge capacity *in vitro* [51]. Chronic *in vivo* recordings with PEDOT probes [52] have shown that PEDOT coated sites can record single unit and local field potentials and outperform control sites with bare metal electrodes. However we believe that the significant benefits of PEDOT coatings lie in applications which involve microstimulation. The efficacy of PEDOT probes in comparison to 'state of the art' electrodes and coatings for microstimulation applications has not been well quantified nor has its behavior in chronic *in vivo* microstimulation applications been established.

2.2.1 Materials and Methods

Microwire arrays (Plexon Inc., Dallas, Tx) made with 25 or 75μm diameter teflon-coated PtIr wires with flat, exposed tips were coated with poly(3,4-ethylene dioxythiophene)-poly(styrene sulfonate) (PEDOT-PSS). PEDOT-PSS was deposited from a solution containing 0.1% (w/v) ethylene dioxythiophene (EDOT; H.C. Starck) and 0.2% (w/v) poly (styrene sulfonate) sodium salt (PSS; Acros Organics) in deoinized water. The microwire array was immersed in the

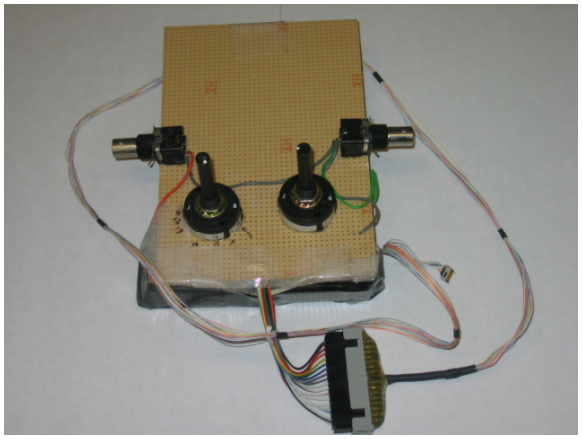

Figure 2.6: Breakout box used to measure impedances from the electrode array without having to change connections for every electrode.

monomer solution and served as the working electrode (anode). A platinum foil served as the counter electrode (cathode). For the 75μm diameter wire, galvanostatic charge of 86.4μC was applied using an AutoLab PGStat12 Potentiostat/Galvanostat (EcoChemie) to individual sites. The coated array was then rinsed in deionized water and stored dry for testing / implantation. Figure 2.7D shows a typical scanning electron micrograph of PEDOT deposited onto the electrode sites of PtIr microelectrodes and the inset shows roughened surface features of the deposited PEDOT which lowers the interface impedance.

Iridium oxide was electrochemically deposited onto PtIr electrodes from solution according to methods similar to those used in [53]. 75mg of $IrCl_4$ (Alfa Aesar) was added to 50ml of deionized water and stirred for 30 minutes at room temperature. 0.5ml of 27.7 $\%$ hydrogen peroxide was then added to the solution, resulting in a yellowish colored liquid. The solution was again stirred for 10 minutes. 250mg oxalic acid dihydrate (Alfa Aesar) was then added to the solution and stirred for 10 minutes. By adding small amounts of anhydrous potassium carbonate (Alfa Aesar), the pH of the solution was slowly raised to 10.5. This solution was then left to equilibrate for 2 days at room temperature prior to use. Deposition of the iridium oxide film was performed using an AutoLab PGSTAT12 Potentiostat/Galvanostat (EcoChemie) to deliver galvanostatic charges of 16.2μC. The resulting films were rinsed twice in deionized water and stored dry. The deposition charges used for PEDOT-PSS (86.4μC) and for IrOx (16.2μC) were selected to provide the best charge transfer properties without compromising mechanical stability and adhesion of each coating.

Cyclic voltammetry (CV) was measured at a 500mV/s sweep rate between potential limits of -0.6V and 0.8V. All CVs were measured in a three-electrode cell comprising a Ag—AgCl reference electrode, a large-area Pt mesh counter electrode, and the test microelectrode immersed in phosphate buffered saline (PBS). The deposition of PEDOT and IrOx as well as CV measurements were performed at Univ. of Michigan by collaborators. Current pulsing

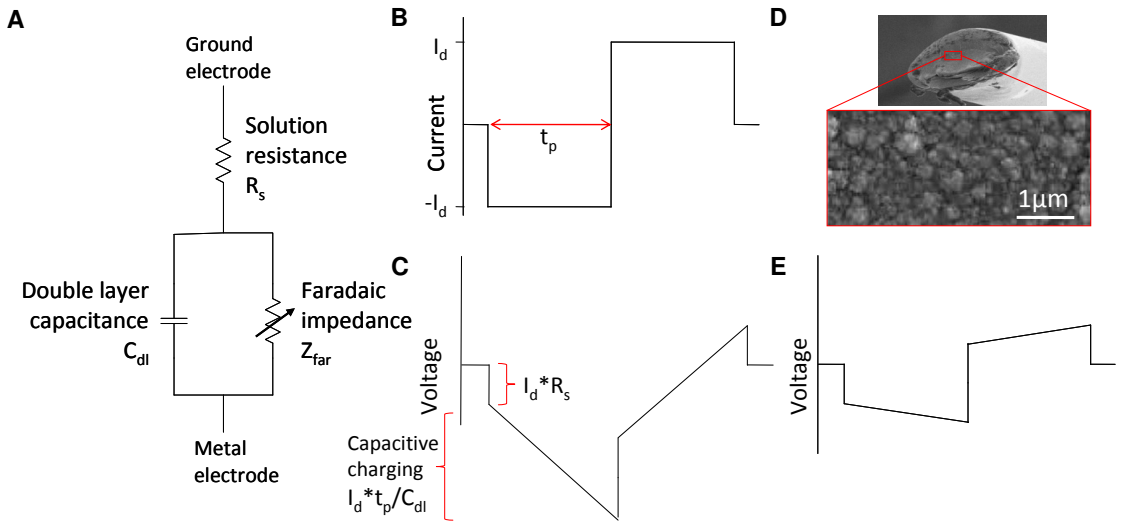

Figure 2.7: Model of electrode interface. (A) Model of electrode tissue interface as a series capacitance (double layer capacitance) and resistance (tissue). (B) Biphasic current pulse used in microstimulation. (C) Voltage expected at metal electrode in model upon injection of biphasic current waveform with one component due to IR_s drop and one component due to capacitive charging of C_{dl}. (D) PEDOT deposited on PtIr microelectrode and a close-up view of the rough surface of deposited film. (E) Voltage transient expected with increased capacitance.

was performed at Berkeley using a stimulator from AM Systems (Sequim, WA) that provides biphasic current pulses of desired amplitudes and precise pulse widths. All potential transient responses were measured in a three-electrode cell comprised of a low impedance Pt reference electrode, a separate low impedance Pt counter electrode and the test electrode immersed in saline to closely match *in vivo* testing conditions.

Electrode impedances were measured *in vivo* using an impedance meter from FHC. Most commercial impedance meters only measure the impedance of a single electrode but we wished to measure the impedance of all electrodes on an array without having to change connections for every electrode. This was achieved by building a breakout box (Figure 2.6) which connects to the impedance meter and uses an omnetics connector to connect to the electrode array. It then uses two 8/1 switches to couple different electrodes from the 16 electrode array to the impedance meter. All impedance measurements in this work were performed using this breakout box.

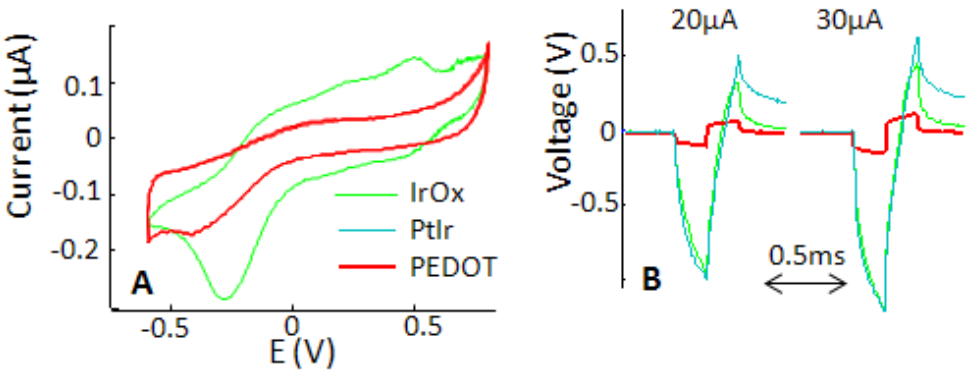

Figure 2.8: (A) Cyclic voltammetry measurements on PEDOT and IrOx coated electrodes show that IrOx exhibits larger charge capacity for the particular parameters of deposition used in test electrodes. (B) The same PEDOT coated electrodes exhibit a much smaller voltage transient compared to IrOx and bare PtIr.

2.2.2 *In Vitro* Testing

A simple electrical model of the tissue-electrode interface is shown in Figure 2.7A which helps to predict the voltage transient seen on electrodes during neural stimulation (Figure 2.7C,E). The electrode interface can be modeled as a series resistance (due to the cellular medium) and capacitance (due to the double layer capacitance) in parallel with a faradaic impedance (due to chemical reactions). A constant amplitude current pulse causes an IR drop across the resistance (referred to as the access voltage V_a) and capacitive charging of the double layer capacitance. Neural stimulators typically use constant current pulses, hundreds of microseconds in duration. These pulses are designed to be biphasic (Figure 2.7B) to minimize irreversible chemical reactions on the electrode interface. However, simply using biphasic pulses does not ensure that no irreversible reactions occur; it is also important to ensure that the voltage transient on the electrode stays smaller than the water window (-0.6V to 0.8V). When the voltage across the double layer exceeds the water window, it initiates irreversible electrolysis of water. Rough materials like PEDOT increase the double layer capacitance and thus decrease the voltage developed across it. Moreover, PEDOT also allows reversible faradaic reactions at the electrode-electrolyte interface thus injecting charge through the faradaic impedance. Thus the voltage transient on PEDOT electrodes is expected to be smaller, thus reducing the probability of irreversible faradaic reactions at the interface.

Cyclic voltammetry (CV) is a commonly used technique to measure the charge transfer capacity of materials. Figure 2.8A shows that the IrOx electrodes possess a larger charge capacity compared to PEDOT electrodes when measured using CV. However, CV measures the charge capacity of electrodes when subjected to a slow voltage ramp (5-1000mV/s) and only a fraction of this charge capacity is available when using sub-millisecond current pulses. Note that a 600mV transient caused in 200μs translates to 3,000,000mV/s! Hence, the charge

injection limit measured using voltage transients provides a more accurate measure of electrode performance. The charge-injection limit is defined as the quantity of charge which polarizes the electrode interface to the potential for water reduction (E_{mc} = -0.6 V). The potential transients were recorded with an oscilloscope, and the maximum negative potential excursion (E_{mc}) was calculated by subtracting the access voltage (V_a), associated with the ohmic resistance of the electrolyte from the maximum negative voltage in the transient. The charge injection limit for electrodes of identical geometrical surface area (GSA=4500μm^2) were measured to be PtIr = 0.13mC/cm^2, IrOx = 0.19mC/cm^2 and PEDOT = 2.92mC/cm^2. These measurements show that PEDOT-coated electrodes can safely deliver 15 times more charge compared to IrOx and PtIr electrodes.

The measurement of charge injection limit requires that we be able to subtract the access voltage (V_a) which, while possible *in vitro*, is often impossible *in vivo*. We therefore chose an equivalent measure which was the actual voltage drop across the electrode for a constant current pulse. We found that upon applying a current pulse of 20μA, 200μs, the PEDOT-coated electrodes show a 579mV smaller voltage drop across the electrode interface (Figure 2.8b) compared to the IrOx electrodes. A second measure of performance was to look at the residual voltage seen 200μs after the end of the biphasic pulse. This measure takes into account the fact that in a perfectly reversible reaction, the potential at the end of the charge balanced biphasic pulse should revert to 0V. Any residual voltage implies that irreversible reactions have taken place during the current pulse. The residual voltage 200μs after 20μA biphasic pulses was measured to be PEDOT = 2.27mV, IrOx = 32.3mV and PtIr = 222mV. Hence, PEDOT-coated electrodes were superior on this measure (Figure 2.8b) followed by IrOx, and lastly bare PtIr.

It is known that IrOx performs best at a DC voltage bias of +0.6V and its charge injection limit drops at low DC bias [54]. This explains its poor performance compared to PEDOT in our experiment. Most commercial current stimulators do not offer the functionality to deliver short constant-current pulses while maintaining a constant voltage bias, and this is not a functionality used in typical scientific applications. We therefore decided to compare charge injection limits and voltage transients on all electrodes at zero voltage bias. The above measurements demonstrate that PEDOT coatings provide much better performance than IrOx and PtIr when using zero voltage bias constant-current stimulation, as is the norm.

It is possible to increase the charge injection limit obtained with PEDOT electrodes by increasing the thickness of the coatings. However, this also decreases the mechanical stability of the coating. The significance of these results lies in the demonstration that PEDOT electrodes which show a lower performance when considering cyclic voltammetry actually perform a lot better when considering zero voltage bias current pulses as is the norm in actual applications.

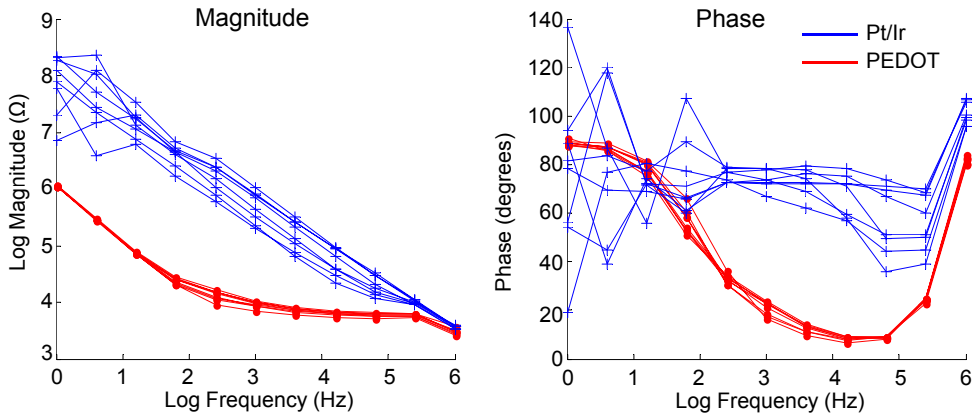

Figure 2.9: Impedance spectra of PEDOT coated probes and bare PtIr probes. Magnitude of impedance of PEDOT coated probes (measured at 1kHz) was 17x smaller than bare Pt/Ir probes.

2.2.3 *In Vivo* Testing

Many scientific and prosthetic applications require microelectrodes to be implanted in subjects for many months. Chronic implantation of electrodes leads to gliosis and scar formation around the electrodes [55]. Therefore, it is important to test whether the improvements measured *in vitro* are preserved *in vivo* under chronic conditions. We did so by implanting arrays of 16 PtIr microelectrodes (25μm diameter) in three adult female Sprague Dawley rats (250-300g) where every alternate electrode was coated with PEDOT. The surgical techniques used are described elsewhere [56].

As a first measure of electrode performance, we measured the impedance of implanted electrode arrays for three weeks post-implantation. Figure 2.9 shows the magnitude and phase of the impedance spectra on PEDOT-coated sites and bare sites of the electrode array measured in saline prior to implantation. The magnitude of impedance at 1kHz is a commonly used metric and the average electrode impedance measured on PEDOT sites was 17 times smaller than PtIr sites at 1kHz prior to implantation. The variability between sites on the PEDOT-coated electrodes was significantly smaller in terms of the magnitude and phase angle of the impedance. Interestingly, PEDOT coated probes show a significantly more resistive behavior over the frequencies of interest than PtIr electrodes indicating that a significant fraction of the charge injection might be occurring through reversible faradaic reactions at these frequencies. The exact nature of the charge injection process in PEDOT at high current densities has not been fully explored.

Figure 2.10 shows impedances measured at 1kHz over 2 weeks post-implantation. Similar to previous reports [52], we saw a gradual increase in electrode impedance over days 1-9

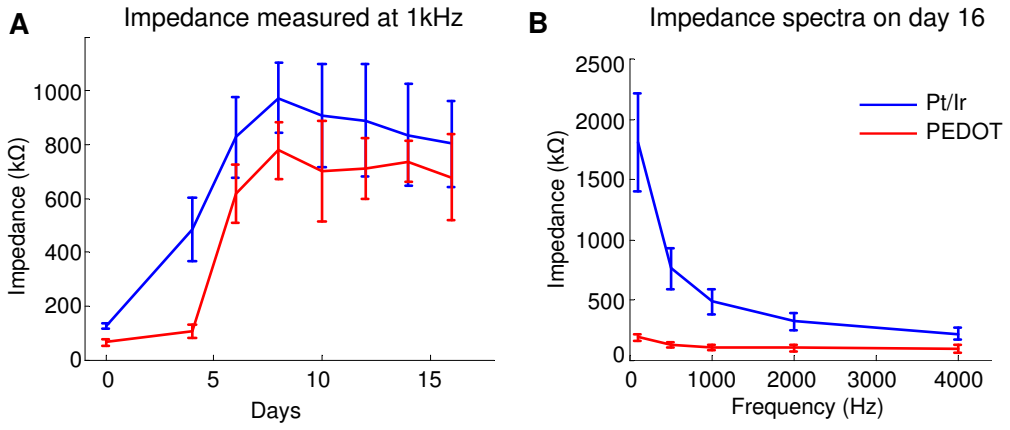

Figure 2.10: (A) Average magnitude of impedance recorded over two weeks after implantation (B) Impedance spectra measured *in vivo* on day 6 post implantation. PEDOT electrodes show significantly lower impedance especially at low frequencies

post-surgery followed by a slow decrease. This trend is believed to be associated with glial scar formation around the electrodes after implantation. However, the PEDOT-coated electrodes consistently displayed impedances $\approx$200kΩ lower. Impedance spectra measured on day 6 post-surgery showed that PEDOT electrodes perform significantly better at lower frequencies, which may be significant for recording local field potentials as well as stimulation experiments.

Neural signals were recorded from rats using a multichannel neural recording system (Plexon Inc., Dallas, TX). Figure 2.11A shows spikes recorded on PEDOT and bare PtIr electrodes a week after surgery, demonstrating that PEDOT-coated electrodes can record neural activity equally well as uncoated PtIr electrodes. For a quantitative measure of signal strength, we measured the average power spectral density on PEDOT and PtIr electrodes during surgery (Figure 2.11B) with rats under high isoflurane (2% vol). Isoflurane significantly reduces neural activity in the cortex, so the resultant spectrum is largely caused by thermal noise. The recorded power on PEDOT electrodes in this condition was 7.4dB lower. Data measured two weeks after implantation showed a similar trend with an improvement of 5dB. Taken together, these results demonstrate that the signal strength on PEDOT electrodes remains identical to PtIr electrodes with lowering of noise power leading to better signal to noise ratio.

We believe that the significant advantage of using PEDOT-coated probes is in microstimulation applications. The lowered impedance of PEDOT-coated electrodes is promising for this application. For a more accurate test of performance, we applied biphasic current pulses *in vivo* and measured the resultant voltage transients. The average maximum negative voltage recorded on the array of PEDOT-coated electrodes upon stimulation with 20μA 200μs

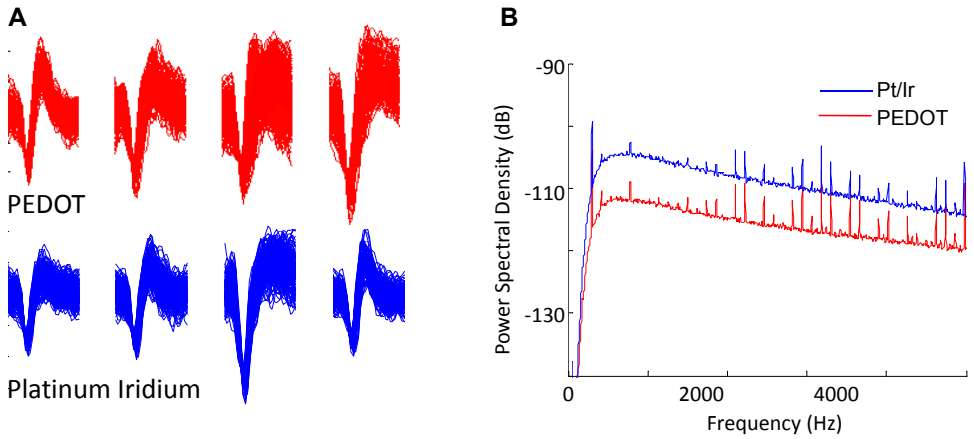

Figure 2.11: (A) 100 overlaid action potential waveforms (0.8ms each) recorded on different electrodes of the same array on one rat. No difference was observed in number or magnitude of neuronal action potentials recorded on PEDOT or bare PtIr electrodes. (B) Average power spectral density measured on PEDOT and PtIr electrodes during surgery under high isoflurane. Isoflurane significantly reduces neural activity in the cortex, so resultant spectrum is largely caused by thermal noise.

pulses was 0.8V smaller than that recorded on PtIr electrodes (Figure 2.12). Furthermore, the average residual voltage 200μs after a 20μA biphasic pulse was measured to be PEDOT = 218mV and PtIr = 568mV. These measurements demonstrate that the improvements seen *in vitro* are preserved in chronic conditions. The increase in the voltage transient compared to Figure 2.8B is likely caused by an increase in access resistance due to glial scar formation around the electrodes and the nature of the *in vivo* electrolyte [57]. It is difficult to accurately calculate this access resistance *in vivo*, hence no measurements of charge injection limit were made.

It should be noted that a reduced voltage transient caused due to stimulation will also serve to reduce the stimulation artifact caused in the neural recording system. Thus PEDOT coated electrodes further help to reduce the stimulation artifact and allow better recording of the neural response to stimulation.

2.2.4 Summary

We have developed tools to simultaneously stimulate and record neurons in awake behaving animals [58]. Similar tools can be used for applications like deep brain stimulation, epilepsy research etc where groups are studying the neural response to stimulation. Further, we demonstrate that PEDOT-coated microelectrodes have superior performance compared to PtIr electrodes and IrOx-coated electrodes for recording and stimulation applications [59].

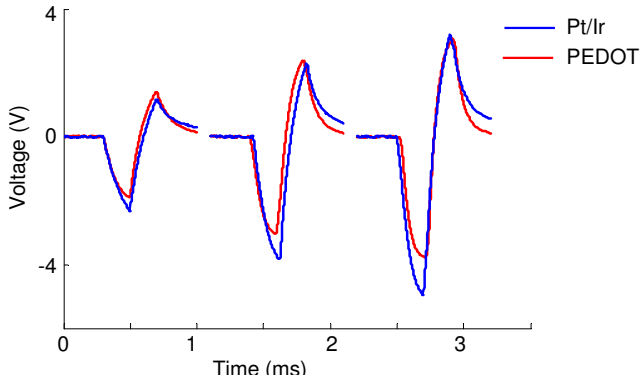

Figure 2.12: Average voltage transients recorded on PEDOT and PtIr electrodes two weeks after implantation on application of biphasic current pulses of different magnitudes. The PEDOT electrodes show a smaller voltage transient and a smaller residual voltage 200μs after the end of the pulse.

The experiments in this manuscript were performed on PtIr microwire arrays (Plexon Inc., Dallas, TX), but the conclusions are also valid for MEMS based implantable neural recording/stimulating arrays, like the Michigan probe and the Utah array [21, 9]. Future work in this direction would be to further characterize the performance of PEDOT coated electrodes *in vivo* over extended periods. It should be noted that the effectiveness of any coating, like PEDOT or IrOx, is limited by the significant increase in impedance around the electrodes after chronic implantation, presumably due to glial scar formation. It is therefore essential that biological approaches be pursued in parallel with material advances to develop ideal microelectrode arrays. One of the advantages of using PEDOT is the possibility of surface modification with physiologically active species in the future to enhance the biocompatibility and functionality of such electrodes.

Since we wish to investigate cortical microstimulation in awake behaving rodents, the next requirement was to develop techniques to monitor the behavior of rodents. In the next chapter, we discuss two technologies developed to monitor the behavior of awake rodents; namely wireless accelerometers to monitor gross behavior and a real-time video based whisker tracking system to track whisking.

Chapter 3

Tracking Rodent Behavior

We wished to study cortical microstimulation in awake behaving rodents, therefore it was essential to accurately track rodent behavior. To track the movements and gross behavior of freely moving rats, we designed a wireless inertial sensor sensor which could be carried by rodents (Section 3.1). This provided us with information of the general activity of the animal as well as timing of movement initiation. Movement initiation is of interest due to its relevance to behavioral training as well as disease models of Parkinsons. Since we implant electrode arrays in the barrel cortex of rats (which receive inputs from the whisker system), we decided to also study the whisking behavior of rats. To do so, we designed a real-time whisker tracking system (Section 3.2) based on high-speed video recordings of restrained rats. This system proved crucial for the neuroscience results described in the following chapters.

3.1 Wireless Inertial Sensors

Many systems have been proposed to track the behavior of freely roaming rodents. One commonly used technique is video surveillance which has the important advantage of being non-intrusive [60, 61]. Algorithms have been developed for automatic behavior analysis from video data but these algorithms typically do not detect subtle movements or the precise instant of movement initiation. Moreover, many of these algorithms fare poorly when multiple animals are present in the same cage. Some other approaches developed include the use of piezo or pressure sensors on the floor of the cage and the use of Continuous-Wave Doppler radar (CWDR) signals to discriminate animal behaviors [62]. Both technologies lack precision and fare poorly in the presence of multiple animals in a cage.

The last few years has seen an explosion in sensor networks research with the development of many different hardware and software platforms; see for example the proceedings of SenSys, 2003 - present. Concurrently, advances in Micro Electro Mechanical Systems (MEMS) technologies have enabled the development of packaged low power accelerometers and other

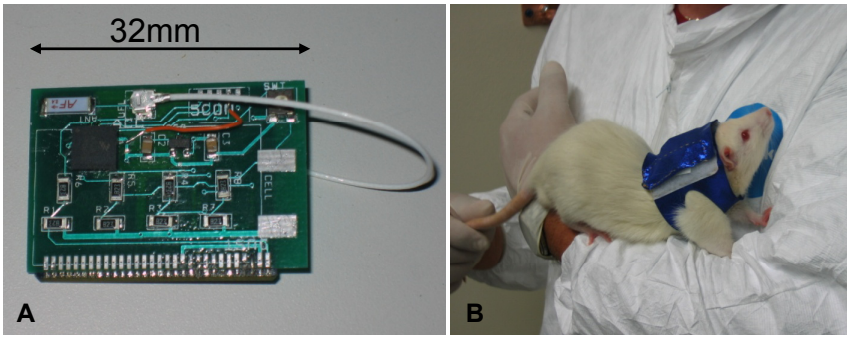

Figure 3.1: Wireless inertial sensor. (A) The 32mm x 25mm wireless accelerometer prior to packaging (B) The wireless sensor being tested on adult rats.

inertial sensors. In recent years, significant effort has been expended into making wireless inertial sensors small enough to enable biological applications. For example, Hitachi has demonstrated a wristband sensor node which can record the motion and pulse of a person and transmit it wirelessly to a base station [63]. This device measures 6cm x 4cm and weighs 50grams. Researchers have attempted analysis of animal behavior using inertial sensors in the past but these have been restricted to large systems unsuitable for small animals and lacking wireless telemetry capabilities [64, 65]. Ideally, the sensor used for small animals such as rats or mice would be less than $1cm^3$ in size and weigh less than 5grams. Wireless sensors at this size scale have also been demonstrated in recent years [66].

As a first generation device, we built a wireless accelerometer which was 3cm x 2.5cm in size and weighed 10grams. This sensor was small enough to be tested on rats. Three axes acceleration data was recorded from rats and wirelessly transmitted to a base station using this system. This data was used to record and measure the activity of the animal over time. Multiple animals and hence multiple transmitters in close proximity was not an issue so long as appropriate protocols are used for data transmission. Further, we demonstrated that various behaviors of the animal such as standing, eating and grooming could be extracted from this acceleration data using neural network based algorithms.

3.1.1 Hardware

As a wireless frontend, a SmartMesh mote from Dust Networks which contains a radio transceiver, a microcontroller, analog to digital converters etc. on a single board was used. This board controlled the sampling of data from the sensors, providing accurate timestamps and transmission of data over the 2.4GHz frequency band. It used frequency-hopping spread-spectrum communication for interference immunity and duty cycled components like the transceiver when not in use to extend battery life.

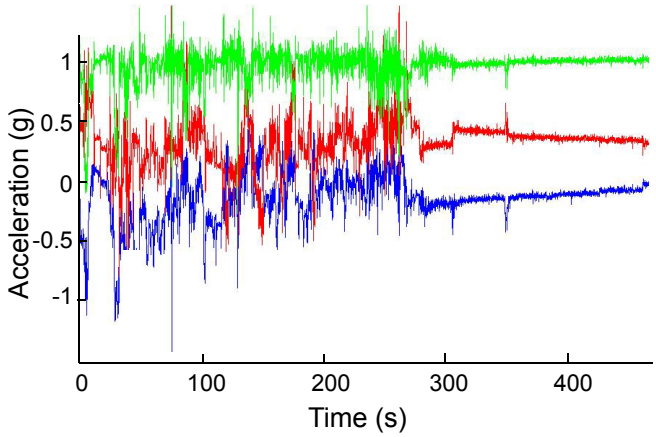

Figure 3.2: Three axes acceleration data as recorded from a rat moving freely in a cage show that the rat was initially active and then fell asleep.

A sensor interface was developed as a separate board which could be attached to the SmartMesh mote. This sensor board contained a three axis accelerometer (MMA7260Q, Freescale Semiconductor), a chip antenna (Rainsun), a 150mAh rechargeable lithium polymer battery (Roomflight), voltage regulator, switch and passive components. The completed wireless sensor weighed 10.2grams and measured 32mm x 25mm and is shown in Figure 3.1A. The accelerometer could be sampled at 36samples/s using our protocol. However this number can be increased in the future using modifications to the software. At this data rate, the transceiver used approximately 600μA and the accelerometer approximately 500μA which gave the device a lifetime of over 5 days.

The sensor was tested on adult Sprague Dawley rats which weighed approximately 300g and were 1 foot long. The sensor was mounted using a specially designed vest or a rat jacket from Harvard Apparatus and is shown in Figure 3.1B. This jacket was often used during behavioral training of rats and the rat comfortably moved around the cage with the sensor. It was also verified that multiple animals in a cage with sensors did not disturb each other's jackets. More long term testing is required to verify that the presence of the sensor does not significantly alter the behavior or stress level of the animal.

The acceleration sensors measure both acceleration caused by movements of the animal and gravitational acceleration (g). Figure 3.2 shows three axes acceleration data collected from a rat freely moving in a cage. Typically one axis showed a mean of 1g due to gravity and the other two axes showed around 0g as we would expect. During the period of this recording, the rat was initially moving around the cage and then fell asleep and that is clearly seen from the acceleration data. Hence the recorded acceleration data can be used to obtain some quantitative measure of 'activity' of the animal and also to monitor its sleep patterns. Clinical relevance of these two metrics is expected to be high and needs to be studied over longer

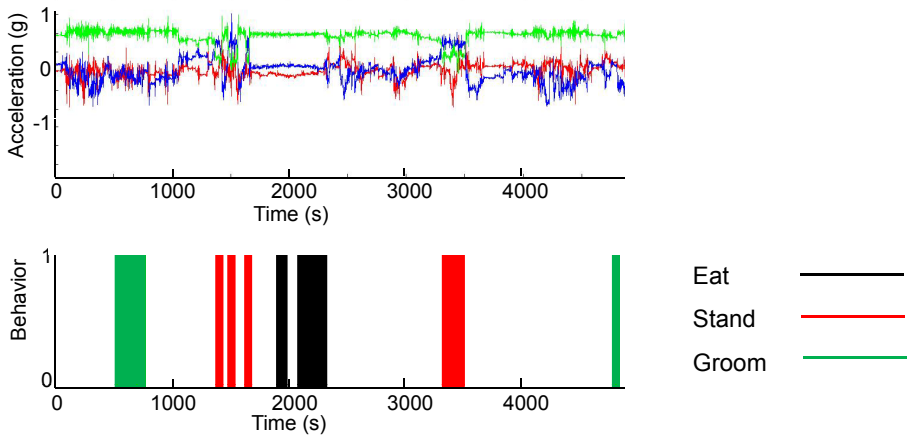

Figure 3.3: Behavior of the rat as recorded manually along with simultaneous recording of acceleration data.

trials. We also wanted to extract periods of relevant behaviors from this acceleration data and this was an interesting pattern recognition problem.

3.1.2 Behavior Recognition

The behaviors which we decided to categorize were standing, eating and grooming. Standing is when the animal stands on its rear legs, eating is when the animal eats a small piece of food and grooming is when the animal uses its forearms to clean itself. Grooming is a behavior of particular interest since rats groom themselves to keep clean and tend not to do so when unhealthy. Hence length of time spent grooming each day could be a good indicator of well being of the animal. These three behaviors were manually recorded in order to train the algorithms. Figure 3.3 shows three axes acceleration as recorded from a rat along with recordings of its behaviors.

The acceleration data used for behavior recognition was obtained using a wired version of the same accelerometer to aid in accurate time-stamping of data with respect to behavioral and neural data. 36 gauge wires attached to a multichannel commutator (Plexon Inc, Dallas Tx) were used to allow the animal free movement in the cage. The acceleration data was sampled at 20samples/sec and preprocessed depending on the behavior being detected. Eating and grooming performed best with data high-pass filtered at 2Hz while standing algorithms performed best using raw data.

To analyze the data and recognize patterns of behavior, we used a supervised learning algorithm. A 2 layer neural network with 5 hidden units was chosen for this purpose. Each unit performs the computation

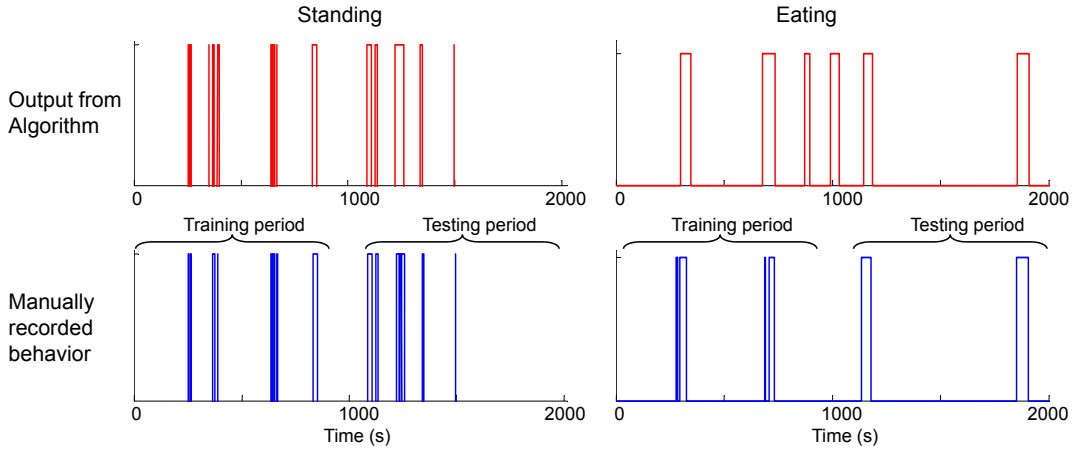

Figure 3.4: Neural network recognition of standing and eating.

$$y_i = \sigma \cdot \left(\sum_j W_{ij} \cdot x_j \right)$$

where y_i is the output of the unit, x_j are the inputs to the unit, W_{ij} are the weights assigned to individual inputs and σ is a nonlinear (sigmoidal) function.

It is essential to provide the neural network with information regarding the frequency content of the acceleration data. This can either be done by performing a sliding window Fourier transform on the data and feeding this as the input or by feeding data for the current time instant as well as 'n' previous time instants. The second approach showed better performance and hence was chosen. The recorded behavior served as the desired answer for the neural network during the training period. The network was trained using a standard back-propagation algorithm. Other possible algorithms for this purpose include Independent component analysis (ICA), Support vector machines (SVM) and the K nearest neighbor algorithm. It is still an open question as to which algorithm is optimally suited to analyzing data from such inertial sensors [67].

Post processing involved low pass filtering and thresholding the neural network output and the results are shown in Figure 3.4. In this figure, the first part of the data was used to train the algorithm and the second part of the data was used to test the algorithm. The algorithm achieved 97% accuracy in recognition of periods of standing and 93% accuracy in periods of eating. This is a typical value of the performance of the algorithm over multiple trials. The performance in grooming is similar to that in eating.

The performance of the algorithm was worse if it was trained on data from one day and its performance tested on another day's data. One reason for this problem was that the sensor was mounted in a slightly different way each time it was taken off and put back on. This caused a rotation in space and 1g was distributed among the three axes in a different way. One method to reduce this problem would be to mount the sensor in an identical fashion on the animal everyday or calibrate the sensor during characteristic movements. This problem

was solved in later experiments where the wired accelerometer was firmly attached to the neural recording headstage, thus ensuring that it was mounted identically every day.

3.1.3 Applications in Behavioral Neuroscience

A potential application of this technology is to measure movement initiation of rodents. We would like to measure movement initiation to measure the reaction times of rodents being trained on a behavioral task. Operant conditioning of rodents is typically performed in a test chamber with the animal performing tasks such as a forelimb reach for food or activating an infrared sensor within a nose poke. These methods have some inherent limitations since they tend to record only part of the behavior of the animal. For example, it has been shown that reach-related activity in shoulder muscles and shoulder movement can precede attainment of the goal of the movement (attaining food) by 400 ms or more [68]. Such analysis is of particular importance for studies of motor areas of the brain, if it is desired to assign neural activity to the pre-motor and motor phases of the task. Researchers typically solve this problem by designing more complex tasks or by using other techniques such as subcutaneous Electromyogram (EMG) recordings [68] or frame by frame video monitoring to accurately measure the behavior of the animal. Our goal was to develop a non-invasive rodent monitoring system to help record rodent behavior during the collection of electrophysiological data that avoids experimenter intervention and bias. Measuring the acceleration of the animal during the performance of a task or during free behavior provided us with such a system.

Figure 3.5 shows an example recording of acceleration data from a rat while it performed a variable delay stimulus detection task based on a tone. The rat was trained to react to a tone and poke its nose in a nose poke within 3 seconds after the tone. The reaction time of the rat was measured using the time the rat entered the nose poke, which provides an overestimate of the reaction time. A more accurate estimate was obtained using the accelerometer data which showed the instant when the rat started moving after hearing the tone. Thus we can use wireless inertial sensors to provide an accurate estimate of the reaction time of rats.

Next generation accelerometers were also tested on mice (Figure 3.6). These sensors face a more stringent weight and size specification due to the small size of mice. The wired version of these sensors were built to interface directly with standard neuroscience recording setups so would be transparent from the point of view of the investigator. The wireless version was built using the DN2400 2.4GHz Mote-on-Chip from Dust Inc interfaced to a custom PCB. This wireless sensor faced some implementation issues due to difficulties in soldering to all the chips on the small package. However, there is no fundamental reason why a completely functional wireless accelerometer is not realizable in a cm^3 package using off-the-shelf components. This technology has now been adopted by other neuroscience labs and is being used to study movement initiation in Parkinson models in mice.

In addition to tracking the behavioral states of freely roaming rodents, we wished to measure the whisking behavior of rats. This is very difficult in freely roaming animals (though see [69]) so we chose to study whisking in head-restrained rats using a real-time whisker tracker.

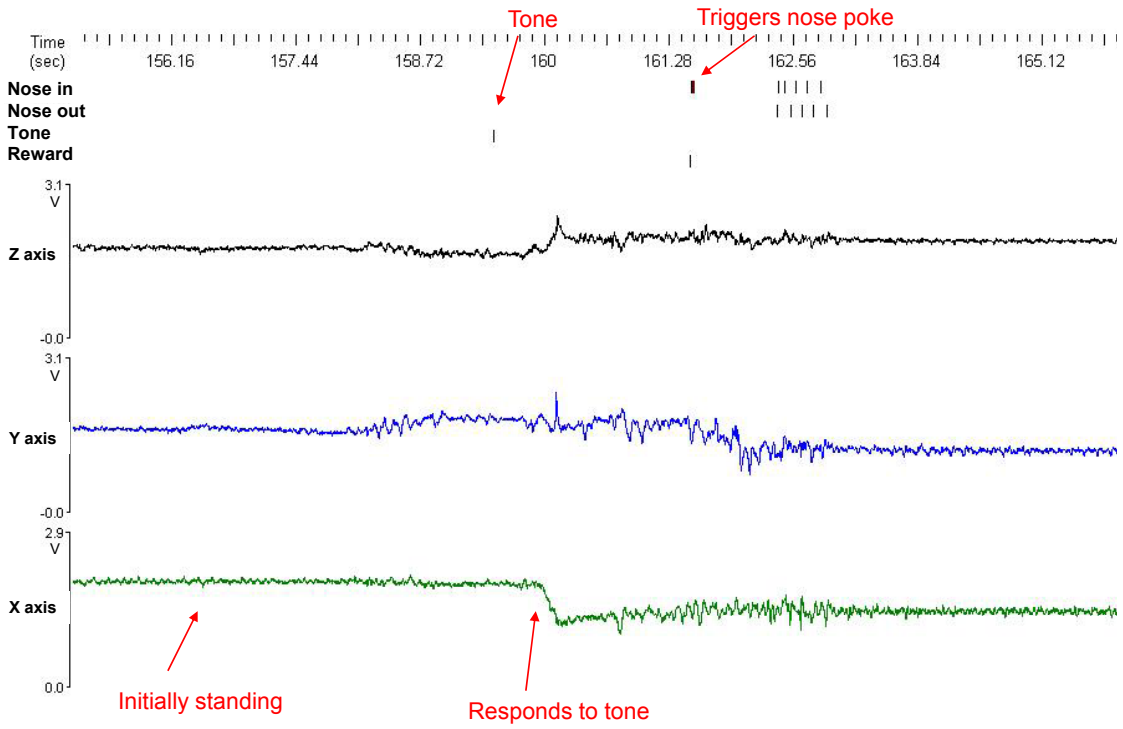

Figure 3.5: Recording of movement initiation during an operant conditioning task provides information on reaction time of the rat.

3.2 Whisker Tracking

Rats use their vibrissa (whisker) system to actively sense the world around them since they have a poorly developed visual system. By using their whiskers, they can build spatial representations of their environment, locate objects and discriminate between different textures. They do so by actively moving their whiskers in concert at 8-12Hz. Since we study the effects of microstimulation in the barrel cortex, we decided that it might be useful to track the whiskers of the rat. Moreover, we figured that it might be useful to trigger microstimulation in real-time based on the movements of the whiskers therefore real-time tracking would be beneficial.

Since rats whisk at 10Hz, we designed our system to track whiskers in real-time using video recorded at 100 frames a second. Rat whisker tracking using high-speed video has been demonstrated previously [70] but has never been implemented in real-time. We found that rats are more amenable to be body restrained than to be head restrained. Hence rats in our experiment were restrained using a harness but were capable of moving their heads to a small degree. An EC-640C camera (Prosilica, Burnaby, B.C., Canada) was placed above the rat facing down to capture images of the rat's head and whiskers. The whisker was tagged by a light self-adhesive foam marker (weather proofing foam from Ace Hardware, Berkeley, CA) as shown in Figure 3.7A.

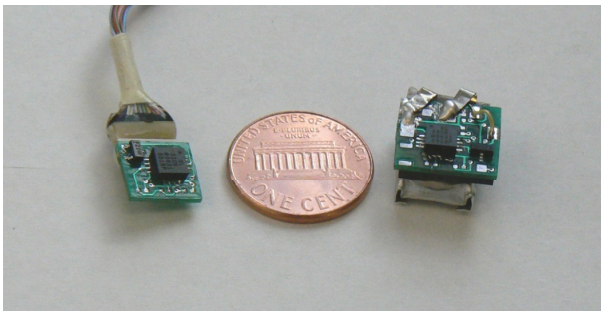

Figure 3.6: Wireless and wired accelerometers for measuring activity of mice

The whisker tracking system ran on a high-performance Dell Dimension 690 machine with the following specifications: Two dual core Xeon 3Ghz processor, 3GB of RAM, and a SATA 3.0GB/s 7200RPM hard drive. It received input from the camera which provides 100 frames per second (fps) at a 659x498 resolution over firewire. The tracking software was implemented in C++ and used Intel's Open Computer Vision Library (OpenCV) in conjunction with the Prosilica Firewire Software Development Kit. A large fraction of the code for this tracking sofware was written by Ken Elkabany (B.S. EECS, UC Berkeley) under my guidance.

Real-time video tracking has been implemented by a number of researchers to track people and objects in video recorded at 10-30fps [71]. However, our application demands real-time tracking at 100fps which is a significant challenge since it necessitates that each frame be processed in under 10ms. The time taken to process a complete frame (659x498 pixels) and search for pixels meeting a color threshold is (mean $\pm$ SD) 11.3ms $\pm$ 5.2ms clearly indicating that a more intelligent approach was required. Hence we adopted a number of techniques used in video tracking and optimized them for our fast application. The stringent processing-time specification imposed by 100fps tracking necessitates the use of computationally minimal and memory efficient algorithms. Our tracking algorithm was successful in spite of these constraints because we had the advantage of a specified white background and a clearly defined marker.

3.2.1 Region of Interest

A Region of Interest (ROI) is the portion of an image frame that is scanned for markers and can be initialized by the experimenter at the beginning of the trial. OpenCV's Kalman filter implementation is used to efficiently estimate the future locations of the whisker marker. The ROI is moved after each processed frame to the estimated marker location. The choice of model used to estimate future marker locations significantly affects the performance of the estimator hence we spent some time optimizing the model of rat whisker motion.

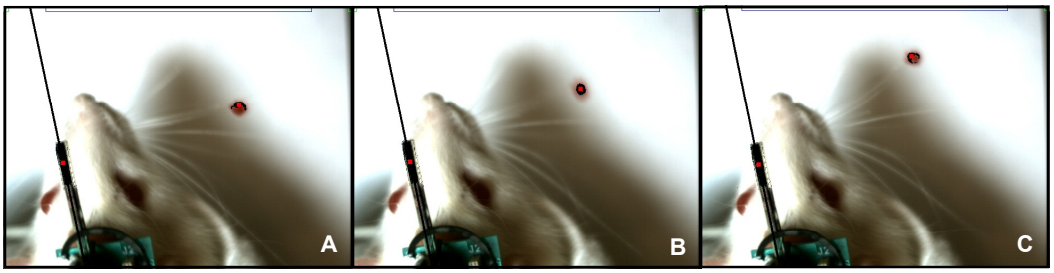

Figure 3.7: Whisker tracking system in action. A, B and C show three frames captured 20ms apart showing the rat whisking and the head angle, head position and whisker position being tracked in real time with a black line and small red dots.

3.2.2 Modeling Whisker Motion

The prediction of whisker positions using a Kalman filter requires a good model of rat whisking. To build a good model, a stream of data from a tracked whisker is required - for which we require a working Kalman filter predictor. This necessitates an iterative solution to the problem as mentioned in [72]. The most inexpensive estimate of the whisker location is to simply center the ROI at the previous location of the marker as in equation (1). A more intelligent approach is to use a Kalman filter with a simple model assuming constant linear velocity of the marker as in equation (2). We used such a simple model to record data of whisking.

Model 1:

$$\hat{x}(k) = x(k-1) \tag{3.1}$$

$$\hat{x}(k) = x(k-1) + \dot{x}(k-1) \tag{3.2}$$

Using recorded data on whisker motion, we then optimized parameters for a linear tracking algorithm by minimizing the square error of the estimate to arrive at

Model 2:

$$\hat{x}(k) = 1.00x(k-1) + 0.75\dot{x}(k-1) + 0.35\ddot{x}(k-1) \tag{3.3}$$

Each of these models can be incorporated into a standard Kalman filter formulation

$$\mathbf{x}(k) = \mathbf{A} \cdot \mathbf{x}(k-1) + \mathbf{w}(k-1) \tag{3.4}$$

$$\mathbf{z}(k) = \mathbf{H}(k) \cdot \mathbf{x}(k) + \mathbf{v}(k) \tag{3.5}$$

where **x** is composed of the x and y position of the marker and its derivatives, **A** is the transition matrix, and **H** is the measurement matrix. $\mathbf{w}(k-1)$ and $\mathbf{v}(k-1)$ are zero-mean normal noise distributions in the process and measurement model respectively. We also modeled the system using an oscillatory tracking algorithm based on [73] which takes into account the fact that the whisker oscillation is often centered between 8- 10Hz.

Model 3:

$$\hat{x}(k) = b_0 + b_1 \cos(\omega \cdot t + \varphi) \tag{3.6}$$

Incorporating this model into a Kalman filter requires that equation 3.6 be linearized as

$$\hat{x}(k) = b_0 + b_1 \cos(\omega \cdot t)\cos(\varphi) - b_1 \sin(\omega \cdot t)\sin(\varphi) \tag{3.7}$$

And the Kalman filter is implemented as

$$\mathbf{x} = \begin{bmatrix} b_0 \\ b_1 \cos(\omega \cdot \varphi) \\ b_1 \sin(\omega \cdot \varphi) \end{bmatrix} \tag{3.8}$$

We found that the oscillatory model performs well during periods of sustained oscillations but is prone to large errors during sudden changes in behavior. The performance of the three models are shown in Figures 3.8(B, D). The models were tested on a new dataset of recorded whisker trajectories using a Kalman filter implemented in MATLAB (Mathworks, Natick, MA) after being optimized on training data. The oscillatory model had a higher standard deviation of error compared to the optimized linear model as well as having larger number of errors crossing a particular threshold for size of ROI.

Hence we implemented the optimized linear tracking algorithm (Model 2) as the real-time Kalman filter.

3.2.3 Model-based Tracking

Model-based tracking is a technique commonly used to track objects and people in real-time tracking applications. It consists of an *a priori* model that defines the tracked object and the background. In our usage, the model defines (i) the shape and size of the tracked object and background (ii) the areas in the frame where the points of interest are most likely to reside and (iii) blacklisted areas where tracked objects cannot enter due to the constraints of the experiment. If a whisker is tracked into a blacklisted area, the current whisker position is invalidated and the search is restarted with the entire non-blacklisted frame as the ROI. This technique helps us reduce false positive marker identifications and errors due to occlusion.

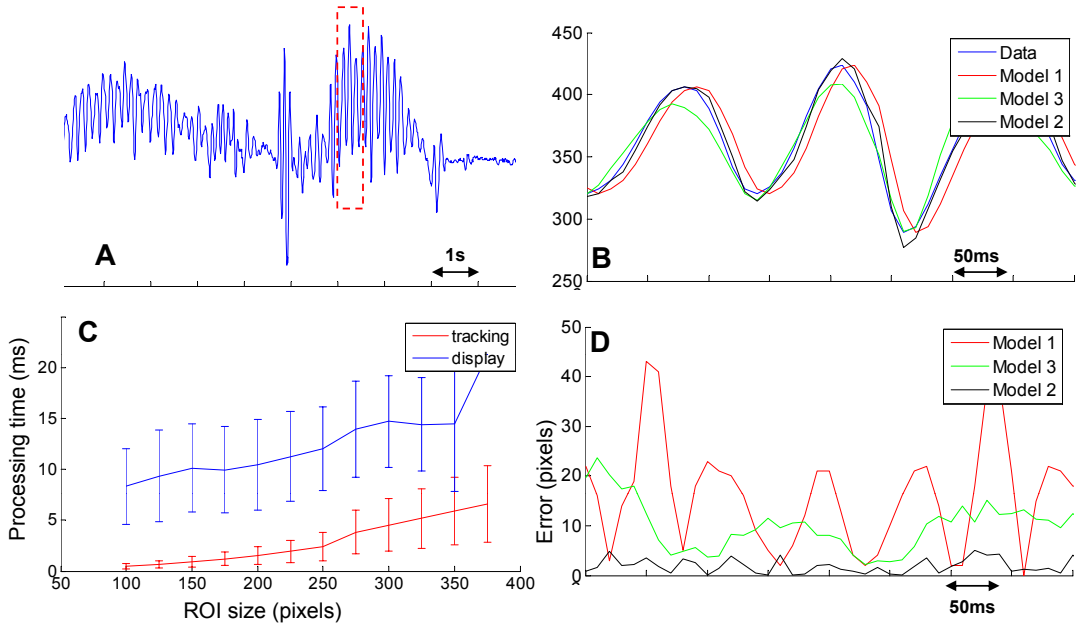

Figure 3.8: Real-time whisker tracking system. (A) 10s data showing whisker trajectories of a rat which was used to test Kalman filters. Snippet shown in further figures in highlighted in red (B) Estimation of whisker trajectories by Kalman filters based on equations 1, 3 and 6. (C) Processing time of our algorithm as a function of ROI size. (D) Errors in estimation by the three models.

3.2.4 Color Estimation

Color filters are used to judge whether a pixel is part of the head or whisker marker. Each marker has an expected color and the location of the marker is determined by filtering for the expected colors and finding the center of mass of the activated pixels. To account for color changes caused by shadows and motion blur, thresholds for the color filter are updated based on previous frames. We attempted transforming colors to the HSV scheme to minimize lighting effects but discovered that the conversion required 8.3 ± 4.8ms per frame and was hence not suitable for 100fps implementation.

The time taken to identify the marker is a strong function of the size of the ROI as shown in Figure 3.8C with the blue curve showing the processing times for frames which were displayed and the red curve showing the processing time for frames which were not. We typically display 1 in every 10 frames to allow the user to monitor the performance of the tracking algorithm in real-time. We provide a 2 frame buffer to ensure that all processing is completed within a lag of 20ms. It should be noted that a larger ROI leads to a larger number of frames being dropped due to large processing times but leads to a smaller number of errors from the Kalman filter.

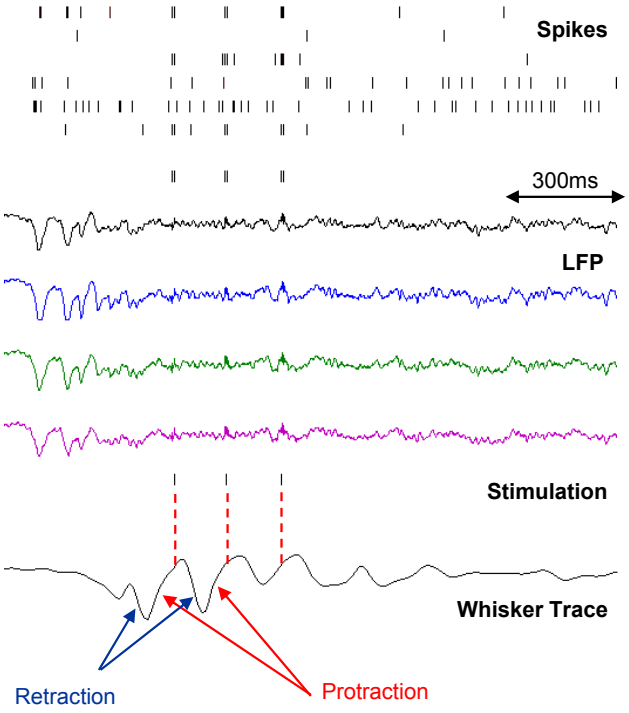

Figure 3.9: Neural responses to microstimulation in the form of spikes and LFP are shown along with y-coordinate of whisker trace. Real-time triggering of ICMS during the protraction phase of whisking allows us to study behavioral modulation of neural responses to ICMS.

Given an ROI size of 100x100 pixels, the processing time of our algorithm is 2.3 ± 4.0ms. Figures 3.7 A, B and C show three non-consecutive frames with the whisker and head angle being tracked in real time. The whisker phase during protraction in Figure 3.7C crosses a user defined threshold, triggering the stimulation system. Thus our whisker tracking system is capable of triggering ICMS in real-time based on the whisking of the animal.

Figure 3.9 demonstrates the working of the entire closed-loop stimulation and recording system. A whisker of a freely whisking rat is tracked in real-time and shows sinusoidal 8-10Hz oscillations during active whisking. ICMS in barrel cortex is triggered towards the end of the protraction phase of whisking. Neural responses to ICMS in the form of spikes and LFP are recorded with the help of the artifact reduction system. This data can be used to study behavioral modulation of neural responses to microstimulation.

3.2.5 Summary

This chapter demonstrates the development of technologies to track rodent behavior using wireless inertial sensors [74] and using high speed real-time video tracking [58]. Small inertial sensors are now being explored by a number of groups studying topics as diverse as Parkinsonian models of rats, beetle flight dynamics and mouse thermoregulation. The real-time whisker tracking system proved to be essential to place the recorded neural data into behavioral context as demonstrated in the next chapter.

Chapter 4

Behavioral Modulation of Evoked Oscillations

The neural response to cortical microstimulation has been extensively studied in anesthetized and awake animals [2]. The response typically consists of an initial burst of spikes followed by a prolonged period (approximately 100ms) of reduced neural activity. This is sometimes followed by a rebound excitation before returning to the baseline firing rate [40]. However, little is known about how this neural response to microstimulation is modulated by the behavior of the animal. The only previous studies which characterized such modulation looked at the ability of microstimulation in visual pathways to elicit a saccade and its modulation by active fixation [75]. Therefore, we explore the neural response to microstimulation in the rat barrel cortex and its modulation by active whisking.

Cortical microstimulation in sensory areas is known to elicit an oscillatory response in both anesthetized and awake animals [76, 77]. These oscillations are similar to the tone-evoked oscillations observed in the auditory system and their thalamic origin has been well established [77, 78]. While the occurrence of stimulus-evoked oscillations in anesthetized animals has been well documented, experiments on awake subjects have yielded conflicting results [79]. To shed light on the functional significance of these oscillations, it is essential to study their occurrence and behavioral modulation in alert, awake animals.

Modulation of afferent sensory transmission by active movement is a well known phenomenon [80]. The rodent vibrissa system provides an excellent model to study this modulation. During quiet immobility, whisker deflections evoke large-amplitude, highly distributed cortical sensory responses. Whereas, during active whisking, passive whisker deflections evoke small-amplitude localized sensory responses. Hence sensory responses in the rat whisker system are thought to be dynamically modulated by motor behavior.

It is believed that this may function as a sensitive detection system (a wake-up call), alerting the animal to unexpected sensory inputs [81]. We show that this effect can be recapitulated by replacing sensory stimulation with cortical microstimulation. The neural response to mi-

crostimulation can be considered to be the impulse response function of the thalamocortical loop [82]. Thus studying microstimulation evoked neural responses presents an excellent method to explore modulation of the thalamocortical loop by behavioral state.

Further, we explore whether cortical microstimulation evoked oscillations in the rat somatosensory system are also modulated by motor behavior. Similar modulation to that observed in sensory responses would suggest that both phenomena are brought about by common or related underlying causes. It would also provide an experimental link between stimulus-evoked oscillations and modulation of afferent somatosensory circuits by motor behavior.

4.1 Material and Methods

4.1.1 Animals

Five adult female Sprague-Dawley rats weighing 200-300g were used in this study. They were initially handled for 1 week and trained to sit calmly while restrained in a cloth bag and body restrained in a semi-cylindrical tube. Once rats learned to sit quietly, they were implanted with microwire arrays.

4.1.2 Surgical Procedure

Microwire arrays with two 35μm diameter Platinum/Iridium stimulating electrodes (CD Technologies, Durham NC) and 16 tungsten recording electrodes (35μm diameter , 8x2 array) were implanted in barrel cortex. Rats were anesthetized with ketamine-xylazine supplemented with isoflurane gas anesthesia. After a craniotomy and durotomy, the electrode array was stereotactically inserted into the infragranular layer of the primary somatosensory barrel field (S1bf) in one hemisphere. Stereotaxic coordinates relative to bregma were used to center the arrays in S1bf [anteroposterior (AP), -3.0mm; mediolateral (ML), +5.5mm; dorsoventral (DV), -1.2mm]. The craniotomy was sealed with cyanoacrylate and the array was firmly attached to the skull using dental acrylic. Intraoperative recording of multiunit activity and post-operative receptive field mapping, using the MAP system (Plexon Inc, Dallas, TX), were used to ensure that arrays were located in barrel cortex. Placement of electrodes in the infragranular layer was verified by comparing the polarity of observed spontaneous oscillations to known depth profiles of oscillations [83].

4.1.3 Cortical Microstimulation

Biphasic stimulating pulses were delivered through bipolar 200-500kΩ platinum/iridium microelectrodes (AM Systems pulse generator and stimulus isolation unit, Sequim, WA). Pulse

length was set to 250μs and the stimulation typically consisted of two pulses of 10-20μA separated by 3ms. Microstimulation was delivered while rats were restrained and the interval between pulses was varied in a pseudo-random manner between 1-5seconds.

4.1.4 Correlation Analysis

We defined the power of the evoked neural oscillation as the power in the 10-20Hz band of the local field potential (LFP) 100-500ms post-microstimulation. The strength of whisking was defined as the power in the 5-20Hz band of the recorded whisker trace 0-100ms pre-stimulation. The correlation between these two metrics was defined as the correlation between the power of the evoked oscillation and the strength of whisking.

It is conceivable that state dependent evoked responses could occur if rats were 'quiet' for the first half of the trials and awake and 'whisking' for the next half. To demonstrate that rats showed rapid transitions between behavioral states, we calculated the correlation between evoked neural oscillations and whisking strength at some time lag (t secs, t$<$1). If behavioral states changed on the order of tens of seconds, one would expect that whisking strength 't' secs prior to stimulation would be highly correlated to the strength of stimulus evoked oscillations. However, if behavioral states changed rapidly, one would expect that this correlation would drop off rapidly with increasing magnitude of 't'.

4.2 Results

4.2.1 Behavioral Modulation

Neural responses to cortical microstimulation have been studied by several researchers (reviewed in [2]). Cortical microstimulation typically triggers nearby neurons to fire spikes immediately after stimulation. This is followed by a prolonged period ($\approx$100ms) of decreased firing rate (mediated by inhibitory circuits [84]) followed by a short rebound excitation and return to baseline firing rate [40]. We observed a similar neural response to microstimulation in awake, freely roaming rats [58]. However we also noticed a fraction of trials where this response was followed by oscillations phase-locked to the stimulation.

To investigate whether the variability in evoked oscillations was related to motor activity in the whisker system, we tracked the position of a single whisker in awake rats while microstimulating at random intervals (1-5s). The neural response to microstimulation when rats were actively whisking showed a small initial inhibition and no subsequent oscillations (Figure 4.1A). In contrast, we found that when rats were quietly immobile, the LFP response to microstimulation consisted of $\approx$15Hz oscillations following the initial prolonged inhibition (Figure 4.1B). The multiunit activity showed burst firing coherent with the negative deflections of the LFP.

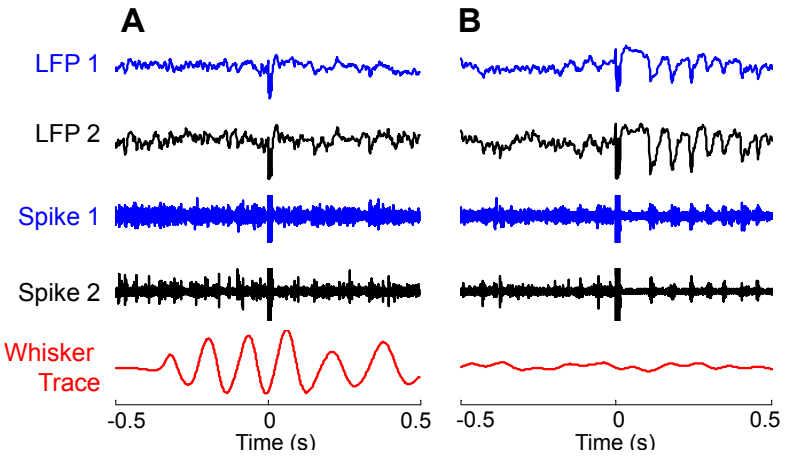

Figure 4.1: Evoked responses to cortical microstimulation. (A) 1-200Hz local field potential (LFP) and 0.5-10kHz multiunit activity (Spike) recorded from two electrodes in infragranular layer of barrel cortex of awake rats are shown along with traces of whisker movements. Microstimulation (at 0s) delivered during active whisking typically induced a small neural response which is partially obscured by the stimulus artifact at 0s. (B) On the other hand, microstimulation delivered during periods of no whisker movement typically induced a long period of reduced neural activity followed by a series of 15-18Hz rhythmic oscillations in the LFP and concomitant spike bursts in multiunit recordings.

We observed a significant negative correlation between the power of the evoked LFP oscillation and the strength of whisking (R= -0.50, P$<$0.001) (Figure 4.2). This is further illustrated in Figure 4.3 where 50 trials with lowest whisking strength were classified as 'Quiet' and 50 trials with the highest whisking strength were classified as 'Whisking'. The raster and average LFP response when 'Quiet' show evoked oscillations in response to cortical microstimulation (Figure 4.2A). We calculated the power spectral density of the LFP response during time 100-500ms post-microstimulation in each trial. The average of all such power spectral densities shows a peak at 17Hz (Figure 4.2B). The initial multiunit response to cortical microstimulation (2-10ms post stimulation in Figure 4.2 C) in 'Quiet' trials was statistically similar to 'Whisking' trials (considering 15 multiunits from the same animal, paired Student's t-test, P$>$0.25) suggesting that cortical excitability is not modulated by behavior. However, microstimulation in 'Quiet' trials evoked a stronger inhibition (comparing LFP 20-100ms after stimulation, Mann Whitney two-tailed test, P$<$0.001) and more pronounced evoked oscillations (comparing power spectral density of LFP 12-18Hz, Mann Whitney two-tailed test, P$<$0.001). 94% of the evoked responses in 'Quiet' trials showed higher spectral power in the 12-18Hz band compared to the average power in whisking trials showing that oscillations were reliably evoked in quiet trials.

These analyses show that the neural response to microstimulation is strongly dependent on the behavioral state of the animal. Similar behavioral modulation of neural responses was observed in a total of five rats. It should be noted that there was no explicit sign of bodily

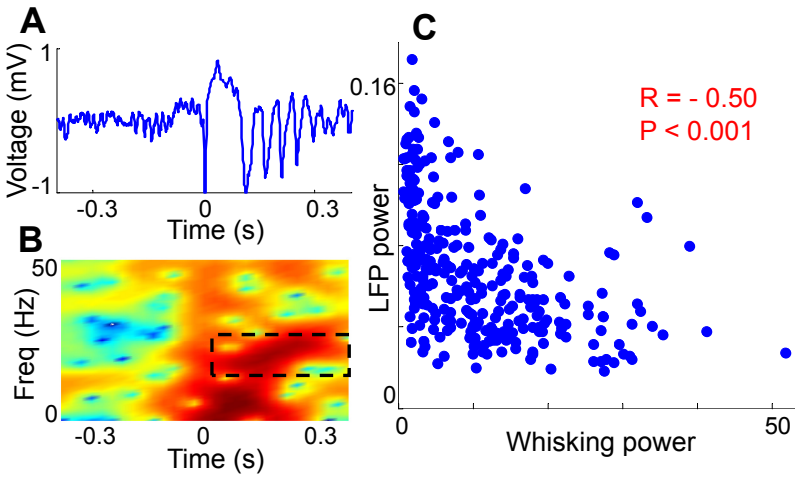

Figure 4.2: Correlation between whisking and evoked LFP oscillations. (A) Example LFP trace of microstimulation evoked oscillations. (B) Spectrogram of above LFP trace. The power in the 10-20Hz band from 100-500ms after microstimulation is used as a metric of the power of the evoked LFP oscillation (Dashed black box). (C) Scatter plot shows an inverse relation between the power of the evoked LFP oscillations and the strength of whisking in 300 stimulations on one rat.

activity such as whisker movement or twitching correlated with the evoked oscillations. Further, the evoked oscillations died down within 500ms and never resulted in kindled seizures.

4.2.2 Cause of Modulation

It is conceivable that behavioral modulation of evoked responses could be caused by the state of alertness or arousal of the animal. It is well known that the state of arousal of the animal modulates the response properties of the thalamocortical network (as reviewed in [85, 86]). To explore whether level of alertness played a role in our experimental setup, we measured the power in the delta frequency band (1-4Hz) of the LFP which is often used as a marker of alertness [87]. We found that the power of the microstimulation-evoked oscillations was not significantly correlated to 0-500ms pre-stimulus delta power ($R=0.02$, $P>0.5$). This suggests that level of alertness was not an influencing factor in the observed modulation.

Another potential source of modulation could exist if rats fell asleep when quiet. To rule out this possibility, we examined occasions where the neural response to microstimulation was significantly different on closely spaced stimulations (Figures 4.4A). To demonstrate that rats showed rapid transitions between behavioral states, we calculated the correlation between evoked neural oscillations and whisking strength 't' seconds before or after stimulation. This analysis reveals to what degree whisker movements more distant in time from

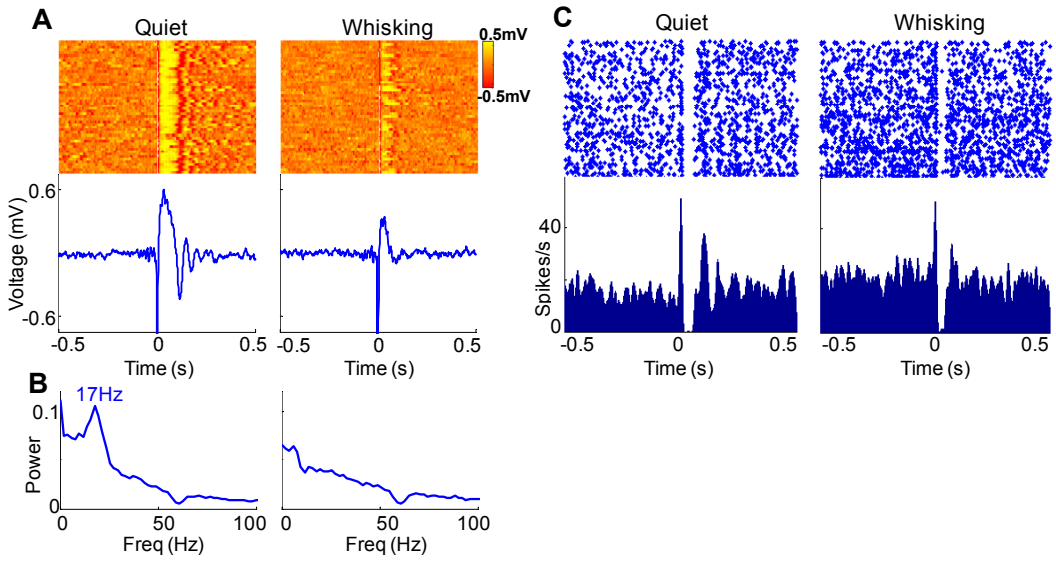

Figure 4.3: LFP and multiunit evoked responses. (A) Raster plot and average evoked LFP responses to cortical microstimulation (at 0s) in 'whisking' and 'quiet' trials. (B) The average power spectral density of the LFP during the period 100-500ms after microstimulation in whisking and quiet trials. (C) Raster and histogram of evoked multiunit responses to microstimulation during whisking and quiet trials. The quiet trials show a lower baseline firing rate, a prolonged inhibition and oscillatory bursting but the initial excitation (0-5ms) is similar to that observed when whisking.

the microstimulation influenced the evoked oscillations. If behavioral states changed slowly, one would expect that whisking strength 't' seconds prior to stimulation would be strongly correlated to the strength of stimulus evoked oscillations. We found that the correlation dropped off rapidly with a time lag as low as 500ms (Figures 4.4B) implying rapid transitions between behavioral states. Such rapid transitions [87] are incongruent with sleep and more likely caused by rapid changes in motor behavior.

To further ensure that animals were awake and alert, we trained two rats on a variable interval tone detection task while restrained. A tone was played after random intervals and rats learned to wait and respond to the tone with a lick within 1s. We also delivered cortical microstimulation randomly 0.5-1s before the occurrence of the tone. During this period, rats would sometimes sit in a quiet immobile state and sometimes actively whisk. This microstimulation did not have any relevance to the behavioral task but we could now analyze the neural response to microstimulation considering only those trials where rats responded within 1s after the tone. We repeated the analysis of Figure 4.2 on this dataset and found very similar results (Figure 4.5). The reaction time on the task was in fact lower when the rats were quiet than when they were whisking (Median response time when quiet=0.30s and whisking=0.56s, Mann Whitney two-tailed test, $P<0.001$) suggesting that the rats were equally if not more alert when quiet. Taken together, these results argue against the possibil-

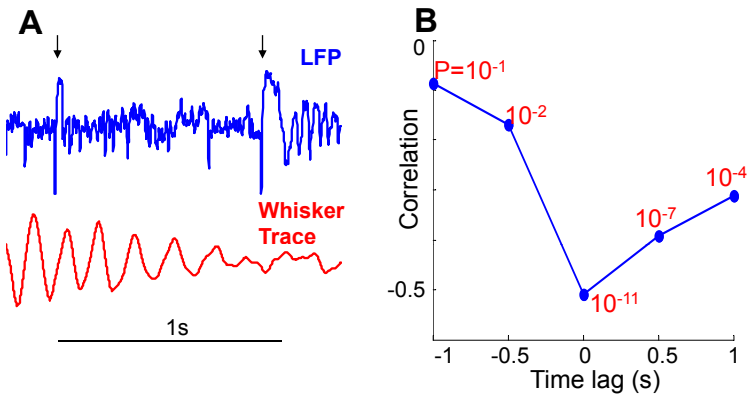

Figure 4.4: Time constant of behavioral states. (A) Example of whisking trace and LFP responses to two closely spaced microstimulations. The time of microstimulation is indicated using black arrows. The significant difference in LFP response shows that evoked responses to microstimulation are rapidly modulated by changes in motor behavior. (B) The correlation between LFP oscillation power and whisking strength is plotted at different time lags with the correlation (R) on the Y axis and the 'P' value of each correlation indicated in red. Note that the correlations are negative with the highest magnitude of correlation (-0.50) occurring at zero lag. The rapid drop-off in the correlation implies rapid switching of behavioral states.

ity that alertness, arousal or sleep play a role in the behavioral modulation observed in this work.

This leads us to the conclusion that the observed effect is likely caused by motor modulation of the somatosensory thalamocortical loop. It should be noted that there exist points in the lower left hand corner of Figure 4.2C and Figure 4.5B demonstrating that the relationship between whisking strength and evoked oscillations in not purely linear. This suggests that although motor behavior is a dominant modulator of the somatosensory thalamocortical loop, other causes of modulation (like attention) exist.

4.2.3 Relation to Spontaneous Rhythms

In the rat somatosensory system, two prominent <20Hz oscillations have been observed. Sleep spindles are 7-14Hz oscillations observed in early stages of sleep that wax and wane over a period of 1-3seconds [88]. Spontaneous spindles are also observed under ketamine-xylazine anesthesia but only show a waning phase [77]. Cortical microstimulation evoked oscillations appear very similar to spontaneous ketamine spindles (Figure 4.6 A). This agrees with the hypothesis that spindles are often initiated by a naturally occurring synchronous volley of spikes from the cortex [89]. The corticothalamic nature of spontaneous ketamine spindles and cortical microstimulation evoked oscillations has been well established [77, 89].

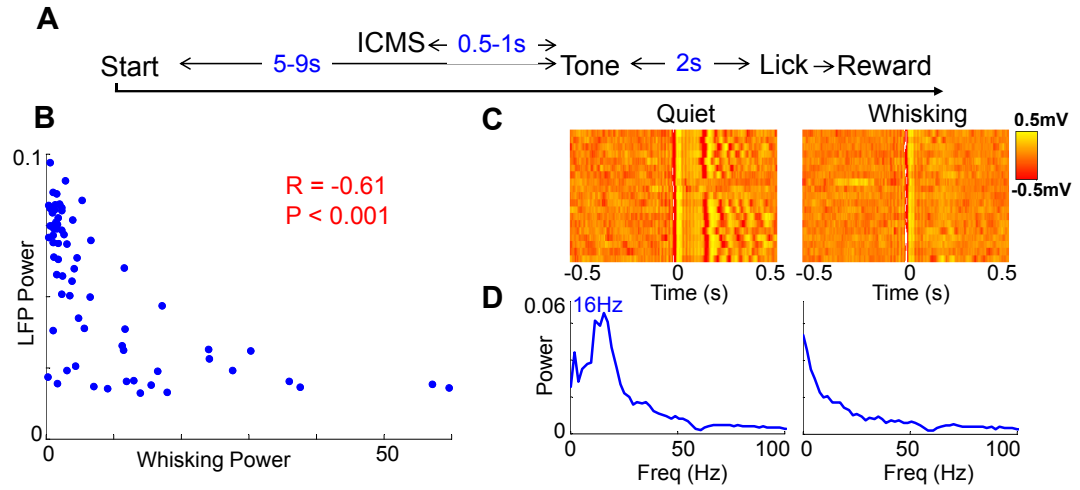

Figure 4.5: Behavioral modulation in alert rats. (A) Structure of a variable interval tone detection task on which rats were trained. Cortical microstimulation was introduced 0.5-1s before the tone stimulus on some trials and had no relevance to the task. (B) The inverse relation between evoked LFP oscillations and whisking strength continued to hold. (C) The raster and (D) power spectral density of evoked oscillations in trials classified as quiet and whisking show clear behavioral modulation of evoked responses.

The second prominent oscillations occur in the 8-10Hz band and are known to spontaneously occur in quiet immobile rats. They have been variously called high voltage rhythmic spikes (HVRS) [90], high voltage spike-and-wave spindles (HVSs) [83], Mu Rhythms [91] and Spike Wave Discharges (SWDs) [92]. An example of such an oscillation in an awake rat is shown in Figure 4.6B and its average power spectral density is shown in Figure 4.6C. This figure clearly demonstrates that SWDs have a different frequency range compared to the observed microstimulation evoked oscillations. It should also be noted that the pre-stimulus period of Figure 4.3 and Figure 4.5 do not show any prominent LFP oscillations. We discarded the few stimuli which occurred during ongoing 8-10Hz oscillations to ensure that they did not play a role in the observed effects.

4.2.4 Modeling

A number of detailed computational models of thalamic and thalamo-cortical networks have been developed [93, 94] which provide insight into some of the basic neuronal mechanisms underlying thalamocortical oscillations. We constructed a population model in MATLAB (MathWorks Inc., Natick, MA) to explore the possible origins of the evoked neural oscillations in response to cortical microstimulation. This model was based on the one developed in [95] to explore the transitions between spontaneous spindle oscillations and SWDs. We extended this model to better account for the effect of modulatory neurotransmitters in the

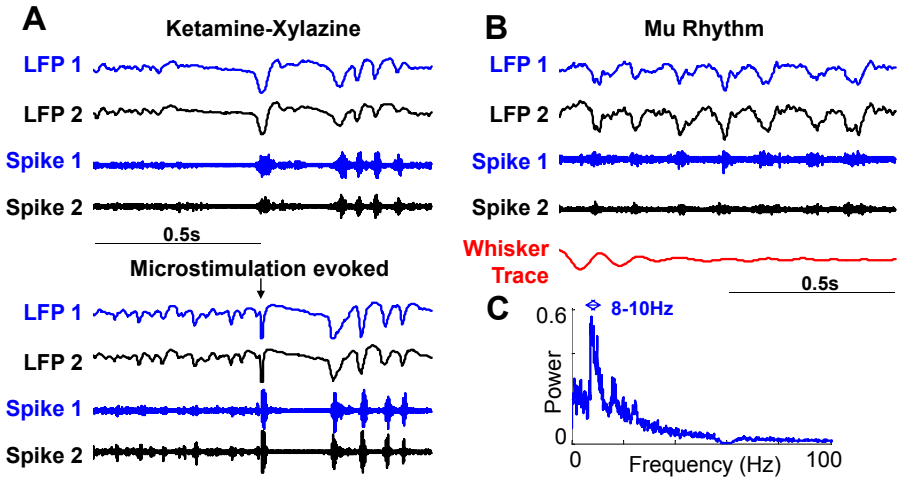

Figure 4.6: Comparison to spontaneous oscillations. (A) Spontaneous waning oscillations in LFP and multiunit recordings while under ketamine-xylazine anesthesia (ketamine spindles) are very similar to microstimulation evoked responses in the same animal. (B) Spontaneous oscillations (SWDs) observed in awake immobile rats often accompanied by whisker twitching. (C) Average frequency spectrum of SWDs shows a peak at 8-10Hz clearly different from that observed in microstimulation evoked oscillations.

thalamus by modeling the Na^+ and K^+ leak currents (g_{Naleak} and g_{Kleak}). This model recreates patterns of evoked oscillations allowing us to infer what properties are necessary and sufficient to account for the observed phenomena.

The model consists of four sub-parts modeling thalamic relay cells (TC), reticular thalamic cells (RE), pyramidal neurons in the cortex (PY) and inhibitory interneurons in the cortex (IN) (Figure 4.7A). The transformation between mean membrane potential and firing rate in thalamic neurons takes into account the I_T current which underlies burst firing. Cortical microstimulation was modeled by the injection of a strong excitatory input on PY and IN neurons for 5ms. It was assumed (as in [95]) that cortical LFP recordings show similar behavior to the negative of the mean membrane potential of the PY cell population. The equations governing the TC neurons are shown in detail in the Appendix in [96].

The model recreates the evoked LFP oscillations in response to cortical microstimulation (Figure 4.7B). According to the model (Figure 4.7C), the initial burst of spikes in response to cortical microstimulation causes a prolonged hyperpolarization of neurons due to the activity of $GABA_B$ receptors in the thalamus and cortex. This is in agreement with [84] and the fact that $GABA_B$ is typically activated only by a strong volley of spikes as created by cortical microstimulation. Prolonged hyperpolarizations of RE neurons are known to precede spontaneously occurring spindle oscillations [89]. This hyperpolarization likely deinactivates the Ca^{2+} dependent T-current (I_T) leading to a low threshold spike and rebound excitation. In a similar manner, the microstimulation evoked hyperpolarization sets off evoked oscillations

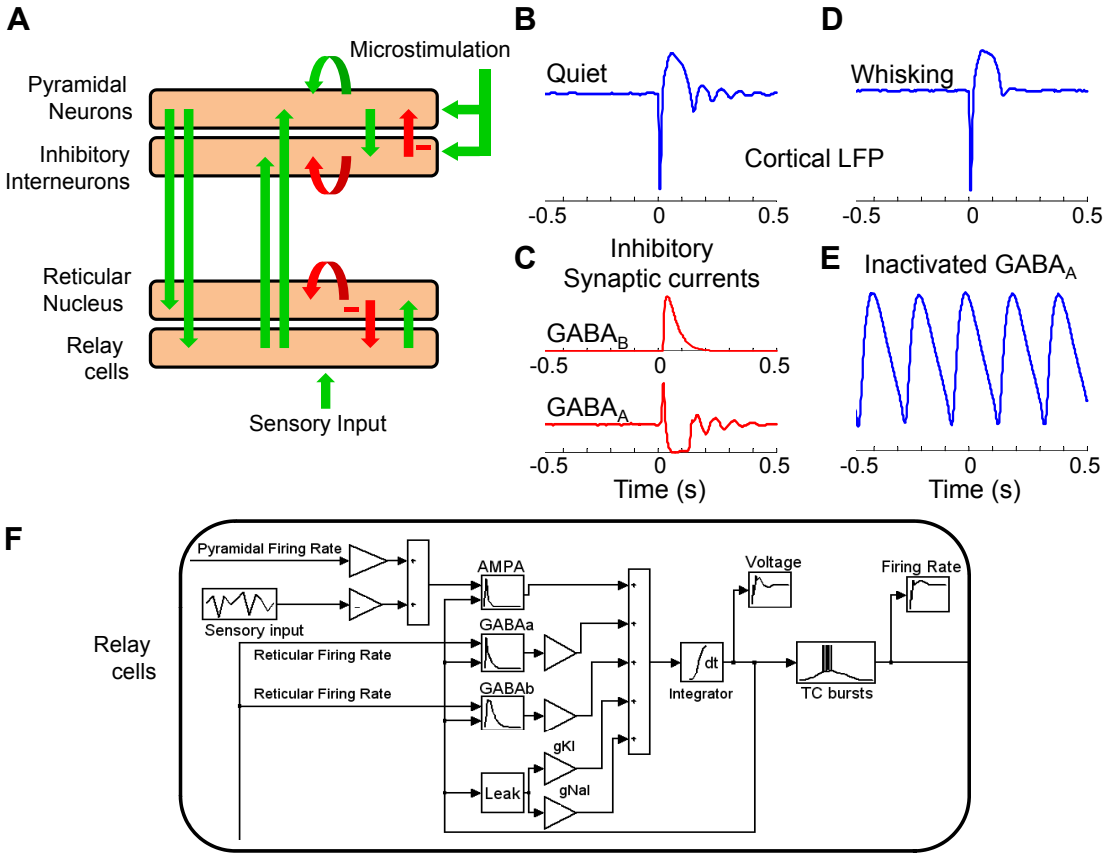

Figure 4.7: Thalamocortical model. (A) Computational model of the thalamocortical loop used to investigate potential mechanisms of the experimentally observed evoked responses. The green arrows denote excitatory connections and the red arrows inhibitory. (B) Evoked LFP response of the thalamocortical model to a burst of spikes in the cortex (at 0s) shows a similar response to experimentally observed data. (C) The model suggests that a $GABA_B$ mediated IPSP in thalamocortical cells plays a significant role in the initial prolonged inhibition. A series of $GABA_A$ mediated IPSPs in thalamic neurons along with their intrinsic bursting properties seem to be responsible for the oscillatory evoked response. (D) The evoked response in the modeled whisking state is similar to that experimentally seen. (E) Application of $GABA_A$ antagonists induces lower frequency sustained oscillations in the thalamocortical model. (F) Representation of the components of the population model for relay cells. Similar blocks were created for the three other neural populations.

in the model by a combination of $GABA_A$ mediated IPSPs (Figure 4.7C) and the intrinsic bursting property of TC and RE neurons. The oscillations are further transferred to the cortex by the TC neurons.

The precise neuromodulatory mechanism by which motor activity modulates the somatosensory thalamocortical system is unknown. Potential modulatory neurotransmitters are acety-

lycholine, serotonin, norepinephrine etc which act primarily by modifying the potassium leak conductance (g_{Kleak}) in thalamic and reticular neurons [97]. Moreover, the sensory input to thalamic neurons is expected to be higher during active whisking. Reducing g_{Kleak} in RE and increasing sensory inputs led to depolarization of RE neurons in the model. We found that the evoked response now showed a reduced inhibition and no oscillations in a manner similar to that observed in actively whisking rats (Figure 4.7D). Further, it is known that the administration of $GABA_A$ antagonists to the ferret LGN *in vitro* slowly perverts normal spindle waves into a highly synchronized slow oscillation similar to SWDs. Blocking of $GABA_A$ in the model led to a similar result (Figure 4.7E).

This model suggests that the oscillatory properties of TC and RE neurons can account for the evoked oscillations and behavioral modulation seen in our experiments. The exact mechanisms underlying spindle initiation and synchronization are not completely understood [98]. Future models of evoked thalamocortical oscillations should include the hyperpolarization-activated current I_h and the Ca^{2+}-activated currents $I_{K[Ca]}$ and I_{CAN} which are thought to play a role in spontaneous spindles [93]. Further, norepinephrine and serotonin are known to abolish spindle wave generation through an enhancement of I_h in TC neurons [99] and this mechanism may contribute to behavioral modulation.

4.3 Discussion

In this work, we have demonstrated that microstimulation-evoked oscillations in rat barrel cortex are strongly modulated by active whisking. This phenomenon is also seen in alert rats engaged in a challenging behavioral task, suggesting that the observed modulation is truly motor driven.

4.3.1 Startle Response

Modulation of the whisker sensory system by motor behavior has been observed by a number of researchers [100, 86, 87, 81, 101]. During active whisker movements, somatosensory afferent circuits seem to act like a linear low-gain input stage to faithfully transmit patterns of spikes from the periphery. In contrast, during quiet immobility, the system seems to act like a non-linear high-gain input stage to optimally detect and magnify single stimuli. This may function as a sensitive detection system (a wake-up call), alerting the animal to unexpected sensory inputs [81]. Moreover, this modulation persists after transaction of the infraorbital nerve [87] suggesting that it is not caused by afferent sensory signals and must be central in origin. This gating of sensory inputs is thought to occur at the level of the brainstem and the thalamus [101]. Our findings show that the neural response to microstimulation in barrel cortex is also modulated by active whisking. This occurs in the form of modulation of the initial inhibition as well as the long-lasting evoked oscillations.

The question then arises as to whether whisker deflection also sets off the kind of oscillatory

evoked responses seen in response to cortical microstimulation? Whisker deflection evoked oscillations at 16Hz have been observed in anesthetized animals [102, 103] but are typically not seen in awake, behaving rats. This could be due to a number of factors. Cortical microstimulation, even at low stimulus levels, might excite more thalamic spikes than caused due to physical whisker deflections. Further, it is known that stimulation of pre-thalamic neurons is less effective at setting off oscillations than cortical stimulation [88]. This is thought to be because cortical stimulation directly excites RE neurons whereas pre-thalamic afferent fibers and incoming sensory stimuli do not.

Intracellular recordings in RE neurons [77] have shown that cortical microstimulation triggered oscillations increase in amplitude as the cells are hyperpolarized from -54mV to -75mV. The modulation of evoked oscillations by whisking of rats suggests that motor behavior rapidly depolarizes somatosensory reticular neurons. This modulation of membrane potential can be readily achieved by neurotransmitters like acetylcholine, serotonin, norepinephrine etc by varying the K^+ leak conductance. This mechanism potentially also plays a role in behavioral modulation of sensory evoked responses observed in the rat whisker system. This hypothesis can be verified in future experiments using patch clamp recordings of RE neurons in awake, behaving rodents.

4.3.2 Evoked Oscillations

The functional role of stimulus-evoked oscillations has been the subject of much debate. It has been suggested that bursting, as seen in microstimulation-evoked responses, may provide better signal to noise and thus facilitate detection of a stimulus [104]. However, it has also been found that the thalamus is insensitive to external inputs during spindles and hence spindles are thought by some to represent a cutoff from the external world [105].

Sensory stimuli like tones and flashes of light also evoke oscillatory responses under certain circumstances and this seems to be an intrinsic property of the thalamocortical loop (reviewed in [106]). One potential significance of this phenomenon is that a single volley of afferent spikes sets up a response outlasting by several hundred times the duration of the original stimulus. This may constitute a mechanism for the persistence of a mental impression aroused by a sensory stimulus. Recent evidence of replay of hippocampal spike trains coinciding with thalamocortical spindles [107] gives further credence to this hypothesis.

4.3.3 Sensory Neuroprostheses

Cortical microstimulation has been proposed as a method to deliver sensory percepts to circumvent damaged sensory receptors or pathways. To achieve desired encoding of percepts, it is essential to better understand the neural response to cortical microstimulation.

Recent work [84] has suggested that the inhibitory period seen following cortical microstimulation is caused primarily through the influence of $GABA_B$ receptors in the cortex. The

evoked oscillations we observe, and our model, suggest that thalamic neurons play a significant role in the observed response. These results can be reconciled since the experiment used to infer the role of $GABA_B$ involved an intraperitonal administration of $GABA_B$ antagonist making it impossible to distinguish between the role of $GABA_B$ at the level of the cortex or thalamus. Further, previous research [108] has shown that the reticular nucleus plays a leading role in the rebound excitation observed in the cortex. It is therefore essential to keep in mind the excitation of thalamic neurons by cortical microstimulation during the design of stimulation protocols.

Thalamic gating modulates sensory inputs based on the behavioral state of the animal. As shown in this work, this mechanism also modulates the neural response to cortical stimulation. Further, behavioral state dictates whether thalamic neurons are in the tonic or burst firing mode and the resultant response to cortical microstimulation. Therefore it may be essential, in future sensory neuroprostheses, to modify stimulation parameters based on the behavioral state or background neural activity of the user in order to deliver desired percepts.

Having studied neural responses to ICMS and their modulation by behavior [96], we now explored the perceptual effects of microstimulation and the extent to which they could be used to encode somatosensory information.

Chapter 5

Active Sensing

5.1 Introduction

Active sensing, namely the active movement of sensory organs to better sense the environment, forms an essential component of somatosensation [109, 110, 111]. While humans move their fingers for tactile sensing [112], rodents scan their mystacial vibrissae (whiskers) with stereotypical rhythmic motions at 8-12Hz to explore their surroundings [113]. The dynamic perception of the environment derived from active sensing [110] is fundamentally different from sensations produced by feed-forward transformation of inputs from external sensors since active sensing requires the integration of information across sensory and motor modalities. For example, the perception of object location through contact requires the integration of position of the external mechanoreceptor (finger or whisker) with the activation of those sensors by contact with the object.

The rodent vibrissa system and its associated neuronal architecture is a well studied model of tactile sensory processing [114, 26, 115]. Rats can use their whiskers to sense object shape [116], judge distances [117], and discriminate textures [118, 113, 119], widths of apertures [120], and surface orientations [121]. Furthermore, rats can discriminate offsets in horizontal location of less than 0.24mm (1^o) by actively moving their whiskers [122]. The recent demonstration that rats can discriminate between two objects whose rostro-caudal angle differed by 15^o by actively scanning a single whisker [123], provides an excellent model to study object localization through active touch [124, 125]. The performance of rats in the aforementioned task suggests that they infer object location by using sensorimotor integration; namely by combining whisker contact information with knowledge of whisker position. Here we use a similar behavioral paradigm to study target localization in rats and further exploit the fact that whisking of rats can be brought under operant control [126]. The novelty of our paradigm lies in the use of intracortical microstimulation (ICMS) to deliver sensory inputs in real-time based on motor movements of the animal.

Research in non-human primates has shown that microstimulation in somatosensory cortex

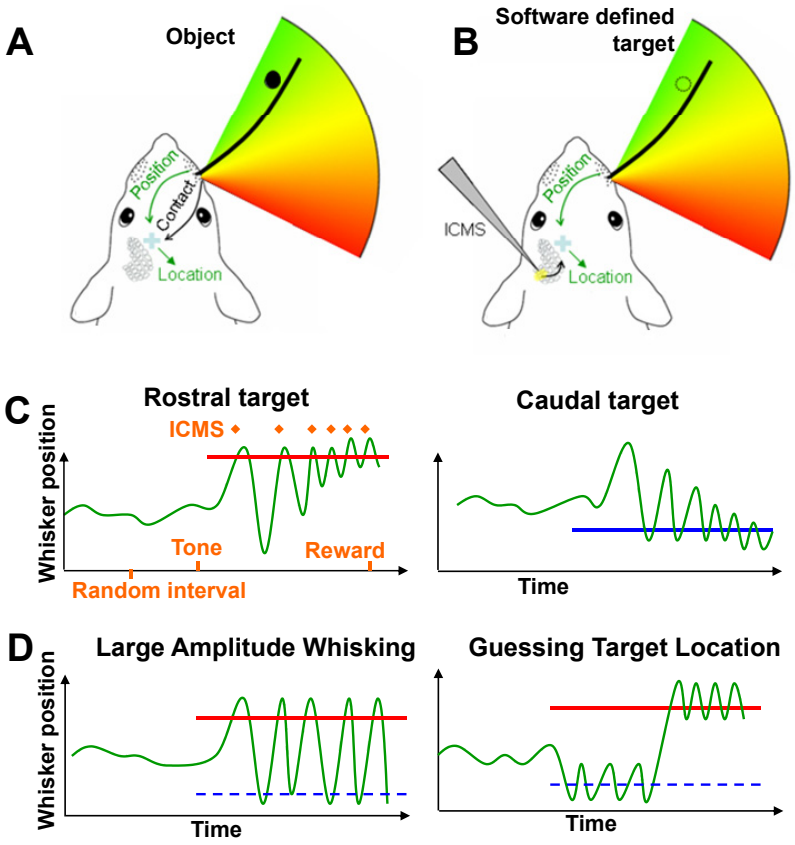

Figure 5.1: Target location cued using cortical microstimulation. A. Schematic depicting a rat actively whisking to contact a small object (black circle) and the resulting neural streams afferent to the vibrissa somatosensory cortex. B. Schematic of behavioral task to test whether rats can replace contact signals with microstimulation in barrel cortex triggered by crossing a software-defined target (dotted circle) to infer target location. C. In each trial, the target is positioned randomly at one of two possible locations (red and blue lines). Rats must cross the target N_{stim} times within 2 seconds after the tone to obtain a reward. Rats often adopted a strategy where they locate the target and then concentrate on it. D. Alternate strategies to obtain a reward in this task.

can be used to provide behavioral cues [127, 38, 128]. Similarly, behavioral studies have shown that rats can detect microstimulation in somatosensory cortex and use it to perform a discrimination task [27, 28, 129, 130]. However, previous experiments have only demonstrated passive encoding of sensory inputs and the integration of such inputs in an active sensing paradigm remains to be seen.

In this work, we investigate whether actively whisking rats can substitute vibrissa contact signals with microstimulation in the barrel cortex to infer spatial locations along the rostrocaudal axis (Fig. 5.1A,B). Performance of such a task would suggest that animals can incorporate electrically delivered stimuli into active sensing systems to form dynamic percepts of the environment.

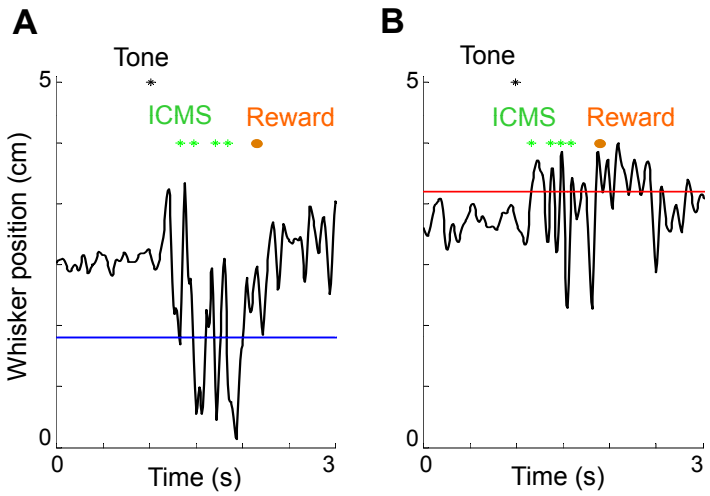

Figure 5.2: Y-coordinate of whisker traces during example red and blue trial along with occurrence of tone, microstimulations and reward.

5.2 Results

We implanted four rats with chronic microwire arrays in somatosensory barrel cortex. After recovery from surgery, they were trained to sit head-restrained while one whisker was tracked in real-time using a custom whisker-tracking system [58]. In each trial, a software-defined target was created at one of two possible spatial locations (rostral and caudal targets indicated by red and blue lines) in a pseudo-random manner and rats were required to cross the target with their whisker 4-6 times (N_{stim}) within 2 seconds to obtain a reward (Fig. 5.1C). Each target crossing triggered microstimulation across two neighboring electrodes and the timing of this microstimulation was the only information rats received regarding target location. Two biphasic pulses separated by 3ms, each 250μs in length and 25μA in amplitude, were used for microstimulation.

5.2.1 Analysis of Whisker Motion

Rats started each trial by actively whisking to detect the position of the target and we concluded whether they had inferred target location by analyzing whisker trajectories (Fig. 5.2). Observations of whisker trajectories during the task suggested that rats concentrated their whisking near the location of the target (Fig. 5.1C). This would only be possible if rats could infer target location from microstimulation delivered cues. There are alternative strategies to obtaining a reward in this task which do not require knowledge of target position: performing a number of high amplitude whisks which would trigger microstimulation at either target location or guessing target location and moving to other possible locations if no re-

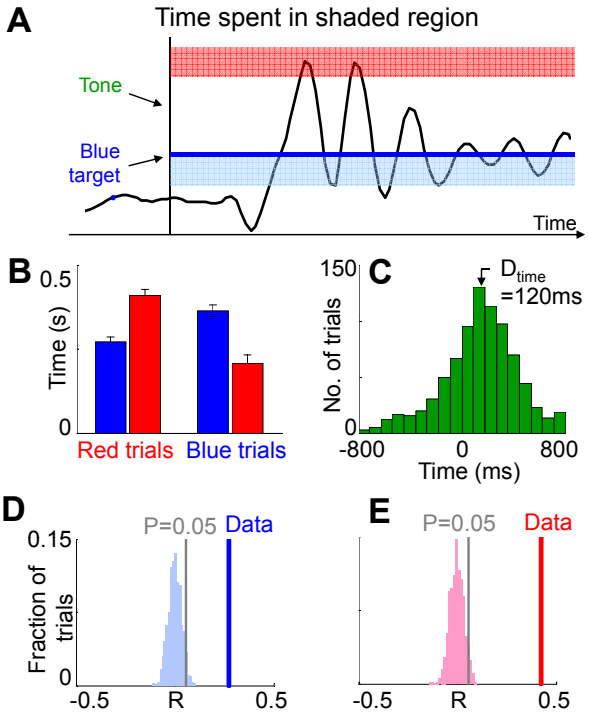

Figure 5.3: Measures of performance. A. Time spent in a rectangle drawn around both target positions is used as a metric to evaluate whether rats whisk near the location which triggers microstimulation. The black trace shows the recorded whisking during a trial. B. Data for this figure was obtained from all 27 sessions (862 trials) performed by one rat during a two month period with the number of required target crossings (N_{stim}) set to 6. Bar graph of mean +/- 2σ (standard error of mean) time spent in the vicinity of red and blue targets during red and blue trials. C. Histogram of the difference in time spent near the correct and incorrect position on each trial. The median of this distribution is denoted as D_{time}. D, E. Correlation between time spent in the vicinity of each position and the location of the target is indicated as Data. The distribution of possible correlations and P=0.05 levels are found by correlating the observed values of time spent near each position with shuffled target locations. The calculated correlation (Data) is greater than the P=0.05 value showing that it is significant.

ward was obtained at the first (Fig. 5.1D). While rats can switch strategies between trials, we performed a number of statistical analyses to reject the null hypothesis that the observed performance could be achieved without knowledge of target location. Once this hypothesis was ruled out, we could infer that rats actually infer target location encoded by microstimulation and concentrate their whisking in its vicinity.

To rule out the possibility that rats used only large amplitude whisking to obtain a reward, we measured the average time spent in the vicinity of the rostral and caudal positions during red and blue trials (Fig. 5.3A). If rats recognized target location and concentrated on it, we would expect longer time spent near the rostral target (red line) on red trials and vice versa,

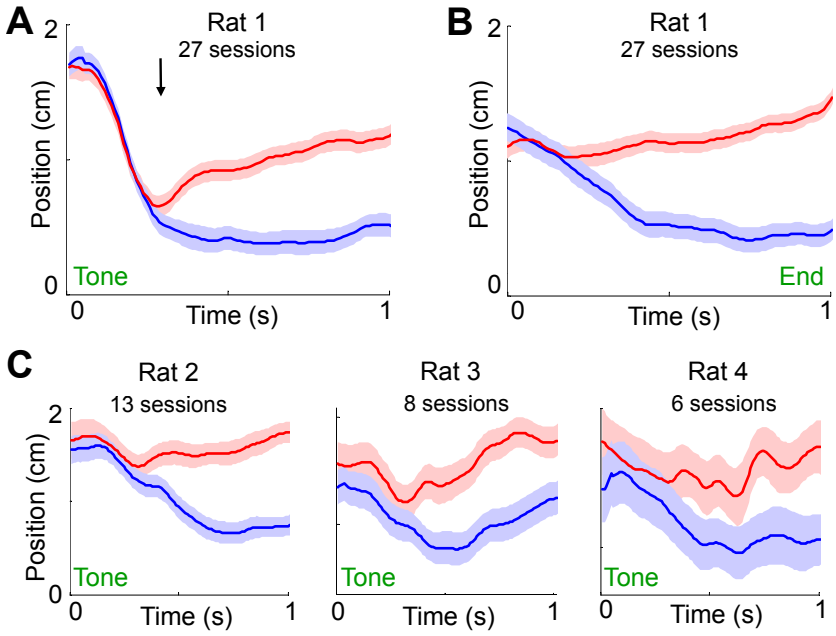

Figure 5.4: Average whisker position. A. Mean whisker position starting from the tone on red and blue trials +/- 2σ (standard error of mean) on same 27 sessions as Fig. 2. The black arrow indicates the time after which the 2σ error regions remain non-overlapping. B. Since trials lasted for variable periods of time, a second metric was used to calculate the average whisker trace looking backwards in time for 1s until the end of each trial. In trials where the rat receives a reward, the end is the instant of reward and in trials without a reward the end is calculated as tone+2s. C. The performance of three others rats on the same task showing above chance performance.

as was seen (Fig. 5.3B). The median difference between time spent near the correct and incorrect position on each trial (D_{time}) was 120ms (Fig. 5.3C) (significantly different from 0, P$<$0.001, Wilcoxon Signed Rank Test). A median of zero would imply no difference in whisking strategy between correct and incorrect position, whereas the positive median implies that rats prefer the correct position. Rats were sometimes biased to one side and spent more time there even though the time spent on each side covaried with target location. To account for this behavior, we also calculated the correlation between the time spent on each side and target location (marked 'Data' in Fig. 5.3D,E). We calculated the distribution of possible correlations by shuffling target locations, to ensure that the measured correlations were significant. The calculated correlation ('Data') being positive and larger than 95% of the distribution indicates that the time spent on each side is correlated to target location. These measures are similar to the metrics used to evaluate the performance of rats in a Morris Water Maze task [131]. Thus we can rule out the possibility that rats only used large whisks to obtain a reward.

To rule out the possibility that rats guessed target location, we measured the average whisker

position over the course of red and blue trials (Fig. 5.4A,B). Rats typically started whisking 120ms after the tone (t_{tone}), and the traces were statistically different after 300ms ($t_{diverge}$, P<0.01, t-test). If rats simply guessed target location, information on target location could only be obtained after crossing the location a sufficient number of times to obtain a reward. We verified that this occurred in the first 300ms of the task in only 1.5% of the trials (N_{stim}=6 in this dataset). In other words, if the animals had learned nothing about target location from the microstimulation, they would need to adopt a strategy of crossing each target at least six times and the whisker traces would diverge only after a significant period of random whisking. Hence, $t_{diverge}$=300ms rules out the possibility that the observed behavior can be explained by simply guessing target location. For confirmation, we recorded five sessions where we set the minimum interval between microstimulations (t_{min}) to 100ms. We still observed a $t_{diverge}$ of 300ms. If the rat had guessed target location, the minimum tdiverge possible would be $t_{diverge_C} = t_{tone} + N_{stim} \cdot t_{min} = 720ms$. Similar results were obtained from a total of four rats (Fig. 5.4C).

The above analyses rule out the null hypothesis that the observed behavior could be possible without knowledge of target position. This suggests that rats do infer target location cued by microstimulation while actively whisking, and use this information to direct their motor plan.

5.2.2 Controls

We performed a number of controls to verify that discrimination relied solely on microstimulation cues and sensorimotor integration. To estimate chance performance and to guard against inadvertent cues, we measured the performance of two rats on an identical task with the output of the stimulator disconnected from the implanted electrodes. Under this condition, performance dropped to chance levels (Fig. 5.5A,B). D_{time}=-10ms (not significantly different from 0, Wilcoxon Signed Rank Test, P>0.2).

If target localization is mediated by rats sensing microstimulation, we would expect behavioral performance to increase when amplitude of stimulation is increased from zero to threshold levels. We measured the psychophysical threshold for cortical stimulation by training rats to perform a variable interval stimulus detection task triggered by microstimulation. We found that threshold performance occurred at around 15μA on this task (Fig. 5.5C). We then varied stimulation levels while rats performed the target localization task and measured performance. We found that D_{time} increased with stimulation amplitude and was significantly different from zero (Wilcoxon Signed Rank Test, P<0.05) for stimulation at 20μA and 25μA (Fig. 5.5D). The similar performance of rats on these two tasks suggests that both are mediated by rats sensing cortical microstimulation.

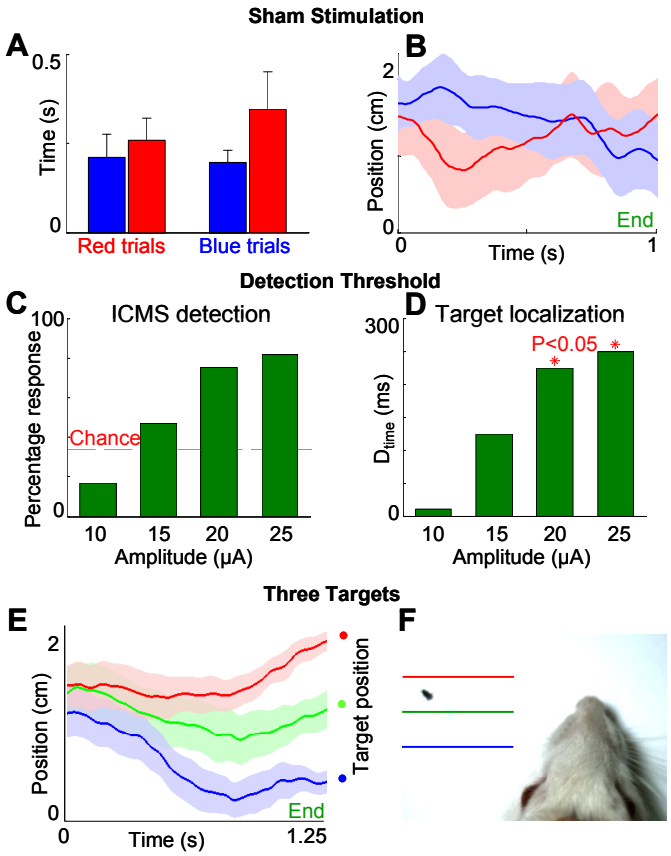

Figure 5.5: Controls. A, B. Performance of rats in an identical task with sham stimulation shows chance levels. C. Behavioral performance on a microstimulation detection tasks at different amplitudes of stimulation to determine the psychophysical threshold of rats. The red line denotes chance levels determined by the frequency of false positives. D. Behavioral performance on the target localization task cued by microstimulation as calculated by the average D_{time} of all sessions at that amplitude. D_{time} being significantly different from 0 (P<0.05) is denoted with a red star. E. Extended version of the same behavioral paradigm with the target placed at one of three possible locations. Average whisker position +/- 2σ (s. e. m.) backwards in time for 1.25s until the end of the trial in red, blue and green trials. Data for this analysis was taken from four sessions performed by two rats. F. Rat head position, whisker marker (red) and location of three possible targets shown as red, green and blue lines.

5.2.3 Whisker Identity

Rats typically move their entire array of whiskers in concert but do have the ability to move individual whiskers to some extent [132]. It was not possible to tag the same whisker on all sessions since rats routinely pulled out tagged whiskers. Moreover, it was only possible to tag one of a small number of macrovibbrisae (typically A2, A3, B2, B3, C2 and C3) which were

strong enough to support the foam marker. We found that varying which whisker was tagged did not modify performance (Comparing distribution of D_{time}, P>0.1, Unpaired t-test).

The spatiotemporal spread of evoked activity caused by cortical microstimulation has been studied by a number of researchers and it is believed that the horizontal spread of excitation upon microstimulation is a function of microstimulation strength (reviewed in [2]). If whisker identity matters in task performance, using higher amplitude stimulation might excite a larger number of barrels and allow more distant barrels to perform the computation required for the task. We found no change in task performance upon varying the stimulation amplitude between 25μA and 50μA (Comparing distribution of D_{time}, P>0.4, Unpaired t-test). These experiments suggest that rats performing our task used synchronous movements of the entire whisker array and this was consistent with visual observations. Recent results [133] suggest that microstimulation activates a sparse distributed population of neurons in an area significantly larger than a single barrel. This further diminishes the importance of stimulating the exact barrel corresponding to the tagged whisker.

5.2.4 Head Movements

Rats in our behavioral task were head restrained but were capable of making minimal head movements. The use of head movements to infer target location is ruled out because this would require very rapid head movements to possible target locations within the time taken for whisker trajectories to diverge ($t_{diverge}$=300ms) and this was not observed in video recordings. Further verification was performed with manual frame by frame analysis of recorded video to extract head position in five randomly chosen sessions. We found that whisker position at the time of first stimulation was correlated with target location ($R > 0.83, P < 0.001$) while head position was not ($R < 0.1, P > 0.2$) on all sessions tested. Head movements are therefore unlikely to be the technique employed by rats to infer target location.

5.2.5 Spatial Location

We next explored the mechanisms that rats used to perform this behavioral task. It is conceivable that rats could perform this task as a two-alternative forced-choice task and decide in each trial whether to whisk in the rostral or caudal direction. To rule out this hypothesis, we tested the performance of three rats on an identical task where the target was placed in one of three possible locations. The average whisker trace for each target clearly shows that rats could infer the 'spatial location' of targets along the rostro-caudal axis (Fig. 5.5E,F). Moreover, the fact that rats could perform the three-target task rules out the use of any position/velocity based algorithm which relies on exploiting the structure of the two-alternative forced-choice task.

This experiment provided us with the opportunity to measure the angular resolution with which rats could determine the position of targets in head-centered coordinates. We found

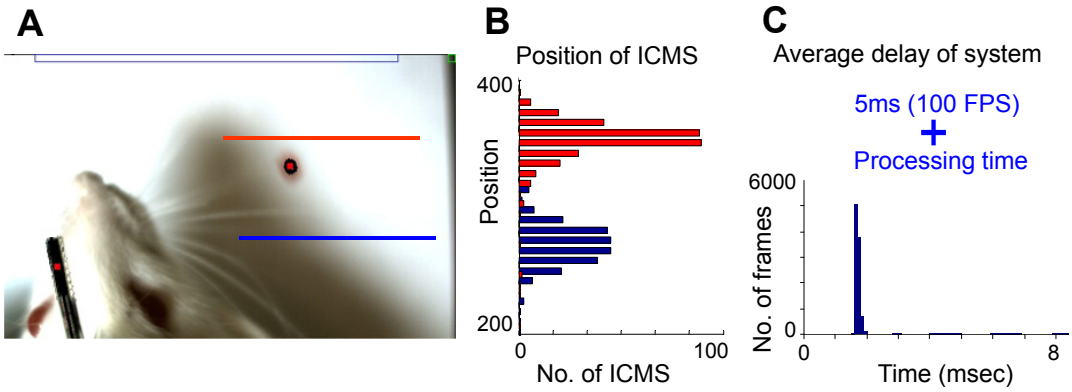

Figure 5.6: Performance of closed-loop real-time whisker tracking and microstimulation system. (A) Rat head position, whisker marker and location of two possible targets. (B) Histogram of marker locations at which the rat received microstimulation. The reason for the spread is the inherent delay of the closed-loop system. (C) There are two primary causes for this delay. The camera used is a 100frames per second video camera which implies one frame every 10ms. Hence there is an average delay of 5ms after target crossing before the frame capture. The actual frame capture, analysis and marker location estimation takes an additional 2ms as shown in the histogram below.

that all three rats could discriminate targets 15^o apart and two of them could resolve targets 10^o apart (considering metrics in Fig. 5.3, 5.4). We believe that this estimate is an upper bound due to the limitations of the closed-loop stimulation system (Fig. 5.6) and the fact that using large whisks becomes more attractive when targets are spaced close together. This hypothesis can be explored using a more accurate real-time feedback system and a modified task structure.

5.2.6 Motor Effects

Microstimulation in rat barrel cortex is known to cause movement of the whiskers [134, 129] and it is conceivable that such a motor twitch could cause the whiskers to spend more time near the location of the target. Two example trials (Fig. 5.7A,B) show that the whisker trace is unaffected by the microstimulation. Further, we measured the microstimulation triggered average of whisker position and velocity over ten sessions (black traces in Fig. 5.7 C,D) and found them both to be flat. To determine chance levels expected in such a triggered average, we shuffled the times of stimulation and recalculated the triggered average. Repeating this a hundred times provided a distribution of expected whisker positions and velocities by pure chance (+/-2σ region indicated by gray region). This suggests that microstimulation at the low levels used (25μA - 2 pulses) did not cause a discernable twitch. This still does not rule out the possibility that stimulation caused freezing of the whiskers, thus causing them

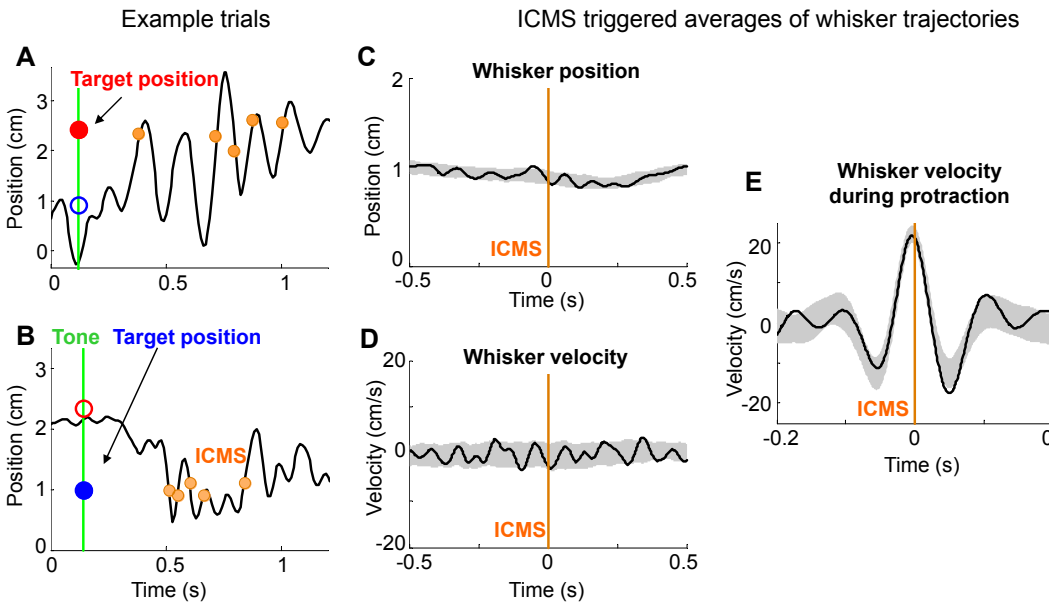

Figure 5.7: Motor effects of cortical stimulation. A. Recorded whisker trace on a trial with a rostral target (red). The green line indicates the tone which initiates the trial and the orange circles indicate times when ICMS was delivered. B. Trial with a caudal target. C. Black trace shows mean whisker position triggered by ICMS. Data for this analysis was taken from ten sessions performed by two rats. D. Black trace shows mean whisker velocity triggered by ICMS. The shaded gray region represents the 95% confidence interval of triggered averages when the triggers are shuffled. E. To rule out the possibility that ICMS inhibits whisker motion thus causing the whisker to spend more time near target position, we look at all trials where ICMS was triggered during protraction. Thus the mean velocity before ICMS is expected to be positive and the sinusoidal nature is due to whisking at 8Hz. If ICMS inhibits whisker motion, we would expect to see a drop in whisker velocity to zero soon after stimulation.

to spend more time near the target. Therefore we analyzed the subset of trials where microstimulation occurred during protraction. The microstimulation-triggered average whisking velocity in this subset of trials (Fig. 5.7E) is expected to be positive (positive velocity during protraction) and show a periodicity of 125ms (due to 8Hz whisking). If stimulation caused freezing of the whiskers, we would expect the velocity to fall to zero immediately after stimulation and this is not observed. The symmetric nature of the triggered average and the fact that it falls within the +/-2σ bounds obtained by triggering with random time instants suggests that microstimulation, at the low levels used in this task, did not cause a motor effect. This is similar to the effect observed in [129] where it was observed that low levels of stimulation could be detected by rats but did not evoke a motor twitch.

The dismissal of these controls suggests that rats can rapidly integrate information about whisker position and timing information from microstimulation to compute the location of targets along the rostro-caudal axis.

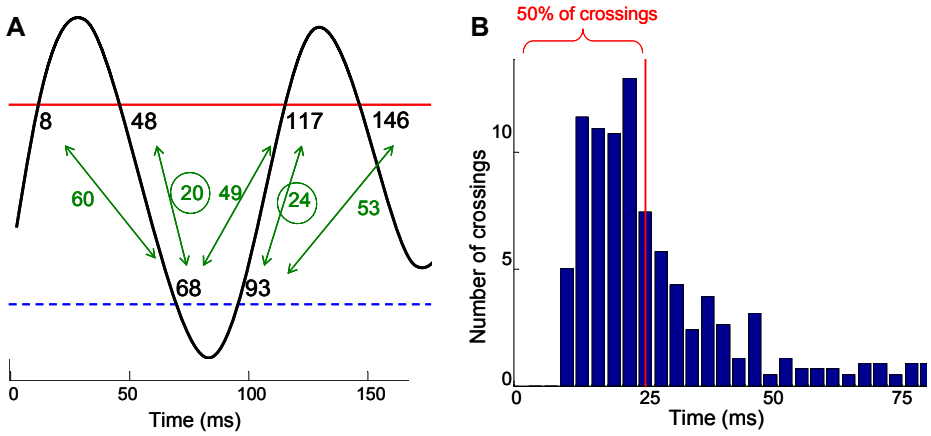

Figure 5.8: Temporal resolution required to perform the task. 50% of the time differences between correct and wrong targets were less than 25ms apart suggesting that rats need to detect the timing of ICMS to within 25ms to accurately perform the task.

5.2.7 Timing of Microstimulation

To measure the temporal resolution with which rats sense the timing of microstimulation, we calculated the time difference between crossings of the correct target and other targets over the length of each trial. The minimum time difference was calculated for every crossing of wrong targets. If the error in the rats estimate of the instant of microstimulation was greater than this value, the rat would have inferred that the target was present at the wrong location. A histogram of these minimum times was then plotted (Fig. 5.8), and it was found that 50% of these time differences were less than 25ms. Therefore 25ms forms an upper bound on the maximum error in the rat's estimate of the instant of microstimulation for the rat to still perform above chance levels on this task.

Another way to estimate the temporal resolution required to perform this task is to introduce a delay between the time at which the whisker crosses the target and the time at which microstimulation is delivered. This temporal delay will lead to a spatial blur in the position at which the rat experiences microstimulation. However, the task can still be performed by simply reducing the speed of whisker motion thus allowing the rat to infer target location. Thus the expected response is that the time taken to infer target location should increase since the task now requires a slower whisking strategy.

We performed exactly this control by introducing a 50ms delay in the timing of the microstimulation in 20% of the trials that the rat performed. We found that this led to a blur in the positions at which the rat receives microstimulation (Fig. 5.9A,B) as expected. The rat could still perform the task but the time taken for the average whisker traces to diverge now increased from 480ms (no delay) to 640ms (50ms delay) (Fig. 5.9C,D). This clearly agrees with the hypothesis that rats should still be able to perform the task but would take longer to infer target location. The performance on 'no delay' trials is also worse in this dataset

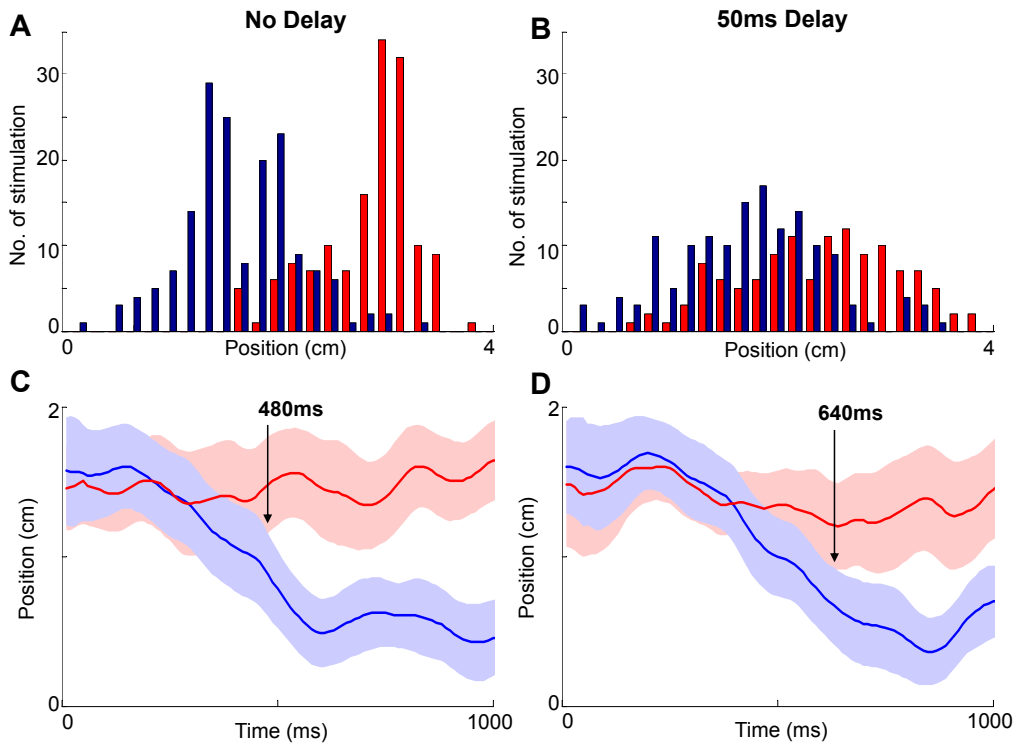

Figure 5.9: Delayed version of task. A, B. The spatial distribution of whisker positions where the rat receives ICMS in the case of minimum delay and 50ms added delay. C. Performance of rat on conventional task with whisker traces diverging after 480ms. D. Performance on delayed version of task where time taken for whisker traces to diverge increases to 640ms.

(compared to Fig. 5.4) presumably because the rat was using a slower whisking strategy due to the presence of catch trials.

5.2.8 Whisking Behavior

We quantified the whisking behavior of rats by computing the power spectral density (PSD) of the whisker velocity. Head restrained rats often suppress whisker movements [126, 135] but we could induce exploratory whisking by introducing a novel object or scent near the rat's head. During such epochs, the whisker traces looked highly sinusoidal and the PSD of whisker velocity showed a narrow peak at 8Hz (Fig. 5.10A,C). This agrees with previous reports of stereotypical 8Hz whisking during exploratory whisking [114, 125, 26]. Fig 5.10B shows two example traces of whisker position recorded during the target localization task. PSD analysis of whisker velocity showed that the frequency of whisking was distributed over a wide range (Fig. 5.10D), with 76% of whisking power concentrated in the range of 5-20 Hz and 88% of dominant whisking frequencies on individual trials occurring in the range of 5-20 Hz. This agrees with previous reports [116, 122, 123] that task-specific requirements

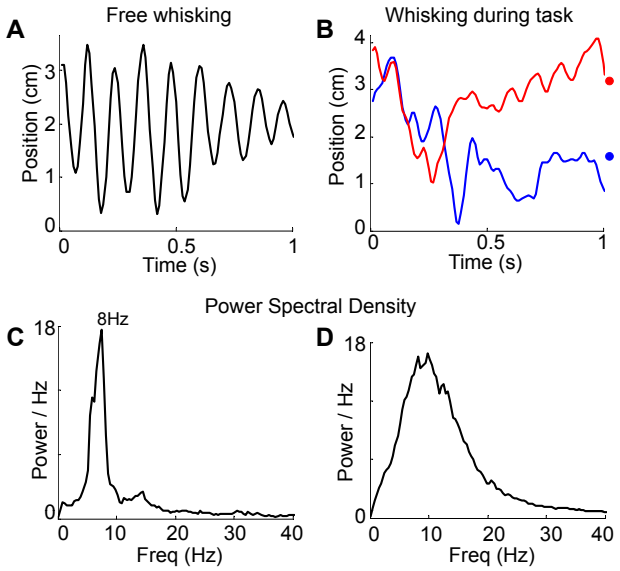

Figure 5.10: Whisking behavior. A. Example of exploratory whisking recorded in a head restrained rat induced by introduction of novel objects/scents near the head. B. Example of whisking during red and blue trials with time 0 indicating the tone and red and blue circles indicating target position. C. Power Spectral Density (PSD) of whisker velocity recorded from two rats during exploratory whisking. The whisking frequency is defined as the peak of the PSD. D. Average PSD of whisker velocity during task performance over 15 sessions. PSDs were calculated for individual trials and averaged.

during target localization and object discrimination lead to a wide distribution of whisking frequencies.

5.2.9 Tactile Percepts

While the previous experiment demonstrates that rats can detect target location as cued by cortical microstimulation, we were curious about the nature of the percept caused by this stimulation. Pioneering work in the monkey somatosensory system [127] has shown that microstimulation of quickly adapting cells can mimic the perception of flutter on fingers. Similar to [136], we asked whether rats would react similarly to physical whisker deflection and microstimulation of randomly sampled neurons in barrel cortex. To explore this question, we trained three rats on a variable interval microstimulation detection paradigm. Rats learned to detect the presence of microstimulation and lick the lickometer for a reward within 2 seconds on $>80\%$ of the trials. We then introduced catch trials (Fig. 5.11A) where a single whisker was magnetically deflected while the animal was waiting for microstimulation.

On the first day, we found that all three rats responded to whisker deflection at above chance

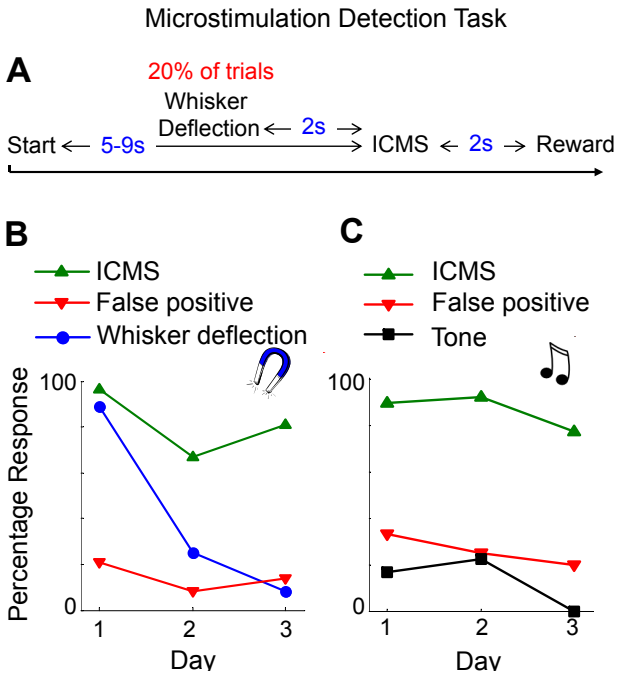

Figure 5.11: Perception of cortical microstimulation. A. Rats were trained to respond to ICMS presented after variable intervals with a lick. Licks were rewarded with water if they occurred within 2s after the ICMS. Once over-trained on this task, a whisker that mapped close to the location of the stimulating electrode was tagged with an iron particle. In 20% of the trials, a distracter was introduced in the form of magnetic deflection of the whisker while the rat was waiting for ICMS. Response to the distracter counted as a false positive in the variable interval stimulus detection task and led to a time-out. B. Responses of one rat to ICMS, whisker deflection and false positives over three days of training are shown. C. Example of performance in an identical task with whisker deflection replaced by a tone.

levels (Fig. 5.11B). It should be noted that rats were not rewarded for this response and were in fact punished with a time-out since this constituted a false positive on the microstimulation task. Over the next two days, all rats learned to stop responding to whisker deflection. This suggests that while whisker deflection and microstimulation of barrel cortex initially produce similar responses, they are not identical and can be discriminated. This agrees with our view that it is highly unlikely that stimulating large populations of neurons in barrel cortex should exactly mirror the percept of whisker deflection.

To ensure that rats were not demonstrating a startle response, we tested three rats (two of which were naive animals which hadn't participated in the magnetic deflection task) on an identical task where whisker deflection was replaced by an auditory tone and found that all three rats ignored the tone (Fig. 5.11C). If the response to whisker deflection that we observed was a non-specific stimulus response, we would expect a similar response to the tone stimulus. The fact that rats ignored the tone but responded to whisker deflection catch trials suggests that microstimulation in barrel cortex and physical whisker deflection are

perceptually similar. This agrees with previous studies in humans [35, 36, 37] which have reported that microstimulation of somatosensory regions evokes tactile percepts.

5.3 Discussion

5.3.1 Target Localization

Previous studies have suggested the rats can calculate the dorsoventral angle of objects [125] and can discriminate the distance of objects along the radial direction [120] in the absence of active whisking. However, the decoding of angle along the axis of vibrissa motion seems to require active whisking and sensorimotor integration [122, 123]. We believe that rats in our behavioral paradigm also locate software defined targets using sensorimotor integration; namely by integrating the timing of cortical microstimulation with knowledge of whisker position while actively whisking. This is supported by the rejection of the null hypothesis that the observed performance could be obtained without knowledge of target position (Fig. 5.3, 5.4).

Rats typically started whisking 120ms after the tone (t_{tone}), and the average whisker traces were statistically different (P$<$0.01) after 300ms. The time taken for whisker trajectories to diverge for different targets ($t_{diverge}$ - Fig. 5.4A) includes the intervals needed to respond to the tone, form a sensory percept and to modify whisking strategy, i.e., $t_{diverge} = t_{tone}+t_{perception}$. A $t_{diverge}$=300ms implies that rats inferred target location in $t_{diverge}-t_{tone} = 180ms$ which translates to one-two whisk cycles for rats whisking at 8-12Hz. Such a low $t_{perception}$ also rules out the use of a purely motor strategy where the rat slowly checks potential target locations. Further controls ruled out the use of inadvertent cues, motor twitches and head movements to infer target location. Thus we can conclude that actively whisking rats can integrate cortical microstimulation cues with their knowledge of whisker position to compute target location along the rostro-caudal axis. We believe that such behavioral paradigms, which precisely control sensory inputs based on animal movements, could shed new light on the mechanisms and neural circuitry underlying active sensing.

Rats performing our task achieve similar angular resolution to rats detecting the position of a physical object in head-centered coordinates [123] suggesting that they may be using a similar mechanism to perform the task. Under this assumption, we can infer details of the encoding scheme used. One potential encoding scheme is based on thalamic gating and phase-locked loops [137]. However, this scheme requires multiple rhythmic whisk cycles to establish a phase reference. The animals in our study did not show periodic sinusoidal whisking (Fig. 5.10) nor did rats in a similar experiment [123]. This ability to form a spatial percept from oscillatory but irregular vibrissa motion, within 1-2 cycles after whisking onset, argues against the use of phase-locked loops.

The other potential encoding scheme, which is consistent with our observations, is thought to consist of an array of coincidence detectors between cortical neurons which encode phase

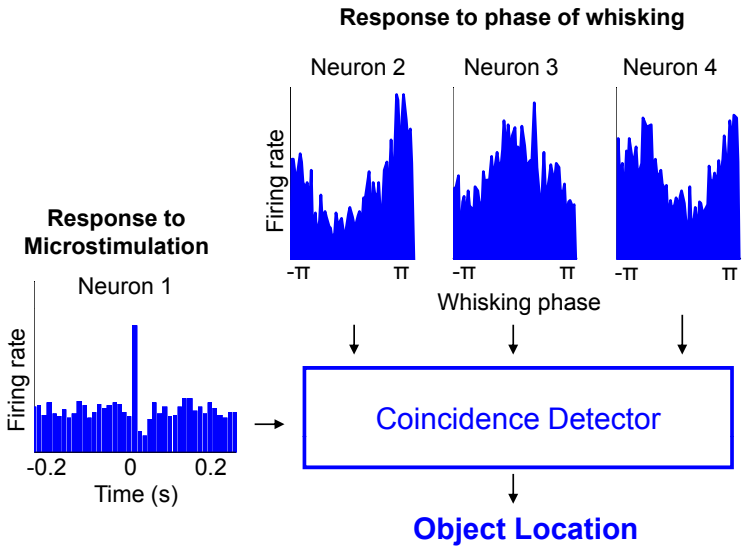

Figure 5.12: Neural Algorithm. All neural responses shown in this figure were recorded from chronically implanted electrodes in barrel cortex of awake behaving rats. Neuron 1 shows the typical response of cortical neurons to microstimulation (at time 0). Neurons tends to fire a brief burst of spikes soon after the microstimulation, shows a short inhibition and returns to baseline firing rate. Neurons 2, 3 and 4 show phase locking of firing rate to the phase of whisking but have different preferred phases. The firing rate of these neurons were recorded along with whisker traces during exploratory free whisking. One potential way to decode object location is to consider a coincidence detector between Neuron 1 and Neurons 2-4. The phase locking neuron which fires the highest number of spikes when microstimulation occurs encodes the phase of the software defined target.

of whisking and those that encode contact [137]. While the details of such a circuit are just being discovered [138], our results suggest that such a circuit must be able to replace specific contact signals from the trigeminal ganglia with neuronal firing induced by cortical microstimulation (Fig. 5.12).

5.3.2 Virtual Objects

The behavioral performance of rats in our task demonstrates that actively whisking rats can identify target location cued by cortical microstimulation. Moreover, rats trained to detect cortical microstimulation respond similarly to whisker deflections but not other stimuli, suggesting that microstimulation in barrel cortex induces tactile percepts. Taken together, these results suggest that rats performing the target localization task likely experience a tactile percept at a particular location in space; which we define as a 'virtual object'. Presumably this would feel similar but not identical to a physical object, since we are bypassing many lower level feedback loops which play important roles in active contact [139]. Moreover, we do

not imply that this percept would have other characteristics of physical objects like rigidity, roughness etc. Nevertheless, the ability to create virtual objects by integrating closed-loop cortical microstimulation of somatosensory areas with real-time tracking of limbs may have numerous applications.

Many researchers are exploring cortical microstimulation of somatosensory areas as a method to deliver such tactile feedback to users of motor prostheses. However, most research in this field has concentrated on encoding binary variables (left/right) using arbitrary associations [27, 38, 28]. We believe that the timing of microstimulation relative to actions of the user represents an excellent dimension along which information can be encoded using cortical microstimulation. For example, one could encode spatial locations, virtual textures, etc., by delivering temporal patterns of microstimulation based on limb position and velocity. Our results provide a proof of concept and suggest that one could integrate closed-loop microstimulation of somatosensory cortex with real-time tracking of prosthetic limbs to create virtual objects in space.

5.4 Conclusion

In summary, we describe a novel behavioral paradigm to study active sensing in rats by precisely controlling sensory inputs based on whisker movements. We found that rats could integrate knowledge of whisker position and timing of microstimulation to compute the spatial location of targets. This demonstration, that rats can perform sensorimotor integration with electrically delivered stimuli, might have significant implications for the future study of active sensing and for the development of sensory neuroprostheses.

Chapter 6

Conclusions and Future Directions

6.1 Conclusions

This dissertation describes technological and neuroscience advances in the quest to provide tactile feedback to users of neurally controlled prosthetic limbs. Providing such tactile feedback requires that we device ways to simultaneously record and stimulate neural activity at will and that we understand the neural and perceptual effects of such stimulation.

Two major technological challenges were addressed to enable chronically implanted stimulating and recording neural interfaces:

- New circuits and systems were developed to allow simultaneous recording and stimulation of neurons from chronically implanted electrode arrays in freely behaving rodents.
- Conductive polymer (PEDOT) electrodes were explored to provide safe and efficacious stimulation using implanted microelectrodes.

Since this research was aimed at awake, behaving rodents, it was essential to monitor rodent behavior in parallel with neural recordings. Towards this goal, two technologies were developed:

- Wireless accelerometers and neural network based algorithms were developed for tracking rodent behavior in a cage.
- To study rat whisking behavior, an OpenCV based software package was implemented that tracks rodent whiskers in real-time at 100 frames/second using a high speed video camera.

These tools and techniques were then used to study the behavioral and neural effects of microstimulation in rat barrel cortex. These results advance our understanding of behavioral modulation of the rat whisker system and present a novel behavioral paradigm to explore active sensing. Moreover, they also have significant implications for the future development of somatosensory neuroprostheses:

- It was discovered that microstimulation-evoked 15-18Hz oscillations in the rat thalamocortical loop are strongly modulated by motor activity.
- Further, it was demonstrated that rats can incorporate cortical microstimulation into an active sensing system and perform sensorimotor integration with electrically delivered stimuli.

6.2 Future Directions

Even with these advances, there remain many technological and neuroscience hurdles which need to be crossed before we can provide realistic tactile feedback to users of prosthetic limbs. Below are described two research directions which I believe will play major roles in this endeavor and in neural prostheses in general.

6.2.1 Stable Long-term Neural Recordings

The recording lifetime of implanted microelectrode arrays is approximately a year, after which the neural signals recorded from the electrodes degrade. Reactive tissue response to the implanted device is considered to be a primary cause of the drop in performance of these devices. The most common observation of the long-term response to chronically implanted electrodes is the formation of an encapsulation layer referred to as the 'glial scar' [55]. This seriously limits the potential clinical usefulness of such cortical implants since clinical adoption would typically require a lifetime of 10 years or more.

With different electrode array technologies, biocompatible materials, and implantation procedures available, various groups have designed novel electrodes in an attempt to minimize or evade the immune response [22, 23]. Investigators better acquainted with the molecular biology of the neural environment have added bioactive agents to the electrodes [140], while others have added microfluidics [24] to allow continuous delivery of anti-inflammatory drugs. A large research effort is proceeding in parallel to develop fully implanted wireless neural interfaces [141] and thus remove the wires connecting to the neural implant and associated infection risks and micromotion. It is possible that many such improvements added together will enable decades of chronic neural recording; however it is also possible that we will need a paradigm shift in chronic neural microelectrode design.

6.2.2 Optical Neural Interfaces

Electrical stimulation, similar to that described in this work, is currently being explored for a number of applications including deep brain stimulation (DBS) for parkinsons [4], cortical stimulation for epilepsy [142], and auditory [143], visual [33], motor control [29] and bladder control prostheses [144]. Thus different parts of this dissertation are likely to have an impact on many of these fields and it is expected that electrical stimulation of neurons will be used for therapeutic applications for many years to come.

As mentioned in the beginning of this dissertation, we have used such electrical neural interfaces for the last two centuries. However, recent years have seen the development of a new generation of neural interfaces based on optical recording and stimulation. A number of optical recording techniques have been developed including voltage sensitive dyes [145] and calcium imaging [146]. Currently, these technologies do not have the combined spatial resolution (1μm) and temporal resolution (1ms) desired for neural applications but many groups are working on exactly such a dye. Such an imaging modality would be revolutionary since it would provide us with single neuron spatial resolution and single spike temporal resolution.

A number of optogenetic techniques [147] based on channelrhodopsin and halorhodopsin have been recently reported for exciting and inhibiting selective neurons using light. This technique also promises to be revolutionary because it allows us to target particular kinds of neurons (like excitatory pyramidal neurons) as opposed to microstimulation which indiscriminately excites all nearby neurons. However, a major stumbling block before this technology reaches patient populations is the requirement to genetically modify neurons in the subject. While this is routinely possible in rodents, it is just being explored in non-human primates [148] and might take some time to gain regulatory approval in humans.

An optical neural interface might consist of a setup similar to a mini two-photon confocal microscope mounted over a craniectomy, recording and stimulating many thousands of neurons in a small patch of cortex. This will allow us to record every spike from every neuron in a small patch of the brain, truly understand the working of neural ensembles, stimulate single spikes in single neurons and watch how it affects the ensemble, and truly 'crack the neural code'. Obviously, such a technology would also have profound implications for the treatment of various neurological disorders like Parkinson's, depression etc., and for building next generation neural prostheses. I believe that this research has the potential to radically improve our understanding of the brain and someday provide us with the ability to seamlessly interface with it.

Bibliography

[1] R. Fowler, *Experiments and observations relative to the influence lately discovered by M. Galvani and commonly called Animal Electricity*. Edinburgh: T. Duncan, P. Hill, Robertson, 1793.

[2] E. J. Tehovnik, A. S. Tolias, F. Sultan, W. M. Slocum, and N. K. Logothetis, "Direct and indirect activation of cortical neurons by electrical microstimulation," *J. Neurophysiol.*, vol. 96, no. 2, pp. 512-521, 2006.

[3] M. Massimini, F. Ferrarelli, R. Huber, S. K. Esser, H. Singh, and G. Tononi, "Breakdown of cortical effective connectivity during sleep," *Science*, vol. 309, pp. 2228–2232, Sept. 2005.

[4] M. L. Kringelbach, N. Jenkinson, S. L. Owen, and T. Z. Aziz, "Translational principles of deep brain stimulation," *Nat Rev Neurosci*, vol. 8, no. 8, pp. 623–635, 2007.

[5] M. Chorost, *Rebuilt: How Becoming Part Computer Made Me More Human*. Houghton Mifflin Harcourt, 2005.

[6] J. D. Weiland, W. Liu, and M. S. Humayun, "Retinal prosthesis," *Annual Review of Biomedical Engineering*, vol. 7, no. 1, pp. 361–401, 2005.

[7] M. A. Lebedev and M. A. Nicolelis, "Brain-machine interfaces: past, present and future," *Trends Neurosci.*, vol. 29, no. 9, pp. 536–546, 2006.

[8] M. A. L. Nicolelis, D. Dimitrov, J. M. Carmena, R. Crist, G. Lehew, J. D. Kralik, and S. P. Wise, "Chronic, multisite, multielectrode recordings in macaque monkeys," *Proc. Natl. Acad. Sci. USA*, vol. 100, no. 19, pp. 11041-11046, 2003.

[9] C. T. Nordhausen, P. J. Rousche, and R. A. Normann, "Optimizing recording capabilities of the utah intracortical electrode array," *Brain Research*, vol. 637, no. 1-2, pp. 27-36, 1994.

[10] J. K. Chapin, K. A. Moxon, R. S. Markowitz, and M. A. L. Nicolelis, "Real-time control of a robot arm using simultaneously recorded neurons in the motor cortex," *Nature Neuroscience*, vol. 2, pp. 664-670, 1999.

[11] M. D. Serruya, N. G. Hatsopoulos, L. Paninski, M. R. Fellows, and J. P. Donoghue, "Brain-machine interface: Instant neural control of a movement signal," *Nature*, vol. 416, pp. 141-142, Mar. 2002.

[12] D. M. Taylor, S. I. H. Tillery, and A. B. Schwartz, "Direct cortical control of 3D neuroprosthetic devices," *Science*, vol. 296, pp. 1829-1832, June 2002.

[13] J. M. Carmena, M. A. Lebedev, R. E. Crist, J. E. O'Doherty, D. M. Santucci, D. F. Dimitrov, P. G. Patil, C. S. Henriquez, and M. A. L. Nicolelis, "Learning to control a BrainMachine interface for reaching and grasping by primates," *PLoS Biol*, vol. 1, pp. e42, Oct. 2003.

[14] M. Velliste, S. Perel, M. C. Spalding, A. S. Whitford, and A. B. Schwartz, "Cortical control of a prosthetic arm for self-feeding," *Nature*, vol. 453, pp. 1098-1101, June 2008.

[15] L. R. Hochberg, M. D. Serruya, G. M. Friehs, J. A. Mukand, M. Saleh, A. H. Caplan, A. Branner, D. Chen, R. D. Penn, and J. P. Donoghue, "Neuronal ensemble control of prosthetic devices by a human with tetraplegia," *Nature*, vol. 442, pp. 164-171, July 2006.

[16] A. B. Schwartz, "Cortical neural prosthetics.," *Annual Review of Neuroscience*, vol. 27, pp. 487–507, 2004.

[17] N. G. Hatsopoulos and J. P. Donoghue, "The science of neural interface systems," *Annual Review of Neuroscience*, vol. 32, no. 1, pp. 249-266, 2009.

[18] A. Abbott, "Neuroprosthetics: In search of the sixth sense," *Nature*, vol. 442, pp. 125-127, July 2006.

[19] E. Kandel, J. Schwartz, and T. Jessell, *Principles of Neural Science*. McGraw-Hill, 2000.

[20] M. Miller, ed., *Brain Facts*. Society for Neuroscience, 2008.

[21] K. Drake, K. Wise, J. Farraye, D. Anderson, and S. BeMent, "Performance of planar multisite microprobes in recording extracellular single-unit intracortical activity," *IEEE Transactions on Biomedical Engineering*, vol. 35, no. 9, pp. 719-732, 1988.

[22] J. Seymour and D. Kipke, "Open-architecture neural probes reduce cellular encapsulation," *Materials Research Society Symposium 2006*, vol. 926, 2006.

[23] A. Mercanzini, K. Cheung, D. Buhl, M. Boers, A. Maillard, P. Colin, J. Bensadoun, A. Bertsch, A. Carleton, and P. Renaud, "Demonstration of cortical recording and reduced inflammatory response using flexible polymer neural probes," in *20th International Conference on Micro Electro Mechanical Systems, MEMS 2007*, pp. 573–576, 2007.

[24] S. Retterer, K. Smith, C. Bjornsson, K. Neeves, A. Spence, J. Turner, W. Shain, and M. Isaacson, "Model neural prostheses with integrated microfluidics: a potential intervention strategy for controlling reactive cell and tissue responses," *IEEE Transactions on Biomedical Engineering*, vol. 51, no. 11, pp. 2063–2073, 2004.

[25] S. F. Cogan, "Neural stimulation and recording electrodes," *Annual Review of Biomedical Engineering*, vol. 10, no. 1, pp. 275–309, 2008.

[26] C. C. Petersen, "The functional organization of the barrel cortex," *Neuron*, vol. 56, pp. 339-355, Oct. 2007.

[27] S. K. Talwar, S. Xu, E. S. Hawley, S. A. Weiss, K. A. Moxon, and J. K. Chapin, "Rat navigation guided by remote control," *Nature*, vol. 417, no. 6884, pp. 37-38, 2002.

[28] G. Fridman, H. Blair, A. Blaisdell, and J. Judy, "Somatosensory feedback for Brain-Machine interfaces: Perceptual model and experiments in rat whisker somatosensory cortex," in *3rd International IEEE/EMBS Conference on Neural Engineering, 2007*, pp. 379–385, 2007.

[29] M. S. A. Graziano, C. S. R. Taylor, and T. Moore, "Complex movements evoked by microstimulation of precentral cortex," *Neuron*, vol. 34, no. 5, pp. 841–851, 2002.

[30] C. D. Salzman, K. H. Britten, and W. T. Newsome, "Cortical microstimulation influences perceptual judgements of motion direction," *Nature*, vol. 346, no. 6280, pp. 174–177, 1990.

[31] S. Afraz, R. Kiani, and H. Esteky, "Microstimulation of inferotemporal cortex influences face categorization," *Nature*, vol. 442, no. 7103, pp. 692-695, 2006.

[32] W. Penfield, *Epilepsy and Cerebral Localization: A Study of the Mechanism, Treatment and Prevention of Epileptic Seizures.* C.C. Thomas, 1941.

[33] J. R. Bartlett, E. A. DeYoe, R. W. Doty, B. B. Lee, J. D. Lewine, N. Negrao, and W. H. Overman, "Psychophysics of electrical stimulation of striate cortex in macaques," *J Neurophysiol*, vol. 94, no. 5, pp. 3430–3442, 2005.

[34] R. Romo, A. Hernandez, A. Zainos, and E. Salinas, "Somatosensory discrimination based on cortical microstimulation," *Nature*, vol. 392, no. 6674, pp. 387-390, 1998.

[35] K. D. Davis, Z. H. Kiss, R. R. Tasker, and J. O. Dostrovsky, "Thalamic stimulation-evoked sensations in chronic pain patients and in nonpain (movement disorder) patients," *J. Neurophysiol.*, vol. 75, no. 3, pp. 1026-1037, 1996.

[36] S. Ohara, N. Weiss, and F. A. Lenz, "Microstimulation in the region of the human thalamic principal somatic sensory nucleus evokes sensations like those of mechanical stimulation and movement," *J. Neurophysiol.*, vol. 91, no. 2, pp. 736-745, 2004.

[37] H. T. Z. Kiss, T. Anderson, T. Hansen, D. Kirstein, O. Suchowersky, and B. Hu, "Neural substrates of microstimulation-evoked tingling: a chronaxie study in human somatosensory thalamus," *Eur. J. Neurosci.*, vol. 18, no. 3, pp. 728–732, 2003.

[38] N. A. Fitzsimmons, W. Drake, T. L. Hanson, M. A. Lebedev, and M. A. L. Nicolelis, "Primate reaching cued by multichannel spatiotemporal cortical microstimulation," *J. Neurosci.*, vol. 27, no. 21, pp. 5593–5602, 2007.

[39] K. J. Otto, P. J. Rousche, and D. R. Kipke, "Cortical microstimulation in auditory cortex of rat elicits best-frequency dependent behaviors," *J. Neural Eng.*, vol. 2, no. 2, pp. 42–51, 2005.

[40] S. Butovas and C. Schwarz, "Spatiotemporal effects of microstimulation in rat neocortex: A parametric study using multielectrode recordings," *J. Neurophysiol.*, vol. 90, no. 5, pp. 3024-3039, 2003.

[41] J. Freeman, "An electronic stimulus artifact suppressor," *Electroencephalography and clinical neurophysiology*, vol. 31, no. 2, pp. 170–172, 1971.

[42] Y. Jimbo, N. Kasai, K. Torimitsu, T. Tateno, and H. Robinson, "A system for MEA-based multisite stimulation," *IEEE Transactions on Biomedical Engineering*, vol. 50, no. 2, pp. 241–248, 2003.

[43] D. A. Wagenaar and S. M. Potter, "Real-time multi-channel stimulus artifact suppression by local curve fitting," *Journal of Neuroscience Methods*, vol. 120, pp. 113–120, Oct. 2002.

[44] M. Knaflitz and R. Merletti, "Suppression of simulation artifacts from myoelectric-evoked potential recordings," *IEEE Transactions on Biomedical Engineering*, vol. 35, no. 9, pp. 758–763, 1988.

[45] R. Blum, J. Ross, E. Brown, and S. DeWeerth, "An analog VLSI stimulation and recording system for extracelluar interfacing," in *2nd International IEEE EMBS Conference on Neural Engineering, 2005*, pp. 381–384, 2005.

[46] R. Harrison and C. Charles, "A low-power low-noise CMOS amplifier for neural recording applications," *IEEE J. Solid-State Circuits*, vol. 38, no. 6, pp. 958–965, 2003.

[47] P. Mohseni and K. Najafi, "A fully integrated neural recording amplifier with DC input stabilization," *IEEE Trans. Biomed. Eng.*, vol. 51, no. 5, pp. 832–837, 2004.

[48] T. Denison, K. Consoer, W. Santa, A. Avestruz, J. Cooley, and A. Kelly, "A 2 μW 100 nV/rtHz Chopper-Stabilized instrumentation amplifier for chronic measurement of neural field potentials," *IEEE J. Solid-State Circuits*, vol. 42, no. 12, pp. 2934–2945, 2007.

[49] S. Venkatraman, C. Patten, and J. Carmena, "Exploiting the 1/f structure of neural signals for the design of integrated neural amplifiers," in *Proceedings of the IEEE Engineering in Medicine and Biology Society, EMBC 2009*, pp. 2050–2053, Sept. 2009.

[50] D. Merrill, M. Bikson, and J. Jefferys, "Electrical stimulation of excitable tissue: design of efficacious and safe protocols," *Journal of Neuroscience Methods*, vol. 141, no. 2, pp. 171-198, 2005.

[51] Y. Xiao, X. Cui, and D. C. Martin, "Electrochemical polymerization and properties of PEDOT/S-EDOT on neural microelectrode arrays," *Journal of Electroanalytical Chemistry*, vol. 573, no. 1, pp. 43-48, 2004.

[52] K. A. Ludwig, J. D. Uram, J. Yang, D. C. Martin, and D. R. Kipke, "Chronic neural recordings using silicon microelectrode arrays electrochemically deposited with a poly(3,4-ethylenedioxythiophene) (PEDOT) film," *Journal of Neural Engineering*, vol. 3, no. 1, pp. 59-70, 2006.

[53] S. A. M. Marzouk, S. Ufer, R. P. Buck, T. A. Johnson, L. A. Dunlap, and W. E. Cascio, "Electrodeposited iridium oxide pH electrode for measurement of extracellular myocardial acidosis during acute ischemia," *Analytical Chemistry*, vol. 70, no. 23, pp. 5054-5061, 1998.

[54] S. F. Cogan, P. R. Troyk, J. Ehrlich, and T. D. Plante, "In vitro comparison of Charge-Injection limits of activated iridium oxide (AIROF) and Platinum-Iridium microelectrodes," *IEEE Transactions on Biomedical Engineering*, vol. 52, no. 9, pp. 1614–1612, 2005.

[55] V. Polikov, P. Tresco, and W. Reichert, "Response of brain tissue to chronically implanted neural electrodes," *Journal of Neuroscience Methods*, vol. 148, no. 1, pp. 1-18, 2005.

[56] M. A. L. Nicolelis, A. A. Ghazanfar, B. M. Faggin, S. Votaw, and L. M. O. Oliveira, "Reconstructing the engram: Simultaneous, multisite, many single neuron recordings," *Neuron*, vol. 18, pp. 529-537, Apr. 1997.

[57] S. F. Cogan, "In vivo and in vitro differences in charge-injection and electrochemical properties of iridium oxide electrodes," in *Proceedings of the IEEE Engineering in Medicine and Biology Society, 2006*, pp. 82–885, 2006.

[58] S. Venkatraman, J. D. Long, K. Elkabany, Y. Yao, and J. M. Carmena, "A system for neural recording and closed-loop intracortical microstimulation in awake rodents," *IEEE Trans. Biomed. Eng.*, vol. 56, no. 15, 2009.

[59] S. Venkatraman, J. Hendricks, S. Richardson-Burns, E. Jan, D. Martin, and J. Carmena, "PEDOT coated microelectrode arrays for chronic neural recording and stimulation," in *4th International IEEE/EMBS Conference on Neural Engineering, 2009*, pp. 383–386, 2009.

[60] S. Belongie, K. Branson, P. Dollr, and V. Rabaud, "Monitoring animal behavior in the smart vivarium," in *Measuring Behavior*, (Wageningen, NL), pp. 70-72, 2005.

[61] C. J. Twining, C. J. Taylor, and P. Courtney, "Robust tracking and posture description for laboratory rodents using active shape models," *Behavior Research Methods, Instruments, & Computers*, vol. 33, no. 3, pp. 381-391, 2001.

[62] K. Austin and G. Rose, "Automated behavior recognition using continuous-wave doppler radar and neural networks," in *Proc. IEEE Engineering in Medicine and Biology Society, 1997*, vol. 4, pp. 1458-1461, 1997.

[63] S. Yamashita, T. Shimura, K. Aiki, K. Ara, Y. Ogata, I. Shimokawa, T. Tanaka, H. Kuriyama, K. Shimada, and K. Yano, "A 15/spl times/15 mm, 1 /spl mu/A, reliable sensor-net module: enabling application-specific nodes," in *Information Processing in Sensor Networks, 2006. IPSN 2006. The Fifth International Conference on*, pp. 383-390, 2006.

[64] K. Yoda, Y. Naito, K. Sato, A. Takahashi, J. Nishikawa, Y. Ropert-Coudert, M. Kurita, and Y. L. Maho, "A new technique for monitoring the behaviour of free-ranging adelie penguins," *J Exp Biol*, vol. 204, pp. 685-690, Feb. 2001.

[65] T. Pfau, T. H. Witte, and A. M. Wilson, "A method for deriving displacement data during cyclical movement using an inertial sensor," *J Exp Biol*, vol. 208, pp. 2503–2514, July 2005.

[66] C. Park and P. Chou, "Eco: ultra-wearable and expandable wireless sensor platform," in *International Workshop on Wearable and Implantable Body Sensor Networks*, 2006.

[67] L. Bao, *Physical Activity Recognition from Acceleration Data under Semi-Naturalistic Conditions*. PhD thesis, MIT, 2003.

[68] B. J. Hyland and J. N. Reynolds, "Pattern of activity in muscles of shoulder and elbow during forelimb reaching in the rat," *Human movement science*, vol. 12, pp. 51-69, 1993.

[69] J. Voigts, B. Sakmann, and T. Celikel, "Unsupervised whisker tracking in unrestrained behaving animals," *J Neurophysiol*, vol. 100, pp. 504-515, July 2008.

[70] P. M. Knutsen, D. Derdikman, and E. Ahissar, "Tracking whisker and head movements in unrestrained behaving rodents," *J Neurophysiol*, vol. 93, pp. 2294–2301, Apr. 2005.

[71] T. B. Moeslund, A. Hilton, and V. Kruger, "A survey of advances in vision-based human motion capture and analysis," *Comput. Vis. Image Underst.*, vol. 104, no. 2, pp. 90–126, 2006.

[72] A. Blake and M. Isard, "3D position, attitude and shape input using video tracking of hands and lips," in *Proceedings of the 21st annual conference on Computer graphics and interactive techniques*, pp. 185–192, ACM, 1994.

[73] S. Soliman, "Linear kalman filter algorithm for analysis of transient stability swings in large interconnected power systems," *Fuel and Energy Abstracts*, vol. 37, pp. 110, Mar. 1996.

[74] S. Venkatraman, J. Long, K. Pister, and J. Carmena, "Wireless inertial sensors for monitoring animal behavior," in *Proc. IEEE Engineering in Medicine and Biology Society, 2007*, pp. 378–381, 2007.

[75] E. J. Tehovnik, W. M. Slocum, and C. E. Carvey, "Behavioural state affects saccadic eye movements evoked by microstimulation of striate cortex," *Eur. J. Neurosci.*, vol. 18, no. 4, pp. 969-979, 2003.

[76] D. Contreras, A. Destexhe, T. J. Sejnowski, and M. Steriade, "Spatiotemporal patterns of spindle oscillations in cortex and thalamus," *J. Neurosci.*, vol. 17, no. 3, pp. 1179-1196, 1997.

[77] D. Contreras and M. Steriade, "Spindle oscillations in cats: The role of corticothalamic feedback in a thalamically generated rhythm," *J. Physiol.*, vol. 490, pp. 159-179, 1996.

[78] N. Cotillon and J. Edeline, "Tone-evoked oscillations in the rat auditory cortex result from interactions between the thalamus and reticular nucleus," *Eur. J. Neurosci.*, vol. 12, no. 10, pp. 3637-3650, 2000.

[79] N. Cotillon-Williams and J. Edeline, "Evoked oscillations in unit recordings from the thalamo-cortical auditory system: an aspect of temporal processing or the reflection of hyperpolarized brain states?," *Acta Neurobiol Exp*, vol. 64, pp. 253-270, 2004.

[80] H. Shin and J. Chapin, "Movement induced modulation of afferent transmission to single neurons in the ventroposterior thalamus and somatosensory cortex in rat," *Exp. Brain Res.*, vol. 81, no. 3, pp. 515-522, 1990.

[81] I. Ferezou, F. Haiss, L. J. Gentet, R. Aronoff, B. Weber, and C. C. Petersen, "Spatiotemporal dynamics of cortical sensorimotor integration in behaving mice," *Neuron*, vol. 56, pp. 907-923, Dec. 2007.

[82] W. J. Freeman, *Neurodynamics: An exploration of Mesoscopic Brain Dynamics*. London UK: Springer, 2000.

[83] A. Kandel and G. Buzsaki, "Cellular-Synaptic generation of sleep spindles, Spike-and-Wave discharges, and evoked thalamocortical responses in the neocortex of the rat," *J. Neurosci.*, vol. 17, no. 17, pp. 6783-6797, 1997.

[84] S. Butovas, S. G. Hormuzdi, H. Monyer, and C. Schwarz, "Effects of electrically coupled inhibitory networks on local neuronal responses to intracortical microstimulation," *J. Neurophysiol.*, vol. 96, no. 3, pp. 1227-1236, 2006.

[85] D. A. McCormick and T. Bal, "SLEEP AND AROUSAL: thalamocortical mechanisms," *Annu. Rev. Neurosci.*, vol. 20, no. 1, pp. 185-215, 1997.

[86] M. A. Castro-Alamancos, "Dynamics of sensory thalamocortical synaptic networks during information processing states," *Prog. Neurobio.*, vol. 74, pp. 213-247, Nov. 2004.

[87] H. Hentschke, F. Haiss, and C. Schwarz, "Central signals rapidly switch tactile processing in rat barrel cortex during whisker movements," *Cereb. Cortex*, vol. 16, no. 8, pp. 1142-1156, 2006.

[88] M. Steriade, E. Jones, and R. R. Llinas, *Thalamic oscillations and signaling*. Wiley-Interscience, 1990.

[89] P. Fuentealba, I. Timofeev, and M. Steriade, "Prolonged hyperpolarizing potentials prececde spindle oscillations in the thalamic reticular nucleus," *Proc. Natl. Acad. Sci. USA*, vol. 101, no. 26, pp. 9816-9821, 2004.

[90] F. Shaw, "7-12 hz High-Voltage rhythmic spike discharges in rats evaluated by antiepileptic drugs and flicker stimulation," *J. Neurophysiol.*, vol. 97, no. 1, pp. 238-247, 2007.

[91] M. A. L. Nicolelis and E. E. Fanselow, "Thalamocortical optimization of tactile processing according to behavioral state," *Nat. Neurosci.*, vol. 5, no. 6, pp. 517-524, 2002.

[92] K. M. Kelly, "Spike-wave discharges: Absence or not, a common finding in common laboratory rats," *Epilepsy Currents*, vol. 4, no. 5, pp. 176-177, 2004.

[93] A. Destexhe, D. McCornick, and T. J. Sejnowski, "A model for 8-10Hz spindling in interconnected thalamic relay and reticularis neurons," *Biophysical Journal*, vol. 65, pp. 2473-2477, Dec. 1993.

[94] X. J. Wang, D. Golomb, and J. Rinzel, "Emergent spindle oscillations and intermittent burst firing in a thalamic model: specific neuronal mechanisms," *Proc. Natl. Acad. Sci. USA*, vol. 92, no. 12, pp. 5577-5581, 1995.

[95] P. Suffczynski, S. Kalitzin, and F. L. D. Silva, "Dynamics of non-convulsive epileptic phenomena modeled by a bistable neuronal network," *J. Neurosci.*, vol. 126, no. 2, pp. 467-484, 2004.

[96] S. Venkatraman and J. M. Carmena, "Behavioral modulation of stimulus-evoked oscillations in barrel cortex of alert rats," *Frontiers of Integrative Neuroscience*, vol. 3, no. 10, 2009.

[97] D. McCormick, "Neurotransmitter actions in the thalamus and cerebral cortex and their role in neuromodulation of thalamocortical activity," *Progress in Neurobiology*, vol. 39, no. 4, pp. 335-388, 1992.

[98] P. Fuentealba and M. Steriade, "The reticular nucleus revisited: Intrinsic and network properties of a thalamic pacemaker," *Prog. Neurobio.*, vol. 75, pp. 125-141, Feb. 2005.

[99] K. H. Lee and D. A. McCormick, "Abolition of spindle oscillations by serotonin and norepinephrine in the ferret lateral geniculate and perigeniculate nuclei in vitro," *Neuron*, vol. 17, no. 2, pp. 309-321, 1996.

[100] E. E. Fanselow and M. A. L. Nicolelis, "Behavioral modulation of tactile responses in the rat somatosensory system," *J. Neurosci.*, vol. 19, no. 17, pp. 7603-7616, 1999.

[101] S. Lee, G. E. Carvell, and D. J. Simons, "Motor modulation of afferent somatosensory circuits," *Nat. Neurosci.*, vol. 11, pp. 1430-1438, Dec. 2008.

[102] E. Ahissar, D. Derdikman, R. Hildesheim, A. Arieli, and A. Grinvald, "Imaging spatiotemporal dynamics of surround inhibition in the barrels somatosensory cortex," *J. Neurosci.*, vol. 23, no. 8, pp. 3100-3105, 2003.

[103] J. Muthuswamy, P. Tran, R. Rangarajan, F. A. Lenz, D. F. Hanley, and N. V. Thakor, "Somatosensory stimulus entrains spindle oscillations in the thalamic VPL nucleus in barbiturate anesthetized rats," *Neurosci. Lett.*, vol. 262, pp. 191-194, 1999.

[104] S. Sherman, "Tonic and burst firing: dual modes of thalamocortical relay," *Trends Neurosci.*, vol. 24, pp. 122-126, Feb. 2001.

[105] R. R. Llinas and M. Steriade, "Bursting of thalamic neurons and states of vigilance," *J. Neurophysiol.*, vol. 95, no. 6, pp. 3297-3308, 2006.

[106] H. R. Dinse, K. Kruger, A. C. Akhavan, F. Spengler, G. Schoner, and C. E. Schreiner, "Low-frequency oscillations of visual, auditory and somatosensory cortical neurons evoked by sensory stimulation," *J. Psychophysiology*, vol. 26, pp. 205-227, June 1997.

[107] A. G. Siapas and M. A. Wilson, "Coordinated interactions between hippocampal ripples and cortical spindles during Slow-Wave sleep," *Neuron*, vol. 21, pp. 1123-1128, Nov. 1998.

[108] F. Grenier, I. Timofeev, and M. Steriade, "Leading role of thalamic over cortical neurons during postinhibitory rebound excitation," *Proc. Natl. Acad. Sci. USA*, vol. 95, no. 23, pp. 13929-13934, 1998.

[109] E. von Holst, "Relations between the central nervous system and the peripheral organs," *The British Journal of Animal Behaviour*, vol. 2, pp. 89–94, July 1954.

[110] J. J. Gibson, *The Senses Considered as Perceptual Systems*. Boston, MA: Hougton Mifflin, 1966.

[111] E. Ahissar and A. Arieli, "Figuring space by time," *Neuron*, vol. 32, no. 2, pp. 185–201, 2001.

[112] J. Scheibert, S. Leurent, A. Prevost, and G. Debregeas, "The role of fingerprints in the coding of tactile information probed with a biomimetic sensor," *Science*, vol. 323, pp. 1503–1506, Mar. 2009.

[113] G. Carvell and D. Simons, "Biometric analyses of vibrissal tactile discrimination in the rat," *J. Neurosci.*, vol. 10, pp. 2638–2648, Aug. 1990.

[114] D. Kleinfeld, E. Ahissar, and M. E. Diamond, "Active sensation: insights from the rodent vibrissa sensorimotor system," *Curr. Opin. Neurobiol.*, vol. 16, no. 4, pp. 435–444, 2006.

[115] J. T. Ritt, M. L. Andermann, and C. I. Moore, "Embodied information processing: Vibrissa mechanics and texture features shape micromotions in actively sensing rats," *Neuron*, vol. 57, no. 4, pp. 599–613, 2008.

[116] M. Harvey, R. Bermejo, and H. Zeigler, "Discriminative whisking in the head-fixed rat: optoelectronic monitoring during tactile detection and discrimination tasks," *Somatosen. Mot. Res.*, vol. 18, no. 3, pp. 211–222, 2001.

[117] E. W. Jenkinson and M. Glickstein, "Whiskers, barrels, and cortical efferent pathways in gap crossing by rats," *J Neurophysiol*, vol. 84, pp. 1781–1789, Oct. 2000.

[118] E. Guic-Robles, C. Valdivieso, and G. Guajardo, "Rats can learn a roughness discrimination using only their vibrissal system," *Behavioural Brain Research*, vol. 31, no. 3, pp. 285–289, 1989.

[119] M. von Heimendahl, P. M. Itskov, E. Arabzadeh, and M. E. Diamond, "Neuronal activity in rat barrel cortex underlying texture discrimination," *PLoS Biology*, vol. 5, no. 11, pp. e305, 2007.

[120] D. J. Krupa, M. C. Wiest, M. G. Shuler, M. Laubach, and M. A. L. Nicolelis, "Layer-specific somatosensory cortical activation during active tactile discrimination," *Science*, vol. 304, no. 5679, pp. 1989–1992, 2004.

[121] D. B. Polley, J. L. Rickert, and R. D. Frostig, "Whisker-based discrimination of object orientation determined with a rapid training paradigm," *Neurobiology of Learning and Memory*, vol. 83, pp. 134–142, Mar. 2005.

[122] P. M. Knutsen, M. Pietr, and E. Ahissar, "Haptic object localization in the vibrissal system: Behavior and performance," *J. Neurosci.*, vol. 26, pp. 8451–8464, Aug. 2006.

[123] S. B. Mehta, D. Whitmer, R. Figueroa, B. A. Williams, and D. Kleinfeld, "Active spatial perception in the vibrissa scanning sensorimotor system," *PLoS Biology*, vol. 5, no. 2, 2007.

[124] M. Hartmann, "Active sensing capabilities of the rat whisker system," *Autonomous Robots*, vol. 11, pp. 249–254, 2001.

[125] M. E. Diamond, M. von Heimendahl, P. M. Knutsen, D. Kleinfeld, and E. Ahissar, "'Where' and 'what' in the whisker sensorimotor system," *Nat. Rev. Neurosci.*, vol. 9, no. 9, pp. 601–612, 2008.

[126] P. Gao, B. O. Ploog, and H. P. Zeigler, "Whisking as a 'voluntary' response: operant control of whisking parameters and effects of whisker denervation," *Somatosensory and Motor Research*, vol. 20, no. 3, pp. 179–189, 2003.

[127] R. Romo, A. Hernndez, A. Zainos, C. D. Brody, and L. Lemus, "Sensing without touching: Psychophysical performance based on cortical microstimulation," *Neuron*, vol. 26, pp. 273–278, Apr. 2000.

[128] B. London, L. Jordan, C. Jackson, and L. Miller, "Electrical stimulation of the proprioceptive cortex (Area 3a) used to instruct a behaving monkey," *IEEE Transactions on Neural Systems and Rehabilitation Engineering*, vol. 16, no. 1, pp. 32–36, 2008.

[129] A. R. Houweling and M. Brecht, "Behavioural report of single neuron stimulation in somatosensory cortex," *Nature*, vol. 451, pp. 65–68, 2008.

[130] D. Huber, L. Petreanu, N. Ghitani, S. Ranade, T. Hromadka, Z. F. Mainen, and K. Svoboda, "Sparse optical microstimulation in barrel cortex drives learned behaviour in freely moving mice," *Nature*, vol. 451, pp. 61–64, 2008.

[131] H. Maei, K. Zaslavsky, C. Teixeira, and P. Frankland, "What is the most sensitive measure of water maze probe test performance?," *Front. Integr. Neurosci.*, vol. 3, no. 4, 2009.

[132] R. N. S. Sachdev, T. Sato, and F. F. Ebner, "Divergent movement of adjacent whiskers," *J. Neurophysiol.*, vol. 87, no. 3, pp. 1440–1448, 2002.

[133] M. H. Histed, V. Bonin, and R. C. Reid, "Direct activation of sparse, distributed populations of cortical neurons by electrical microstimulation," *Neuron*, vol. 63, pp. 508–522, Aug. 2009.

[134] Y. Gioanni and M. Lamarche, "A reappraisal of rat motor cortex organization by intracortical microstimulation," *Brain Research*, vol. 344, pp. 49–61, Sept. 1985.

[135] S. Butovas and C. Schwarz, "Detection psychophysics of intracortical microstimulation in rat primary somatosensory cortex," *Eur. J. Neurosci.*, vol. 25, no. 7, pp. 2161–2169, 2007.

[136] R. Leal-Campanario, J. M. Delgado-Garca, and A. Gruart, "Microstimulation of the somatosensory cortex can substitute for vibrissa stimulation during pavlovian conditioning," *Proc. Natl. Acad. Sci. USA*, vol. 103, no. 26, pp. 10052–10057, 2006.

[137] M. Szwed, K. Bagdasarian, and E. Ahissar, "Encoding of vibrissal active touch," *Neuron*, vol. 40, no. 3, pp. 621–630, 2003.

[138] J. C. Curtis and D. Kleinfeld, "Phase-to-rate transformations encode touch in cortical neurons of a scanning sensorimotor system," *Nat Neurosci*, vol. 12, pp. 492–501, Apr. 2009.

[139] Q. Nguyen and D. Kleinfeld, "Positive feedback in a brainstem tactile sensorimotor loop," *Neuron*, vol. 45, no. 3, pp. 447–457, 2005.

[140] Y. Zhong and R. V. Bellamkonda, "Dexamethasone-coated neural probes elicit attenuated inflammatory response and neuronal loss compared to uncoated neural probes," *Brain Research*, vol. 1148, pp. 15–27, May 2007.

[141] R. R. Harrison, P. T. Watkins, R. J. Kier, R. O. Lovejoy, D. J. Black, B. Greger, and F. Solzbacher, "A Low-Power integrated circuit for a wireless 100-Electrode neural recording system," *IEEE J. Solid-State Circuits*, vol. 42, no. 1, pp. 123–133, 2007.

[142] M. Kinoshita, A. Ikeda, M. Matsuhashi, R. Matsumoto, T. Hitomi, T. Begum, K. Usui, M. Takayama, N. Mikuni, S. Miyamoto, N. Hashimoto, and H. Shibasaki, "Electric cortical stimulation suppresses epileptic and background activities in neocortical epilepsy and mesial temporal lobe epilepsy," *Clinical neurophysiology : official journal of the International Federation of Clinical Neurophysiology*, vol. 116, pp. 1291–1299, June 2005.

[143] K. J. Otto, P. J. Rousche, and D. R. Kipke, "Microstimulation in auditory cortex provides a substrate for detailed behaviors," *Hearing Research*, vol. 210, pp. 112-117, Dec. 2005.

[144] V. Pikov, L. Bullara, and D. B. McCreery, "Intraspinal stimulation for bladder voiding in cats before and after chronic spinal cord injury," *Journal of Neural Engineering*, vol. 4, no. 4, pp. 356–368, 2007.

[145] H. Orbach, L. Cohen, and A. Grinvald, "Optical mapping of electrical activity in rat somatosensory and visual cortex," *J. Neurosci.*, vol. 5, pp. 1886–1895, July 1985.

[146] C. Stosiek, O. Garaschuk, K. Holthoff, and A. Konnerth, "In vivo two-photon calcium imaging of neuronal networks," *Proc. Natl. Acad. Sci. USA*, vol. 100, pp. 7319–7324, June 2003.

[147] K. Deisseroth, G. Feng, A. K. Majewska, G. Miesenbock, A. Ting, and M. J. Schnitzer, "Next-Generation optical technologies for illuminating genetically targeted brain circuits," *J. Neurosci.*, vol. 26, no. 41, pp. 10380-10386, 2006.

[148] X. Han, X. Qian, J. G. Bernstein, H. hui Zhou, G. T. Franzesi, P. Stern, R. T. Bronson, A. M. Graybiel, R. Desimone, and E. S. Boyden, "Millisecond-Timescale optical control of neural dynamics in the nonhuman primate brain," *Neuron*, vol. 62, pp. 191–198, Apr. 2009.